



THESIS APPROVAL
GRADUATE SCHOOL, KASETSART UNIVERSITY

Doctor of Philosophy (Chemistry)

DEGREE

Physical Chemistry

FIELD

Chemistry

DEPARTMENT

TITLE: Experimental and Theoretical Studies of Transition Metals in
 Petrochemical Zeolite Catalysts

NAME: Miss Boonruen Sunpetch

THIS THESIS HAS BEEN ACCEPTED BY

THESIS ADVISOR

(Professor Jumras Limtrakul, Dr.rer.nat.)

COMMITTEE MEMBER

(Assistant Professor Piboon Pantu, Ph.D.)

COMMITTEE MEMBER

(Mr. Pipat Kongpracha, Ph.D.)

DEPARTMENT HEAD

(Assistant Professor Noojaree Prasitpan, Ph.D.)

APPROVED BY THE GRADUATE SCHOOL ON _____

DEAN

(Associate Professor Gunjana Theeragool, D.Agr.)

THESIS

EXPERIMENTAL AND THEORETICAL STUDIES OF TRANSITION METALS IN PETROCHEMICAL ZEOLITE CATALYSTS

BOONRUEN SUNPETCH

**A Thesis Submitted in Partial Fulfillment of
the Requirements for the Degree of
Doctor of Philosophy (Chemistry)
Graduate School, Kasetsart University
2009**

Boonruen Sunpetch 2009: Experimental and Theoretical Studies of Transition Metals in Petrochemical Zeolite Catalysts. Doctor of Philosophy (Chemistry), Major Field: Physical Chemistry, Department of Chemistry. Thesis Advisor: Professor Jumras Limtrakul, Dr.rer.nat. 130 pages.

Catalytic activity of metal supported zeolite catalysts were studied for N_2O decomposition and C_2H_6 oxidative dehydrogenation by N_2O . The activity for N_2O decomposition over different zeolites decreases in the following order, FER > BEA > ZSM5 >> MOR > FAU. With the presence of CH_4 , the activities for N_2O decomposition over FER, BEA, ZSM5 and MOR were significantly enhanced. In addition, the $\text{C}_2\text{-C}_3$ gases were observed in small amount about 8 and 10% selectivity over FER and MOR zeolites, respectively. On ZSM5 zeolite, aromatic products were observed with selectivity of 20% at a conversion of 25%. However, the catalysts suffered with rapid deactivation due to coke formation. The steam treatment was found to improve the catalytic stability. In addition, ZSM5 is also active for C_2H_6 oxidative dehydrogenation. The C_2H_4 yield of 21% was obtained at a reaction temperature of 500°C . The catalytic reactivity for N_2O decomposition of the highly dispersed Fe species in different zeolite frameworks were also studied by computational simulations with the ONIOM method. The framework species played the role in the activity of Fe-zeolites in N_2O decomposition. In the transition state, the smallest pore FER zeolite exerts the strongest van der Waals interactions on the reacting species and, thus, results in the lowest activation energy. Therefore, the predicted intrinsic activity trend is Fe-FER > Fe-ZSM5 ~ Fe-BEA ~ Fe-FAU. The very low activity of Fe-FAU that was observed experimentally could be due to the mass transfer limitation. Moreover, the catalytic N_2O decomposition on Fe-ZSM5, Co-ZSM5 and Ni-ZSM5 were compared. The predicted rate determining step for all catalytic samples is N-O bond breaking. The apparent activation energy predicted for Fe-ZSM5, Co-ZSM5 and Ni-ZSM5 are 46.0, 55.2, and 75.8 kcal/mol, respectively.

Student's signature

Thesis Advisor's signature

ACKNOWLEDGEMENTS

I would like to express gratitude to a number of people who help and support me to reach the goal of this thesis. My first thoughts of gratitude go to my advisor, Prof. Dr. Jumras Limtrakul, for his valuable guidance, continues supported and patiently encouragement along this study. I am particular grateful acknowledge to Assistant Professor Dr. Piboon Pantu for his numerous insightful comment and careful reading for this manuscript, it was his suggestions that made it possible this thesis to be completed.

It is a pleasure to express my gratitude to my teacher, Dr. Pensri Bunsawansong, Associate Professor Dr. Supa Hannongbua and Dr. Chak Sangma who introduced me to the field of physical chemistry. Thanks are also extend to the committee, Dr. Pipat Khongpracha and Associate Professor Dr. Matta Chareonpanich. Thank you my colleagues at LCAC both past and present as a good friend and collaborate in particular of their invaluable source of knowledge and inspiration. The especially indebted to Bundej and Nutchra for they assist in calculation part, to Nipat, Panida, and Wayoon for they help during my laboratory start up, to others who directly and indirectly contributed to my education in this field.

This research was supported by grants from the Commission on Higher Education, Ministry of Education, under the Postgraduate Education and Research Programs in Petroleum and Petrochemicals, and Advanced Materials, Kasetsart University Research and Development Institute, the Kasetsart University Graduate School, the Thailand Research Fund as well as the National Science and Technology Development Agency (2009 NSTDA Chair Professor) and NANOTEC Center of Excellence funded by the National Nanotechnology Center.

Finally, I would like to thank my family, my relations from Trang, and Weerachai and his family, for their love. Without their effort and patience on my long time study, I most certainly could never have accomplished any thing.

Boonruen Sunpetch

October, 2009.

TABLE OF CONTENTS

	Page
TABLE OF CONTENTS	i
LIST OF TABLES	ii
LIST OF FIGURES	iv
ABBREVIATIONS	x
INTRODUCTION	1
LITERATURE REVIEW	5
MATERIALS METHODS	18
Materials	18
Methods	20
RESULTS AND DISCUSSIONS	36
CONCLUSIONS	95
LITERATURE CITED	97
APPENDICES	116
Appendix A Zeolite digestion method for ICP-AES characterization	117
Appendix B Reaction products analysis	121
CURRICULUM VITAE	130

LIST OF TABLES

Table	Page
1 The condition of GC (FID) for characterize the product composition from the reaction of CH ₄ and N ₂ O	29
2 Physicochemical characteristics commercial zeolites used in this study	37
3 Metal content in modified zeolites by FeCl ₂ ion exchange characterized by ICP-AES	38
4 Metal content in modified zeolites by FeCl ₂ ion exchange characterized by ICP-AES	39
5 Surface area and porosity of commercial zeolites	43
6 Surface area and porosity of transition metal exchanged zeolites	43
7 Surface area and porosity of steam treatment zeolites	45
8 Surface area and porosity of coke zeolites	65
9 Products from the reaction of 3% C ₂ H ₆ and 3% N ₂ O in the non-catalytic system	66
10 Products from the reaction of 3% C ₂ H ₆ over ZSM-5(25) 0.15 g	67
11 Gas composition from the reaction of C ₂ H ₆ over 0.150g ZSM-5(25) at 500 °C in the total flow rate 100 cm ³ /min	69
12 Gas composition from the reaction of C ₂ H ₄ over 0.100 g ZSM-5(25) at 500 °C in the total flow rate 100 cm ³ /min	72
13 Products from the reaction of 3% C ₂ H ₆ and 3% N ₂ O over 0.100g zeolites at 500 °C in the total flow rate 100 cm ³ /min.	73
14 The optimized geometry of N ₂ O	75
15 The optimized geometry of Fe-O and Fe-O ₂ in ZSM-5 with various methods and models	77
16 N ₂ O adsorption Energy over FeO _x /ZSM-5 optimized by ONIOM2 model	78

LIST OF TABLES (Continued)

Table	Page
17 The optimized geometric parameters of the isolated zeolite cluster, adsorption intermediates and transition states (TS) for nitrous oxide decomposition over Fe-Zeolite by ONIOM (B3LYP:UFF)	80
18 Optimized geometric parameters of the isolated zeolite cluster, adsorption intermediates and transition states for nitrous oxide decomposition over Fe-ZSM-5	88
19 The optimized geometric parameters of the isolated zeolite cluster, adsorption intermediates and transition states for nitrous oxide decomposition over Co-ZSM-5	89
20 The optimized geometric parameters of the isolated zeolite cluster, adsorption intermediates and transition states for nitrous oxide decomposition over Ni-ZSM-5	90
21 Relative energy for adsorption complex during N ₂ O decomposition over TM-ZSM-5	92
 Appendix Table	
B1 Example of sensitivity and response factor for calculation the gas concentration from MS signal	125

LIST OF FIGURES

Figure		Page
1	Set up diagram for sample pretreatment	22
2	Set up diagram for test the temperature programmed reaction of N ₂ O decomposition	26
3	Set up diagram for test the reaction of N ₂ O with CH ₄ or C ₂ H ₆	28
4	ONIOM model of nitrous dioxide on the Fe-Zeolite: (a) Fe-ZSM-5 12T/144T, (b) Fe-FER 12T/114T, (c) Fe-BEA 14T/176T and (d) Fe-FAU 14T/84T	31
5	The proposed mechanism for N ₂ O decompositions over TM-ZSM-5 (TM= Fe, Co, Ni)	33
6	XRD patterns of the commercial zeolites (a) BEA(26), (b) BEA(51) (c) FER(20), (d) MOR(15), (e) USY(30), (f) Y(6), (g) ZSM-5(25) and (h) ZSM-5(42)	40
7	XRD patterns of the ZSM-5 zeolites (a) ZSM-5(25), (b) ZSM-5(25) st2h, (c) ZSM-5(42), (d) ZSM-5(42) st2h and (e) ZSM-5(42) st4h	41
8	N ₂ adsorption isotherms (—) and desorption isotherms (.....) of commercial zeolites: (a) ZSM-5(25), (b) ZSM-5(42), (c) BEA(26), (d) BEA(51), (e) Y(6), (f) USY(30), (g) FER(20), and (h) MOR(15)	42
9	N ₂ sorption isotherm over steam treatment zeolites: ZSM-5(25) st2h (a), ZSM-5(42) st2h (b), ZSM-5(42) st4h (c)	44
10	H ₂ -TPR profile of 2 vol.% H ₂ in Ar (total flow 30 cm ³ /min) and heating rate 10 °C /min over commercial zeolites: (a) BEA(26), (b) BEA(51), (c) FER(20), (d) MOR(15), (e) USY(30), (f) Y(6), (g) ZSM-5(25), and (h) ZSM-5(42)	46

LIST OF FIGURES (Continued)

Figure		Page
11	H ₂ -TPR profile of Fe zeolites (a) Fe(5,241) ZSM-5(25), (b) Fe(739) ZSM-5(48), (c) Fe(10,734) BEA(26), (d) Fe(7,143) BEA(52), (e) Fe(11,293) Y(6), (f) Fe(7,143) USY(32), (g) Fe(667) FER(20), and (h) Fe(8,592) MOR(15)	47
12	Morphology of starting (a) ZSM-5(25) and (c) ZSM-5(42) and the morphology after steam treatment for 2 h of (b) ZSM-5(25) and (d) ZSM-5(42) characterized by SEM	48
13	Reaction profile of N ₂ O decomposition in the reactor packed with quartz chips. Signal at m/e=28.03, 32 and 43.95 are corresponding to N ₂ , O ₂ , and N ₂ O, respectively	49
14	MS signal profiles of N ₂ O decomposition over FER(55) [N ₂ (— · — ·), O ₂ (.....) and N ₂ O (—)].	50
15	Reaction profile of N ₂ O temperature programmed decomposition over commercial zeolites [BEA (26) (◇), BEA (51) (◆), FER (20) (Δ), MOR (15) (✱), Y (6) (○), USY (30) (●), ZSM-5(25) (□), and ZSM-5(42) (■)] ; 10% conversion (.....), 50 % conversion (—...—) and 100% conversion (— — —)	51
16	Reaction profile of N ₂ O temperature programmed decomposition over Fe exchanged BEA(26) [BEA(26) (◇), Fe(1,861)BEA(26) (□), Fe(6,358)BEA(26) (Δ), Fe(10,734)BEA(26) (○), Fe(14,787)BEA(26) (●)]; 10% conversion (.....) and 50 % conversion (—...—)	52

LIST OF FIGURES (Continued)

Figure		Page
17	Temperature profile of N ₂ O temperature programmed decomposition over the same Fe content over different zeolites species [Fe(6,358)BEA(26) (◇), Fe(667)FER(20) (Δ), Fe(8,592)MOR(15) (✱), Fe(7,143)USY(30) (●), Fe(11,293)Y(6) (○), and Fe(5,241)ZSM-5(25) (□)] at 10% conversion; (— . . .) and 50% conversion (.....)	53
18	MS signal of 5% vol. CH ₄ and 5% vol. N ₂ O temperature programmed reaction in the blank reactor (packed with quartz)	55
19	Conversion of N ₂ O (A) and CH ₄ (B) studied by temperature programmed reaction of N ₂ O and CH ₄ over commercial zeolites [BEA(26) (◇), FER(20) (Δ), MOR(15) (✱), USY(30) (○), Y(6) (●), ZSM-5(25) (□)] at 10% conversion; (— . . .) and 50% conversion (.....)	55
20	Conversion of N ₂ O (A) and CH ₄ (B) studied by temperature programmed reaction of N ₂ O and CH ₄ over Fe exchanged zeolites [Fe(14,787)BEA(26) (◇), Fe(667)FER(20) (Δ), Fe(8,592) MOR(15) (✱), Fe(7,143) USY(32) (○), Fe(11,293)Y(6) (●), Fe(5,241)ZSM-5(25) (□)] at 10% conversion; (.....) and 50% conversion(— . . .)	57
21	Conversion of N ₂ O (A) and CH ₄ (B) studied by temperature programmed reaction of N ₂ O and CH ₄ over TM exchanged BEA(26) [Fe(14,787)BEA(26) (Δ), Co(17,487)BEA(26) (□), Cu(16,500)BEA(26) (◇)] at 10% conversion; (.....) and 50% conversion(— . . .)	57

LIST OF FIGURES (Continued)

Figure		Page
22	Conversion of N ₂ O (A) and CH ₄ (B) studied by temperature programmed reaction of N ₂ O and CH ₄ over TM exchanged ZSM-5(25) [Fe(5,241)ZSM-5(25) (Δ), Co(11,584)ZSM-5(25) (□), Cu(15,878)ZSM-5(25) (◇)] at 10% conversion; (.....) and 50% conversion (— ...)	58
23	N ₂ O conversion (A) and CH ₄ conversion (B) from the reaction of 5% CH ₄ and 2.5 % N ₂ O (in total flow rate 50 cm ³ /min) over 0.100 g commercial zeolites at 500 °C: BEA(26) (◇), BEA(51) (◆), ZSM-5(25) (□), ZSM-5(42) (■), MOR(15) (✕), and FER(20) (Δ)	59
24	CH ₄ and N ₂ O conversion from the reaction of 5% CH ₄ and 2.5 % N ₂ O (in total flow rate 50 cm ³ /min) over 100 mg of Y(6) (A) and USY(30) (B) at 550 °C. ((●) methane conversion, (○) nitrous conversion)	60
25	C ₂ and C ₃ hydrocarbon selectivity from the reaction of 5% CH ₄ and 2.5 % N ₂ O (in total flow rate 100 cm ³ /min) over 100 mg of FER zeolites at 500°C; (A) FER and (B) MOR	60
26	C ₂ and C ₃ hydrocarbon selectivity from the reaction of 5% CH ₄ and 2.5 % N ₂ O (in total flow rate 50 cm ³ /min) over 100 mg of BEA zeolites at 500°C	61
27	C ₂ and C ₃ hydrocarbon selectivity from the reaction of 5% CH ₄ and 2.5 % N ₂ O (in total flow rate 50 cm ³ /min) over 100 mg of ZSM-5(25) (A) and ZSM-5(42) (B) at 500 °C	62
28	CH ₄ conversion (filled symbol) and N ₂ O conversion (blank symbol) from the reaction of 6% CH ₄ and 3 % N ₂ O (total flow rate 50 cm ³ /min) over 0.100 g of steam treatment ZSM-5(25) (◆,◇) ZSM-5(42) (●,○)] at 500 °C ZSM-5(42) (B) at 500 °C	62

LIST OF FIGURES (Continued)

Figure		Page
29	C ₂ -C ₃ hydrocarbon (Δ), aromatic hydrocarbon (\circ), and total hydrocarbon selectivity (\blacklozenge) and hydrocarbon yield (.....) from the reaction of 6% CH ₄ and 3 % N ₂ O (in total flow rate 50 cm ³ /min) over 100 mg of steam treatment ZSM-5(25) (A) and ZSM-5(42) (B) at 500 °C	63
30	Coke content determined by TGA under N ₂ atmosphere (20 cm ³ /min) and heating rate 10 °C/min (\blacksquare) non steam-treatment, (\diamond) steam-treatment)	64
31	General configurations of high level parts in FeO _x -ZSM-5 (a) FeO-ZSM-5, (b) FeO ₂ -ZSM-5 and (c) FeO ₂ -ZSM-5 in tetrahedral form	76
32	ONIOM model of nitrous dioxide on the Fe-Zeolite: (a) Fe-ZSM-5 12T/144T, (b) Fe-FER 12T/114T, (c) Fe-BEA 14T/176T and (d) Fe-FAU 14T/84T	79
33	Energy Profile (kcal/mol) for nitrous decomposition over Fe-Zeolite. The uncertainties are discussed in the text	82
34	Parameter and atomic label defined for TM-ZSM-5 (TM=Fe, Co, and Ni) gases optimized structures [structure (I): TM-O-ZSM-5 straight channel (a) and TM-O-ZSM-5 zigzag channel (b); structure (IV): TM-O ₂ -ZSM-5 straight channel (c) and TM-O ₂ -ZSM-5 zigzag (d); and structure (VIII) TM-O ₂ -ZSM-5 straight channel (e) and TM-O ₂ -ZSM-5 zigzag channel (f)]	84
35	Parameter and atomic label defined for N ₂ O decompositions over TM-O ZSM-5 (TM=Fe, Co, and Ni) gases optimized structures (a) I, (b) II, (c) III, (d) IV, (e) V, (f) VI (g) VII, (h) VIII, and (i) IX TM-O ₂ -ZSM-5	87

LIST OF FIGURES (Continued)

Figure		Page
36	Energy profile of N ₂ O decomposition over TMO _x -ZSM-5	92
Appendix Figure		
B1	Example plot for evaluate the response factor of Ar (A) and N ₂ O (B) at m/e =40 and m/e=44, respectively	124
B2	Example chromatogram from GC (from the reaction of 5%CH ₄ and 2.5% N ₂ O in total flow 50 cm ³ /min over 100 mg ZSM-5-5(25) at 500 °C)	129

LIST OF ABBREVIATIONS

ASAP	=	Accelerated Surface Area and Porosimetry
BEA	=	Beta type zeolite
BET	=	Brunauer-Emmett-Teller
C ₁	=	Molecule contains 1 carbon atom
C ₂	=	Molecule contains 2 carbon atoms
C ₃	=	Molecule contains 3 carbon atoms
CH ₄	=	Methane
CO	=	Carbon monoxide
Co	=	Cobalt
CO ₂	=	Carbon dioxide
C ₂ H ₆	=	Ethane
C ₂ H ₄	=	Ethene
DFT	=	Density functional theory
EXAFS	=	X-ray absorption fine structure analysis
FAU	=	Faujasite type zeolites
Fe	=	Iron
FER	=	Ferrierite type zeolites
Fe-ZSM-5	=	Zeolite Secony Mobil structure 5contain Fe
FID	=	Frame Ionization Detector
FTIR	=	Fourier-transform Infrared
GC	=	Gas Chromatograph
H ₂ O	=	Water
ICP-AES	=	Inductively Coupled Plasma-Atomic Emission Spectroscopy
IR	=	Infrared Spectroscopy
MFI	=	Aluminosilicate MFI-type zeolite type zeolites
MOR	=	Mordenite type zeolites
MS	=	Mass Spectrometer
N ₂ O	=	Nitrous Oxide
Ni	=	Nickel
NMR	=	Nuclear Magnetic Resonance

LIST OF ABBREVIATIONS (Continued)

OCM	=	oxidative coupling of methane
ODE	=	Oxidative dehydrogenation of ethane
ONIOM	=	Our-own-N-layered-Integrated molecular Orbital + molecular Mechanics
O ₂	=	Oxygen
°C	=	Degree Celsius
SBU	=	Secondary Building Unit
SEM	=	Scanning Electron Microscopy
T	=	tetrahedral TO ₄ (T = Si or Al)
TEM	=	Transmission Electron Microscopy
TCD	=	Thermal Conductivity Detector
TGA	=	Thermogravimetric Analyzer
XRD	=	X-ray Powder Diffraction
XRF	=	X-ray Fluorescence Spectrometer
DI	=	Deionized water
S _{ext}	=	External Surface Area
S _{BET}	=	Surface area determined by BET method
TPR	=	Temperature-programmed Reduction
TPD	=	Temperature-programmed Desorption
TS	=	Transition State
TM	=	Transition Metal
V _{micro}	=	micropore volume determined by <i>t</i> -plot method
ZSM-5	=	Zeolite Secony Mobil structure 5

EXPERIMENTAL AND THEORETICAL STUDIES OF TRANSITION METALS IN PETROCHEMICAL ZEOLITE CATALYSTS

INTRODUCTION

Zeolites, acidic molecular sieves aluminosilicate, are widely used as catalysts in organic synthesis and petrochemical processes. These materials are usually used as solid acid catalysts replacing corrosive mineral acid catalysts in many petroleum and petrochemical reactions (Clerici, 2000; Degnan, 2000; Weitkamp, 2000; Jule, *et al.*, 2001; Sheldon and Downing, 1999; Degnan, 2003). The catalytic activity of zeolites can be further modified by introducing new heteroatoms into the framework such as transition metals, alkali and alkali earth metals, which create the new catalytic functions. Zeolites modified with transition metal ions exhibit unique catalytic properties that are quite different from the original (Armor, 1998; Weckhuysen, *et al.*, 1998; Barthomew and Farrauto, 2005; Berthomieu *et al.*, 2005). Added transition metals can be appearing in the form of metallic particle within the channel network that called extra-framework and substituted the atomic framework.

Porous framework of zeolites plays role of molecular sieve and nanoreactor functions. Only molecules of a certain size and shape will be able to access to the nanoreactors. The porous network imposes selectivity of the reaction through the orientation of the molecule inside the channels (Marcilly, 2000; Garcia and Roth, 2002). The catalytic properties of catalysts are determined by its composition and structure on atomic scale. The understanding of structural and electronic properties associated with different metal ions in zeolites, and chemistry of transition metals influenced by the framework are needed. For that, a great number of physical, chemical and computational methods have been developed.

In-situ techniques for study catalyst under operating conditions are quite well suited to monitoring a change in the catalyst during use. Several methods can be used

to characterize active site of heterogeneous catalyst for example chemical characterization, thermochemical characterization, nuclear magnetic resonance (NMR), X-ray absorption, UV-vis, and infrared spectroscopy (IR) (Busca, 1998; Kotrla, *et al.*, 1998; Suits *et al.*, 2000; Mauvezin *et al.*, 2001; Drozdova *et al.*, 2002; Kazaskey, 2003; Paulat *et al.*, 2004; Boissel *et al.*, 2006; Park *et al.*, 2008). Molecular or lattice dynamics techniques have been used to measure sorption processes in the zeolites pore channels (Cruz *et al.*, 1998; Kotrla *et al.*, 1998; Suit *et al.*, 2000; Thiabaut-Starzyk *et al.*, 2004). Electronic structure methods have also been used to elucidate reaction pathways (Berlier *et al.*, 2002; Wood *et al.* 2004b) so that our understanding of zeolites chemistry can be increased. These techniques often determine overall properties of the particles and, however, are usually not sufficiently specific to yield the desired atom-by-atom characterization of the surface. Computational modeling is an ideal candidate to bridge this gap (Berthomieu *et al.*, 2005). It has been proven to be invaluable in this area especially when used in collaboration with experimental work to verify the results.

The accuracy of the computational method depends on the size of system under study and what properties are of interests. Hybrid methods would be good to study the reaction site using a high level electronic structure method, whilst representing the long range interactions using an approximate method (Smirnov and Thibault-Starzky, 1998; Yang *et al.*, 2001; Fella and Onal, 2008). ONIOM method is one of the high accuracy hybrid methods of doing this for zeolites (Limtrakul, *et al.*, 2001; Kasuriya, *et al.*, 2003; Panjan and Limtrakul, 2003; Namuangrak *et al.*, 2004; Pabchanda, *et al.*, 2005). The active site geometries and reaction pathways over zeolites were well predicted through this technique.

Zeolites exchanged with transition metal were reported as the active catalyst for strong greenhouse gas nitrous oxide (N₂O) decomposition. The iron-exchanged zeolites have a high potential for the removal of N₂O from industrial and motor vehicle exhausts (Panov *et al.*, 1998; Sobolev *et al.*, 1993; Kapteijn *et al.*, 1997; Joyner *et al.*, 1999; Perez-Ramirez *et al.*, 2002; Wood *et al.*, 2002; Perez-Ramirez, *et al.*, 2003; Perez-Ramirez, 2004; Pirngruber and Roy, 2004; Wood, *et al.*, 2004a;

Heyden, *et al.*, 2005; Kiwi-Minsker *et al.*, 2005). Moreover, the Fe-ZSM-5 has a unique activity in the selective oxidation of methane to methanol at room temperature using nitrous oxide as an oxidant (Panov *et al.*, 1997; Sobolev *et al.*, 1995; Panov *et al.*, 1998; Dubkov *et al.*, 2002; Veseshchagin *et al.*, 2000; Kuchеров *et al.*, 2002; Wood *et al.*, 2004b; Parmon, *et al.*, 2005). The exact structure of the active site is still widely debated. The states of the iron atoms in the zeolite strongly depend on the method of preparation, the amount of iron loaded in the zeolite, and the pretreatment conditions. Generally, the active site is believed to be highly dispersed iron complexes in the microporous matrix. These fine iron species have a high affinity toward nitrous oxide and cause the molecule to be decomposed and to leave an active surface oxygen species on the iron surface (at a temperature below 300°C) (Kiwi-Minsker *et al.*, 2003; Ates and Reitzmann, 2007). This highly selective and active surface oxygen is generally called the α -oxygen (Panov *et al.*, 1997; Dubkov *et al.*, 2002). This α -oxygen was also reported as the active site for the selective oxidation of benzene to phenol and the oxidations of many hydrocarbons (Yoshizawa *et al.*, 2000; Nowinska *et al.*, 2003; Perez-Ramirez and Llamas, 2004; Parmon *et al.*, 2005; Chernyavsky *et al.*, 2007; Sanchez-Galofre *et al.*, 2007).

Several experimental and theoretical studies have attempted to elucidate the state and the structure of the active site of Fe-ZSM-5 (Joyner and Stockenhuber, 1999; Dubkov *et al.*, 2002; Perez-Ramirez *et al.*, 2002; Choi *et al.*, 2003; Panov *et al.*, 1998; Sun *et al.*, 2006). The highly dispersed iron complexes in the zeolite matrix can be found in the forms of isolated ions, binuclear complexes, oligonuclear complexes, and small aggregates of iron oxide clusters (Lobree *et al.*, 1999; Marturano *et al.*, 2000; Berlier *et al.*, 2002; Ferretti *et al.*, 2002; Jia *et al.*, 2002; Battiston *et al.*, 2003). A recent study has shown that at very low iron loadings ($\text{Fe/Al} \leq 0.1$), the iron is predominantly in the form of isolated ions. At higher exchange levels, the contributions of dimers and oligomers become important (Pirngruber *et al.*, 2006). To preparing the α -active site, the iron metal is normally introduced into zeolite frameworks by conventional ion exchange, solid-state ion exchange or included into chemical reagent during zeolite synthesis.

Small alkane molecules such as methane (CH_4) and ethane (C_2H_6) are the main composition in the natural gas. Moreover, CH_4 was reported as the green house gas mainly released from the nature (Connor, 2008a; 2008b). Finding the way to benefit these abundant and chemical inertness alkanes is the interesting topic. Typically, CH_4 and C_2H_6 are used as the precursor in the production of hydrogen and synthesis gas through the steam reforming or partial oxidation processes (Shilov and Shulpin, 2000; Bartholomew and Farrauto, 2005). Moreover, C_2H_6 can be used as the precursor for ethylene in thermal dehydrogenation and oxidative dehydrogenation (Heracleous and Lemonidou, 2004). This reaction was performed at high temperature at about 1000°C which high energy consumed and high reactor cost (Choundhary *et al.*, 2006). The mild reaction condition can be performed by using of catalysts such as metal oxide and oxidative condition which normally used CO_2 and O_2 . However, it still works at temperature above 650°C (Silberova *et al.*, 2004).

In this research, the catalytic activities of transition metals in petrochemical zeolites were tested for the reaction of N_2O decomposition. The catalytic reactions of CH_4 and C_2H_6 with the N_2O decomposition over these zeolites were also studied. The transition metals supported on several zeolites (MFI, BEA, FAU, FER and MOR) were prepared by conventional ion exchanged method. The activities of trace amount contaminated Fe in the starting zeolites were also compared. The computational simulation was applied to study the reaction geometry and energy of N_2O decomposition on Fe metal accommodated in different zeolite frameworks. From this calculations, the effect of zeolite frameworks on the α -oxygen formation through the N_2O decomposition over Fe-site was investigated. This method is also extended to study the catalytic decomposition of N_2O over different metal species (Fe, Co, Ni) in ZSM-5 zeolite. The effect of transition metal species on the reaction mechanism of N_2O decomposition is also compared.

LITERATURE REVIEW

Petrochemical Zeolite Catalysts

Solid acids are widely used in the chemical and petrochemical industry as catalysts and adsorbents. The important applications of solid acid in petroleum refining and petrochemical are reactions of alkane, including cracking, dehydrogenation, isomerization, and disproportion, etc. Typical catalysts for these reactions are solid proton-donor acids, including zeolites, which are the key components of industrial petroleum cracking catalysts. This catalytic cracking is a majority catalytic process in today's petrochemical industry (Corma, 1995; Degnan, 2000; Degnan *et al.*, 2000; Wietkamp, 2000; Garcia and Roth, 2002). The merits of solid acids, especially zeolites, over soluble acidic catalysts such as corrosion, separation etc., have been adequately underlined in numerous papers and reviews (Jentoft and Gates, 1997; Wietkamp, 2000; Garcia and Roth, 2002; Niwa *et al.*, 2003). They were used in gas phase and liquid phase of many organic in the areas of acid and redox catalysis and also used in environmental issues. Advances of zeolite for refinery applications are driven by the availability of new materials and the demands for improved fuels and chemical. They are attractive because of the structures and variation of pore dimensions leading to shape selectivity, from tunable acidity and from easy regeneration (Creyghton and Dowing, 1998; Cundy and Cox, 2003).

Zeolite catalysts are generally used in petroleum refineries and petrochemical reactions, and some other applications such as dewaxing via isomerization. Significant examples reactions such as acylation, alkylation, hydroxyalkylation of aromatic and heterocyclic compound, and rearrangement reaction have been produced by acid-catalyzed reactions. Light paraffin-olefin alkylation over zeolites catalysts are primary interesting processes. Hydrocracking is an open area that introduction of new and more selective zeolite catalysts. Most of the commercial developments have focused on modifications of zeolite Y to produce either more gasoline or distillate selective catalysts.

Zeolites are crystalline microporous aluminosilicates that exhibit excellent capabilities for catalytic use. Their crystal lattices are formed by TO_4 tetrahedra (T= Si or Al) connected via oxygen bridged in such a way that zeolite frameworks have channels and cages of molecular dimension. The frameworks channels, channel intersection, and/or cage dimension range 2 – 13 Å, which excellent to use as catalyst support material. Original zeolites are active for acid-catalyzed reactions because of the Brønsted-acid sites, which are generated as a charge balancing proton onto bridging oxygen for the substitution of silicon (Si) in the framework with aluminum (Al) (Marcilly, 2000). Others trivalent heteroatoms like Ga, B, or Fe can also introduced into the crystalline zeolite framework via isomorphous substitution of Si atom, results in the formation of strong Brønsted sites affecting acid-catalyzed reaction (Kiwi-Minsker *et al.*, 2003; Perez-Ramirez *et al.*, 2004; Perez-Ramirez and Llamas, 2004; Wood *et al.*, 2004a).

The metal cations are loaded on zeolites by ion exchange at extra-framework position to compensating the charge imbalances created by Al^{3+} ions. Metal ions are thus coupled on the zeolites surface and change their catalytic properties. Interaction between metal cation and zeolites framework seem to be an essential condition for changing the catalytic behavior. This exchanged metal acts as Lewis-acid sites, which active for organic reactions. Transition metal cation exchanged zeolites offer unique and high catalytic activity for a wide variety of important reactions. The combination of zeolites acid sites with transition metal ions build up a series of bi- and /or multifunctional catalysts with unique catalytic properties such as hydrogenation, oxidation, isomerization, and cracking of various organic feed stocks (Amor, 1998).

Different acidities in various zeolite is often attributed to difference in rates and selectivity for a given reaction. However, factors other than the intrinsic proton affinity of a given zeolite structures will also contribute to its catalytic properties (Gorte *et al.*, 1997). Transition metal dispersion in zeolite is varying consequences on the catalytic properties, particularly to the products selectivity. Modification of zeolites with metal by impregnation and ion exchange lead to formation of aggregated oxide clusters that may inactive in variety of reaction. Öhman *et al.* studied the ion

exchange effect on the catalytic activity on direct NO_x decomposition and viable candidate for NO_x reduction with methane. They were found that the preparation is crucial for the efficiency of the conversion and the ion exchange with Cu²⁺, Ni²⁺, or Pd²⁺ and the dual exchange with Cu²⁺/Ni²⁺ or Cu²⁺/Pd²⁺. Di- and trivalent ions frequently by stronger to exchange sites than monovalent ions, but monovalent may act as site blocker for di- and trivalent. Due to their strong interaction di- and trivalent ions may also alter the sites and thus the lattice more than monovalent ions. Different metal ions, depending on size, will exchange differently on different sites, only protons will have equal accessibility to all sites. Diffusion of the second ion is raised by the adsorbed first species (Öhman *et al.*, 2002). These results are correlated to the study of Godelistsas and Armbruster which modified HEU-type zeolite by ion exchange with d- and f-block transition elements and Pb. Structural distribution of the transition elements was determined by single crystal XRD, and combination of microscopic, spectroscopic, and thermal techniques. They found that HEU-type zeolites completely cation exchanged by Ag⁺, Pb²⁺, Cd²⁺, Mn²⁺, and Cu²⁺. Complementary microscopic, spectroscopic, and thermal data (e.g. SEM-EDS, IR, EPR, NMR, EXAFS, XPS, RBS, DTA, TPD) on HEU with Co, Ni, Cu, Pd, and Hg indicated non-homoeionic and non-stoichiometric metal loading. They always observed the excessive accumulation on the crystal surface, due to adsorption and surface precipitation phenomena (Godelistsas and Armbruster, 2003).

Generally, the ion exchange capacity of metal on zeolites is depend on it adsorption ability. Adsorption isotherms of Cu, Co, Mn, Zn, Cd and Ni from their nitrates on A-type zeolites were investigated by Majdan *et al.* They suggested that the adsorption of metals proceeds essentially through an ion-exchange process, surface hydrolysis, and surface complexation. DRIFT, SEM, and XRD results confirmed the presumption about the possible connection between the electronic structure of divalent ions and their adsorption behavior. The ions with d^5 and d^{10} configurations such as Mn²⁺, Zn²⁺, Cd²⁺, with much weaker hydrolytic properties than Cu²⁺ and Ni²⁺, are strongly interact with the zeolite framework. Therefore their affinity to the zeolites phase is much stronger when compared with that of the Ni²⁺ ion, but at the same time not as strong as the affinity of the Cu²⁺ ion, which forming a new phase during the

interaction with zeolite framework. For Zn^{2+} , during inspection of the correlation between the proton concentration H/Al and zinc concentration Zn/Al on the zeolite surface, the formation of the surface complex $\equiv\text{S}-\text{OZn}(\text{OH})$ was proposed. A correlation between the heterogeneity of proton concentrations, H/Al , on metal-zeolite surfaces and the hydrolysis constants, pK_h , of Me^{2+} ions was found (Majdan *et al.*, 2003).

Acidic proton zeolites such as H-BEA, H-ZSM-5, H-MOR, H-FER, and H-FAU are frequently used catalysts and sorptions medium in petrochemical processes. Various kinds of transition metal (TM) can be dope on these zeolites. The loading method for insert the TM into the zeolites framework can be achieved by various methods including as-synthesis and post-synthesis methods. The post synthesis method is applied over the zeolites crystal by adsorption, impregnation, wet ion exchange, solid state ion exchange, sublimation under high vacuum (Gutierrez *et al.*, 2008; Smeets *et al.*, 2008; Sun *et al.*, 2006; Hensen *et al.*, 2005; Tatlier and Kiwi-Minsker, 2005; Wang *et al.*, 2008; Li *et al.*, 2008). Detail about nature and concentration of individual acid sites represents a basic set of the function and performance of these catalysts. The determination of the nature and concentration of individual acid sites will be a basic set of information.

Catalytic activity of nitrous oxide decomposition

One of the most famous topics in transition metal loaded zeolites application is NO_x decomposition concerned. Nitrous oxide (N_2O) is one of the NO_x compound which considered as high ozone depletion and strong global warming species (Jane, 2009). N_2O is also reported as oxidative reagent for hydroxylation of benzene to phenol in $\text{AplphOx}^{\text{TM}}$ process (Gardziella *et al.*, 2000). Many forms of transition metals have been loaded to various kind of zeolite such as $\text{Cu}/\text{ZSM-5}$, ZSM-11 , Y , and MOR , $\text{Fe}/\text{ZSM-5}$, and co-cation loaded such as $\text{Cu}/\text{Ca}/\text{ZSM-5}$, $\text{Cu}/\text{Ni}/\text{ZSM-5}$, etc. in the work of Yokomichi *et al.* It was experimentally found that the addition of a co-cation such as Ca or Ni to Cu ion exchange ZSM-5 zeolite could prevent the catalyst from deactivation caused by O_2 or H_2O in the reaction gas. The theoretical

calculation showed that the addition of these co-cations increased the catalytic activity by promoting desorption of oxygen yielded from NO decomposition and maintained NO adsorption on the catalyst under the coexistence of H₂O (Yokomichi *et al.*, 2000). Armor was illustrated six very different reactions on these zeolites; Co-zeolites are highly active catalysts for the reaction of ethane/NH₃/O₂ to acetonitrile, Pd-ZSM-5 is a good water tolerant catalyst for NH₃ oxidation to N₂, Pd-ZSM-5 is a very active catalyst for CH₄ combustion, Co-ZSM-5 is a very good catalysts for wet N₂O decomposition, Co-ZSM-5 is active of NO_x removal with CH₄/O₂ even in present of water, and Cu-ZSM-5 catalyse the decomposition of NO_x into its elements (Armor, 1998).

Iron (Fe) exchanged zeolites catalysts are frequently used in NO_x decomposition, methanol oxidation, oxidative dehydrogenation of propane, and decomposition of n-butane. The selectivity and apparent energy of NO_x selective catalytic reduction with CH₄ on Mn-ZSM-5 with Co-ZSM-5 and Cu ZSM-5 in the presence of H₂O were independent of the manganese content. It is suggesting that the same surface complexes were formed on all Mn-ZSM-5 catalysts. On Mn-ZSM-5, Co-ZSM-5, and Cu-ZSM-5, the adsorption at room temperature of NO + O₂ or N₂O caused the formation of nitrate. On all these catalysts, NO abatement rates were proportional to the concentration of their monodentates. These findings suggest a role of monodentate nitrate in the SCR reaction (Campa *et al.*, 1998).

The Fe-ZSM-5 and other iron-containing zeolites are active for the nitrous oxide decomposition. The iron zeolites with the pentasil-type frameworks (ZSM-5, beta, ferrierite) are more active than other iron zeolites (mordenite, faujasite). However, the activity order is still not conclusive. The activity for nitrous decomposition is ranked as Fe-FER > Fe-BEA > Fe-ZSM-5 >> Fe-FAU ~ Fe-MOR for the catalysts prepared by liquid-ion exchange with the exchange level ranging from 10-50%. Jisa *et al.* also reported the superiority of Fe-FER over Fe-BEA and Fe-MFI with Fe/Al ratio below 0.15. They proposed the effect of a unique FER structure containing two close collaborating Fe (II) cations accommodated in cationic sites of FER (Jisa *et al.*, 2009). Øygarden and Pérez-Ramírez have recently examined

the effect of zeolite frameworks on the activity of trace iron impurities in zeolites ($\text{Fe/Al} \leq 0.01$). An activity trend of $\text{Fe-BEA} > \text{Fe-FER} > \text{Fe-ZSM-5} \sim \text{Fe-MOR} \gg \text{Fe-FAU}$ was observed (Øygarden and Pérez-Ramírez, 2006). Li *et al.* report the different reactivity trend over Fe wet ion exchanged as $\text{Fe-FUA} > \text{Fe-BEA} > \text{Fe-ZSM5}$. However, the Fe contents in different zeolites species were 0.30, 0.52, and 3.38 % in ZSM5, BEA, and USY that not in comparative range. They also reported the activation energies for N_2O decomposition as 31.1, 36.1, and 37.3 kcal/mol for Fe-FUA, Fe-BEA, and Fe-ZSM5, respectively (Li *et al.*, 2008). This different trend indicates that the activity may be linked with different iron species in the catalysts, derived from different preparation methods and different iron loadings. The additional interactions of the reactant molecule with the framework-cavity environment can assist activation of an adsorbed molecule. This effect include not only the local bonding of the reactant molecule with the Brønsted proton but additional effects arising from host-guest electrostatic and van der Waals interactions and from the long-range influence of the extended solid (Smirnov and Thibault-Staerzyk, 1998; Suits *et al.*, 2000; Yang *et al.*, 2001). The topology of zeolite structure can have a significant effect on reactivities. In case where the reactants and products interact weakly with the acid site, the effect of zeolite topology can be very large.

The transition metal loaded zeolites are reactive for the reaction of N_2O decomposition. The different reactivity of the transition metal on different zeolites framework can be test with this kind of reaction. Furthermore, the different activity of different metal in the same framework species will differentiated by this reaction.

Reaction of Methane Conversion

Methane (CH_4) is the most abundant compound presents in natural gas. It is primary use as fuel in manufacture and electric power plant. Thailand can produce methane both on-shore and off-shore field. It is the interesting fuel because it need and storage system. It is transported from the resource to the using site by pipeline system. However, CH_4 gas from off-shore resource that far away from the land is extremely hard to utilize it as fuel. It is very interesting to use it as chemical feedstock

for industrial process. Nevertheless, the stability of CH₄ is important barrier for this application.

The activation and conversion of methane (CH₄) into more valuable chemicals have attracted much attention and research effort in the last few years. Several researchers tried to find a way to transform CH₄ into higher hydrocarbons. Different transition metal ions, such as Mo, Cu, Zn, and Cr, are able to activate CH₄ and that Mo/H-ZSM-5 is the most promising catalytic system in the absence of an oxidant. Preparation and treatment conditions (treatment method and the metal ion loading) and the zeolite acidity, playing a crucial role in the activity of transition metal ions on the activation CH₄. For Mo, Fe, Cr, W, and V/H-ZSM-5 materials prepared by ether impregnation and solid state ion exchange, the catalytic activities decreased in the order: Mo > W > Fe > V > Cr over H-ZSM-5. Impregnation materials always had a higher activity than solid state ion-exchange materials. It can conclude that the catalytic properties depend on the presence of Brønsted acid sites and the distribution of the transition metal ions in the zeolites materials (Weckhuysen *et al.*, 1998). The dehydroaromatization of CH₄ over Mo/H-ZSM-5 was also investigated by Chu and Qiu. The rate of benzene formation was significantly enhanced with the addition of a few percent of ethane. This conversion of CH₄ to benzene achieved at 3 atm and 725°C (Chu and Qiu, 2003).

The proven natural sources of CH₄ are enormous. The principal methods for the conversion of CH₄ into useful chemical compounds can be divided into indirect and direct processes. The most important indirect methods for CH₄ conversion are based on the production of synthesis gas, which then passed on for the future processing. Three main methods are used for the conversion of methane into synthesis gas:

- Steam reforming of methane: $\text{CH}_4 + \text{H}_2\text{O} = \text{CO} + 3\text{H}_2$
- Carbon dioxide conversion : $\text{CH}_4 + \text{CO}_2 = 2\text{CO} + 2\text{H}_2$
- Partial oxidation: $\text{CH}_4 + 1/2\text{O}_2 = \text{CO} + 2\text{H}_2$

The development of direct methods for the conversion of methane to useful products is possible to three main potentially important: Nonoxidative conversion, oxidative coupling, and partial oxidation to C₁ oxygenates.

The nonoxidative dehydrocondensation of CH₄ make it possible to resolve jointly two important problems – the production of hydrogen and the production of useful higher hydrocarbon. The production of hydrocarbons has a certain thermodynamic limitation- to obtain acceptable yields it is necessary to use fairly high temperatures. The preferential formation of aromatic hydrocarbons was achieved with the use of a series of bifunctional catalysts. More recently, it was found that methane can be converted into benzene in the absence of an oxidizing agent on a deposited molybdenum-oxide catalyst Mo/HZSM5 in a continuous reaction regime at atmospheric pressure and 700 °C (Pyatnitskii, 2003). At atmospheric pressure equilibrium yields of the aromatic compounds are in the order of 10% or more are achieved beginning at 700 °C. A serious problem in this process is carbonization of the catalyst.

The oxidative coupling of methane (OCM) take places by a heterogeneous-homogeneous mechanism. The formation of methyl radicals at OCM catalysts was demonstrated experimentally. Heterogeneous generation of methyl radical is postulated in all models is equation (1):



In the gas phase the methyl radicals recombine with the formation of ethane – a primary C₂ hydrocarbon as equation (2):



Secondary reaction leads to the formation of ethylene and also side products. The selectivity of the process with respect to the C₂ hydrocarbon is limited by reaction paths involving reaction of the methyl radicals with oxygen and oxygen-containing particles.

Ethane oxidative dehydrogenation

Ethane (C_2H_6) is the second most of hydrocarbon presents in natural gas after methane. Nevertheless, only few chemicals could be obtained from the direct reaction of C_2H_6 . Generally, C_2H_6 is utilized by convert it into the most important feed stock in petrochemical industry, ethylene (C_2H_4). One important way to produce C_2H_4 from C_2H_6 is thermal dehydrogenation. Still, the major C_2H_4 feedstock is come from the steam crackers unit (Matar and Hatch, 2000). Steam cracking of pure ethane produced ethylene in yields over 80% at temperature above $800^\circ C$ and a steam: ethane ratio of about 0.3 (Olah and Molnar, 2001).

Ethylene is the important feedstock in petrochemical industry; contribute the greatest volume in the petrochemical industry feed stock (Speight, 2006). Generally, it produced through the thermal cracking that highly endothermic (energy intensive). The thermal cracking process has to run at high temperature up to $1,100^\circ C$ which high energy demand and decrease the reactor lifetime. The presence of oxygen can enhance the thermal cracking of ethane and could be carried out at much lower temperature because it improves the thermodynamic limitation (Sinev, *et al.*, 2003; Kondratenko, *et al.*, 2006). The oxidative dehydrogenation of ethane (ODE) has been considered as a potential route for synthesis of ethylene at lower reaction temperature. The oxidizing gas can be O_2 , CO , CO_2 , H_2O , or N_2O .

The catalytic ($Sr_{1.0}La_{1.0}Nd_{1.0}O_x$) and non-catalytic oxidative dehydrogenation of C_2H_6 to C_2H_4 with O_2 have been carried by Mulla and co-worker. The reaction also test with 30% stem feeding with the inlet mixture. They were reported that the homogeneous gas-phase, reactions were not significant up to $700^\circ C$. Above $700^\circ C$, the non-catalytic reaction occurred to a large extent resulting in C_2H_4 yield of 46% and 53% at 750 and $800^\circ C$, respectively. In the presence of $Sr_{1.0}La_{1.0}Nd_{1.0}O_x$ catalyst the highest C_2H_4 yield amounted to 46% at $700^\circ C$. For this study, they concluded that, the ignition of the reaction mixture which resulted in an increased temperature in catalyst zone as compared to the inlet temperature could not be excluded even at a low space velocity (Mulla, *et al.*, 2002). Moreover, Heracleous, *et al.* reported the

thermal conversion of C_2H_6 in the presence and absence of oxygen in the reaction mixture (Heracleous, *et al.*, 2004). In case of presence oxygen, ethane converts around 600°C. But it was started at about 640 °C when no oxygen was feed.

Carbon dioxide can also act as a mild oxidant, increases ethane to ethylene cracking at 750-900°C (Choudhary *et al.*, 2006). However, they found that ethane conversion was only about 5% at 750°C. Ge *et al.* reported the ethane conversion 0.2 % at 650°C for the system that contained higher CO_2 concentration (Ge *et al.*, 2000). Catalysts can induce this reaction to lower temperature. Ge *et al.* also reported the effect of metal catalyst on that $LiCl/MnOx$ and $CaCl_2/MnOx$ supported on Portland cement were converted 73.3% and 46.9 % ethane at 650°C and produced 63.8% and 30.0% ethylene yield, respectively. The reactivity of $MoOx$ supported on Al_2O_3 was studied for ethane oxidative dehydrogenation with O_2 . This system seem reactive at lower temperature which ethane conversion about 23% over 20% of $MoOx$ over Al_2O_3 at 550°C and $W/F=0.33g\cdot s\cdot cm^{-3}$. Selectivity was about 65% (Heracleous *et al.*, 2004). While the thermal conversion of ethane without catalyst was above 600 °C and 640°C when oxygen was absent.

The activity of Co-zeolites with NFI, BEA, FER, and MOR was studied in ethane and propane oxidative dehydrogenation and amoxidation by Bulanek *et al.* This activity was studied in a through-flow arrangement and temperature range 350-500 °C. The products of oxidative dehydrogenation of paraffins were corresponding olefins, CO, and CO_2 . In the propane reaction only a small part was cracked to ethylene and methane. Ammoxidation of ethane yield CO, CO_2 , ethylene, and acetonitrile. The sequence in activity in both the oxidative dehydrogenation and ammoxidation of Co-zeolites: Co-BEA > Co-MFI >> Co-MOR > Co-FER is ascribed to the location of prevailing amount of Co ions in β cation of pentasil rings zeolites in contrast to Co- β ions in MOR and FER structures occurring in the narrow interconnections and in eight member ring channel, respectively. Presence of ammonia increased substantially the paraffin conversion as well as selectivity and yields of the sum of olefin and nitrile for Co-H-BEA and Co-H-MFI zeolites, while

Co-Na-zeolites the paraffin conversion and selectivity were similar (Blanek *et al.*, 2002).

Computational Approach

Theoretical calculation can provide additional insights into the chemical characteristics of interest system, which essential for the next step of putting them to practical use (Zhidomirov, *et al.*, 1999; Lesthaeghe, *et al.*, 2006). A combination of experimental and computational studies of the reactivities of zeolites can enhance understanding of the elementary process occurring in the real catalyst. It is precious to better understand the system by study thought the model.

Theoretical studies of the catalytic activity of Lewis acid site in zeolites are rather rare. Some attempt was made to model the interaction of Lewis acid sites with probe molecule like CO by Deka and Hirao (Deka and Hirao, 2000). The Lewis acidity and basicity of cation exchanged zeolites were studied by QM/MM and density functional study. They determined structure and geometrics of Li, Na, and K exchanged Faujasite zeolite by cluster model and QM/MM calculations. The quantum chemical calculations were performed using the GASMES program. The geometry was optimization at HF/6-31G**. They investigated the electric field around the extra framework cations by studying the interaction of CO molecule with cation-exchange zeolite and shift of vibrational frequency of adsorbed CO molecule. The strength of Lewis acid acidity of the cations and basicity of framework oxygen atoms is investigated using density functional methods. They used the local reactivity descriptors based on hard-soft acid-base concept as acidity and basicity parameters. The calculated 'relative electrophilicity' values are found to be better descriptors of acidic and basic sites, respectively. From relative electrophilicity value, the Lewis acidity of cation-exchanged faujasite zeolite is found to decrease in the order: [Li-FAU] > [Na-FAU] > [K-FAU], and from relative nucleophilicity value of the framework oxygen atom, the Lewis basicity is found to increase in the order [Li-FAU] < [Na-FAU] < [K-FAU].

Framework is playing the important role in the adsorption processes of probe molecules onto zeolite. Many report showed the proper way of theoretical calculation for study the interaction of molecular probe in zeolites framework. Limtrakul *et al.* used the ONIOM (Our-own-N-layered-Integrated molecular Orbital + molecular Mechanics) method to studied the activity of guesses molecule in zeolites framework. By this method the system can be treating with multi-layer multi-level, cause possible to optimize the bigger system. They were showed that the optimized data were good correlated with experimental data (Limtrakul *et al.*, 2001; Panjan and Limtrakul, 2003; Rakskul and Limtrakul, 2003).

Many authors have been applied quantum chemistry to study the reaction of N_2O in zeolites. Yoshizawa have been success to study the reaction of N_2O and methane hydroxylation and benzene hydrogenation in ZSM-5. Direct methane to methanol and benzene to phenol conversion on Fe-ZSM-5 zeolite have been study through 3T structure and iron-oxo species located on AlO_4 surface site. They optimized this model and the reaction gas with B3LYP method. The system have been treated at sextet and quartet spin. They found the spin crossing in their reaction pathway concern the methane to methanol process. However, they found sextet surface is the most stable form of isolated iron-oxo in ZSM-5 (Yoshisawa, *et al.*, 2000; Yumura *et al.*, 2002; Yoshizawa, 2006). They model the Fe-ZSM-5 with the mononuclear iron exchanged at the Brønsted acid position.

Bell, A.T. groups reported many work on the computational results of N_2O decomposition on transition metal ZSM5. They reported the reactive characteristic of Fe- and Co-exchanged ZSM5 studied by DFT theory on 5T cluster. The apparent activation energies of N_2O dissociation in Fe-ZSM5 and Co-ZSM5 are 39.4 and 34.6 kcal/mol, respectively (Ryder *et al.*, 2002). The extended study about N_2O decomposition over Fe-ZSM-5 also has been done by this group. Heyden *et al.* reported the reaction mechanism of N_2O decomposition over Fe-ZSM5 from DFT calculation over 5T cluster model. They were studied on hydrate and dehydrate mononuclear iron sites. They found that N_2O decomposition is first order with respect to N_2O concentration. They proposed the decomposition of N_2O is first order respect

to N_2O concentration and zero order with respect to O_2 concentration which not agrees with the experiment report (Kapteijin *et al.*, 1997, Wood *et al.*, 2004a). They also found the strong inhibition effect by water on this reaction which present in the range of apparent activation energy vary with the concentration of H_2O (Heyden *et al.*, 2005).

Fellah and Onal were reported the DFT calculation on N_2O decomposition over Fe-ZSM5 and Co-ZSM5 that the framework was important for the energy prediction. The studied model was 5T ZSM-5 cluster and placed Fe atom on the Brønsted acid position. N_2O can decompose on this active site with very low reaction barrier, 4.41 and 6.28 kcal/mol for Fe- and Co-ZSM-5, respectively. After that, they proposed the second N_2O molecule decomposition on the generated active site with activation energy 58.13 and 48.56 kcal/mol for Fe- and Co-ZSM-5, respectively. They found that the activation energy from channel for the first N_2O decomposition is 12.63 kcal/mol (Fellah and Onal, 2008). However, they initial active site $[\text{Fe}^+]$ seem unrealistic because the experiment evidence does not support (Panov *et al.*, 1997; Dubkov *et al.*, 2002; Ryder *et al.*, 2002).

MATERIALS AND METHODS

Materials

1. Instruments

1.1 Mass Spectrometer (Omnistar, Pfeiffer Vacuum Pump, Quadstar QMS422)

1.2 Gas Chromatograph (Thermo Finigan Trace GC) equipped with HayeSep® D, 100/120 10 ft x 1/8" OD, SS column, the detectors were Flame ionization detector (FID) and thermal conductivity detector (TCD)

1.3 Surface area and porosity analyzer (Micromeritics, model ASAP 2020)

1.4 Thermogravimetric Analyzer (TGA) (Perkin Elmer, model TGA7)

1.5 Inductively Coupled Plasma Atomic Emission Spectrometer (ICP-AES) (Perkin Elmer, model PLASSMA4000)

1.6 Powder X-ray Diffractometer (Philips: X'Pert)

1.7 X-ray Fluorescence Spectrometer (WDX (PW 2400) and EDX (ED 2000))

1.8 Scanning Electron Microscope (Hitachi S-3400 Scanning Electron Microscope (SEM) 20kV and 88.0 μ A)

2. Chemicals

2.1 Zeolites

- Beta Type zeolite powder (BEA) CP814E ($\text{SiO}_2/\text{Al}_2\text{O}_3=25$) and CP814Q ($\text{SiO}_2/\text{Al}_2\text{O}_3=50$) NH_4^+ -form, Zeolyst International

- Ferrierite Type zeolite (FER) CP914C ($\text{SiO}_2/\text{Al}_2\text{O}_3=20$) and CP914 ($\text{SiO}_2/\text{Al}_2\text{O}_3=55$) NH_4^+ -form, Zeolyst International

- Modenite Zeolite (MOR) MSM-15 ($\text{SiO}_2/\text{Al}_2\text{O}_3=13-15$) NH_4^+ -form, Al-Si-Penta Zeolithe GmbH

- Zeolite USY (FAU) CBV720 ($\text{SiO}_2/\text{Al}_2\text{O}_3=30$) H⁺-form, Zeolyst International

- Zeolite Y (FAU) CBV400 ($\text{SiO}_2/\text{Al}_2\text{O}_3=5.1$) H⁺-form, Zeolyst International
- ZSM-5 (MFI) (SH27 ($\text{SiO}_2/\text{Al}_2\text{O}_3=22-25$) and SH55 ($\text{SiO}_2/\text{Al}_2\text{O}_3=40-48$) H-form, Al-Si-Penta Zeolithe GmbH

2.2 Transition metal precursors

- Iron (II) Chloride tetrahydrate ($\text{FeCl}_2 \cdot 4\text{H}_2\text{O}$), 99 % (Aldrich)
- Copper (II) Chloride, anhydrous, powder (CuCl_2), 99.995+% (Aldrich)
- Cobalt (II) acetate tetrahydrate ($((\text{C}_2\text{H}_3\text{O}_2)_2 \text{Co} \cdot 4\text{H}_2\text{O})$), 98+% (Aldrich)
- Deionized (DI) water
- Hydrochloric acid (HCl)

2.3 Reagents for catalytic activities

- Air zero (Praxair)
- Argon (Ar) 99.999% (Praxair)
- Helium (He) 99.999% (Praxair)
- Hydrogen (H_2) 99.999% (Praxair)
- Hydrogen (H_2) 2% in Ar (TIG)
- Ethane (C_2H_6) 99.95% (TIG)
- Ethane (C_2H_6) 5% in He (TIG)
- Methane (CH_4) 50% in Ar (TIG)
- Nitrogen (N_2) 99.999% (TIG)
- Nitrous oxide (N_2O) 5% in He (Broach)
- Nitrous oxide (N_2O) 99.998% (Broach)
- Oxygen (O_2) 99.999% (Praxair)

3. Major equipments and Tools

3.1 Oven (Mettler, model UM400)

3.2 Horizontal furnace (Lenton, model LTF 12/75/610, with Eurotherm controller, model 3216)

3.3 Split type vertical furnace (Lenton CSC 12/110/300V with Eurotherm controller, model 3216)

3.4 Digital gas flow controller (AALBOLG Mass Flow Controller, model GFC)

3.5 Ultrasonic bath (Bandelin, SONOREX (frequency 35kHz, P 480W) and BANO De Ultrasons-H)

3.6 Multiposition Sampling Valve with multiposition actuator (VICI ST16 MWE Valco Instruments Co. Inc)

Methods

1. Catalyst preparations

1.1 Zeolites preparation

The commercial zeolites were calcined under atmospheric environment at 550 °C for 6 h. The heating rate was 5 °C/min. These calcined zeolites were used as starting material for all studies.

In this work the transition metal (TM) contained zeolites were typically prepared by exchanging of H-Zeolites in an aqueous solution of transition metal salts. First, the aqueous solutions of transition metal were prepared by dissolving the transition metal salts in DI water. Then the concentration of the solutions was adjusted to be 0.100 M. Iron (Fe) contained zeolites were prepared typically as follows. An aqueous FeCl₂ solution was prepared from Iron (II) Chloride tetrahydrate, FeCl₂·4H₂O in 0.1 M HCl (pH=1.0) to prevent the Fe oxide aggregates (Schwiderer *et al.*, 2005). Then the commercial H-zeolites were added to the solution about 1.0 g zeolite /10 cm³ solution. This ion exchange mixture was contained in plastic bottle (LDPE, NALGENE). The obtained slurry was homogenized in an ultrasonic bath for 30 min and then filtered by Whatman® filter paper (No.42). The precipitate was rinsed with DI water, dried overnight at 110 °C and then calcined at 550 °C for 6 h under air ambient. Next, the final zeolite was pressed into pellet. The pellet was further crushed

to obtain particle size of 250-425 μm which obtained from the fraction between 40- and 60-mesh sieves.

1.2 Steam treatment

Typically, steam treatment of zeolites was performed by following method. Zeolites were packed in the fixed bed reactor between the quartz wool and the quartz chip layer in side quartz tube as shown in Figure 1. The desired steam was generated by the steam generator system, which was attached to the reactor. After the 20 cm^3/min Ar flow was passed through DI water at 80 $^{\circ}\text{C}$, the vapor-contained gas was generated as a steam. Initially, zeolite was heated from room temperature to 650 $^{\circ}\text{C}$ in the Ar ambient by the heating rate of 10 $^{\circ}\text{C}/\text{min}$. Afterward, the mixed stream was introduced to the reactor. The final gas mixture concentration was adjusted to 30% steam and 70% Ar. The reactor was kept under this condition for 2 hours before cool down under the inert ambient, Ar.

2. Characterizations

2.1 Elemental analysis

Chemical composition of the catalysts was obtained by using an X-Ray Fluorescence (XRF) spectrometer and an Inductively Coupled Plasma Atomic Emission Spectroscopy (ICP-AES). The quantities of Al and Fe were measured by using the ICP-AES for all samples. The zeolite samples were prepared as solution form for the elemental analysis by the ICP-AES. The detail of sample preparation and related sample concentration calculation are presented in Appendix A. The quantities of Si and Al contained in zeolites were measured by XRF spectrometer of the solid samples. The results were reported as the molar ratio of Si atom to Al atom (Si/Al).

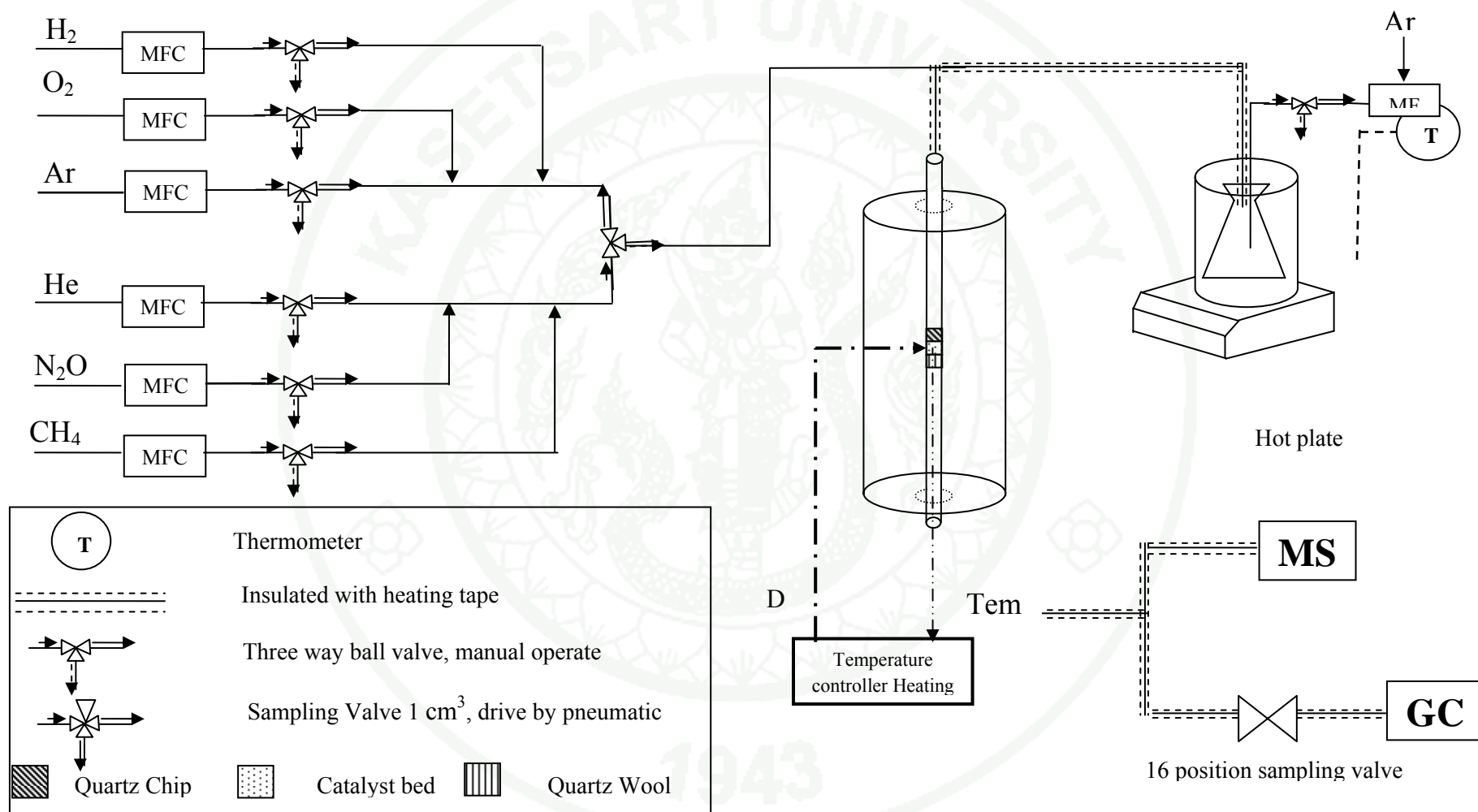


Figure 1 Set up diagram for sample pretreatment

2.2 Surface area and pore structure analysis

Surface and pore characteristic of zeolite samples were described by N₂ sorption isotherm measured from a Micromeritics ASAP 2020 instrument. Prior to each measurement, the sample was degassed for 20 h at 350 °C under vacuum (10 µmHg) to eliminate the volatile component from the sample solid surface.

After that, the treated sample was immersed in liquid nitrogen bath to keep a constant temperature (-169 °C) throughout the sorption isotherm measurement. The adsorbing gas (N₂) was admitted with an increment of 4.0 cm³/g (STP) before reaching the setting relative pressure (P/P_0). Each pressure values were collected out at equilibrium interval 30s. The accumulated quantities of the adsorbed gas that collected at each P/P_0 called adsorption isotherm. The adsorption isotherm pressure was collected around $0.001 < P/P_0 < 0.999$. Similarly, desorption isotherm was a measured from the quantity of nitrogen gas that adsorbed on the sample surface during pressure reduced at the specific P/P_0 .

The BET method was used to calculating the specific surface area (S_{BET}) from the adsorption isotherm. Generally, BET model is fit to describe the adsorption isotherm at P/P_0 lower than 0.3. However, in this work, the BET equation yielded a straight line between P/P_0 values from about 0.001 to 0.100. The external surface area (S_{ext}) and the micropore volume (V_{micro}) were determined using the t -plot method. The appearance of hysteresis loop from desorption isotherm and adsorption isotherm was point out the mesoporous characteristic of zeolite samples.

2.3 Temperature programmed decomposition of coke

Quantities of coke deposition were characterized by a Thermal gravimetric analysis (TGA) with the Thermo gravimetric Analyzer TGA 7, Perkin Elmer. The used catalysts were heated under the flow of N₂ gas 20 cm³/min and a heating rate of 10 °C/min. The study temperature was range between 100 and 800 °C. Weigh loss from catalyst between 200 and 800 °C was calculation to the coke deposition quantities.

2.4 Powder x-ray diffraction (XRD)

Crystalline phase was identified by powder x-ray diffraction (XRD). The zeolites XRD patterns were performed on a Phillips X'pert x-ray diffractometer model X'Pert-MPD using Cu K α radiation ($\lambda = 1.541 \text{ \AA}$). The x-ray tube was operated at 40 kV and 30 mA. X-ray powder diffraction patterns were recorded at step size 0.02 degree with 1.5 s count accumulation per step in the range of 2θ between 5 and 50 degree. The crystalline phases of samples were identified by comparison with x-ray diffraction standard pattern of zeolites on web site <http://izasc.ethz.ch/fmi/xsl/IZA-SC/xrd.xsl>.

2.5 Morphology

Morphology of samples were investigated by scanning electron microscopy (SEM), using a Hitachi S-3400 Scanning Electron Microscope. Zeolite samples have to dried and coated with a thin gold film to improve the electron conductivity before characterized by this technique.

2.6 Temperature programmed reduction (TPR)

The redox property of the catalyst was studied by temperature programmed reduction with hydrogen (H₂-TPR). The H₂-TPR was performed in a fixed-bed reactor (4-mm inner diameter) equipped with a TCD detector. About 0.10 g of the catalyst was pretreated by heat treatment in order to diminish the contaminants contained in the sample. The temperature of the reactor was gradually increased to 600 °C with a constant heating rate of 10 °C/min under atmosphere of mixed gases Ar and O₂ (80:20, v/v). The total flow rate was 60 cm³/min. After the desired temperature was reached, the system was kept for 2 hours. Then, the reactor was allowed to cool down to 100 °C under Ar ambient. After that, the reduction was performed. The gas mixture of Ar:H₂ (98:2, v/v) was passed through the reactor with the total flow rate of 30 cm³/min. After 30 min, the reactor temperature was increased to 800 °C with a heating rate of 10 °C/min. Simultaneously, the change of hydrogen concentration was identified by a thermal conductivity detector (TCD). The detector was conditioned as

follows. The reference flow of was 2% H₂ in Ar (Ar:H₂ = 98:2, v/v) in the total flow rate 30 cm³/min. The transfer temperature and the block temperature were 90 °C and 120 °C, respectively. The filament temperature was kept constant at 270 °C.

3. Catalytic activity test

3.1 Temperature programmed N₂O decomposition

The reactivity of N₂O decomposition was studied by temperature programmed reaction. This study was performed in fixed bed reactor at standard atmospheric pressure, 1 atm. The tubular flow reactor was connected to the gas flow system and mass spectrometer (MS). The gas flow system consists of the pretreatment gas lines (H₂, O₂, Ar) and reactant gas lines (He, Ar and N₂O). The flow rates of gases were controlled by digital gas flow controller (ALLBOLG). Gas inlet species can be changed by a switching valve. The tubular reactor was the quartz tube with 4 mm inner diameter. The reactor was placed in a vertical furnace (Lenton, CSC 12/110/300V). The furnace temperature was controlled by a temperature controller (Eurotherm). The experimental set-up of the reactor is shown in Figure 2.

About 0.05 g of catalyst sample was introduced in the quartz tube at the middle position. The catalyst bed was placed on a layer of quartz wool. The top of the bed was then covered by quartz chips. A thermocouple was placed at the bottom of the catalyst bed and connected to the temperature controller. The quartz tube reactor was placed in the vertical electric furnace. The sample was pretreated by heat treatment at 600 °C under atmosphere of 10% O₂ in Ar (Ar:O₂ = 90:10, v/v) for 1 hour. The total flow rate was 60 cm³/min. After that, the reactor temperature was allowed to cool down to 550 °C under the same gas flow rate. Then, the gas mixture of 10 % H₂ in Ar (Ar:H₂ = 90:10, v/v) was introduced to the reactor. Total flow rate of this gas mixture was also 60 cm³/min. After an hour, the H₂ gas was switched off and allowed the reactor temperature to cool down to 100 °C under the Ar flow.

The catalytic activity was started by introduced the mixed gas of 5% N₂O and 5 % Ar in He with the total flow rate of 100 cm³/min into the reactor that

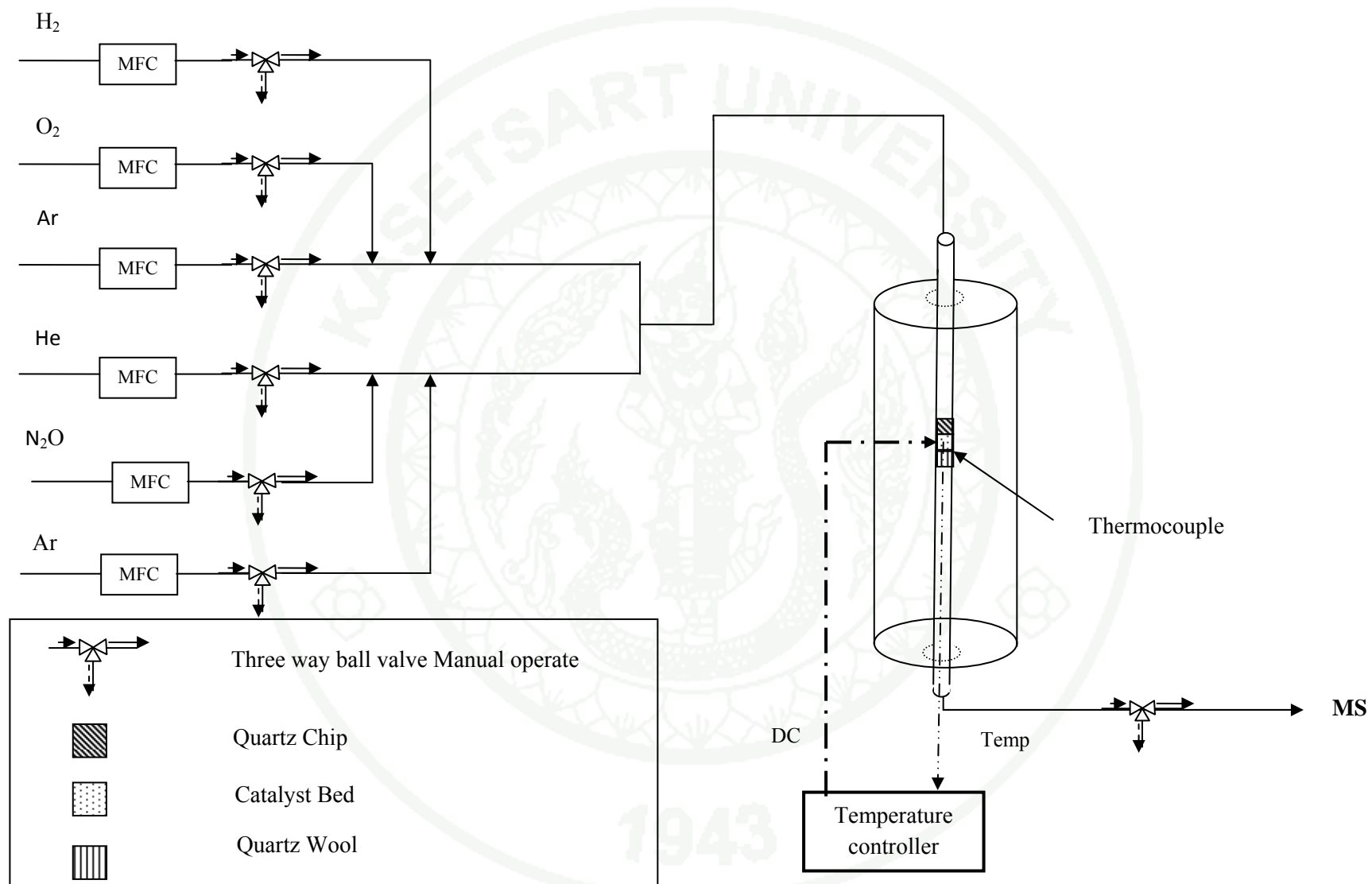


Figure 2 Set up diagram for test the temperature programmed reaction of N_2O decomposition

contained the treated zeolite. The Ar gas was introduced as the internal standard species. Then, reactor was heating with the heating rate 10 °C/min. The effluent gases from the reactor temperature 100°C to about 850°C was analyzed by mass spectrometer (MS). The signal at mass number (m/e) 44, 40, 32, 30, and 28 were collected as the signal of N₂O, Ar, O₂, N₂O and N₂, respectively. The gases concentrations from the reactor effluent were calculated in the basis of Ar signal. The decreasing of N₂O concentration was defined as the catalytic activity of zeolites for N₂O decomposition. The calculation details are presented in Appendix B.

3.2 Temperature programmed reaction for the reaction of N₂O with CH₄

The reducing effect of CH₄ to improve the catalytic decomposition of N₂O over zeolites catalysts were also studied in a fixed bed quartz reactor. The experimental apparatus is set up as for the test of N₂O decomposition in Figure 2. About 0.05 g catalyst was used in each run. Prior to reactivity test, zeolites catalysts were pretreated with the same procedure as for the N₂O decomposition test and cool down to 100 °C in Ar flow. After that, methane was added with 5 % to the flow of 5 % N₂O and 5 % Ar balanced with He in total flow 100 cm³/min. The effluent gases were also detected by MS at m/e= 15, 28, 30, 40 and 44 for CH₄, N₂, N₂O, and Ar, respectively. The gases concentrations in the effluent were all calculated on the basis of Ar signal.

3.3 Catalytic activity of zeolite on reaction of N₂O and CH₄

The product distribution from the reaction of N₂O and CH₄ were also investigated in this study. The catalytic activities at constant temperature were carried out in a tubular fixed bed reactor as Figure 3. The main part of reactor was set up as similar to the N₂O decomposition measurement (Figure 2). A minor modification was applied at the out let part because the products from this reaction can be higher molecular weight species which can be condensed to liquid phase before reach the analyzer. Therefore, the outlet line was wrapped with the heating tapes to kept temperature above 100 °C.

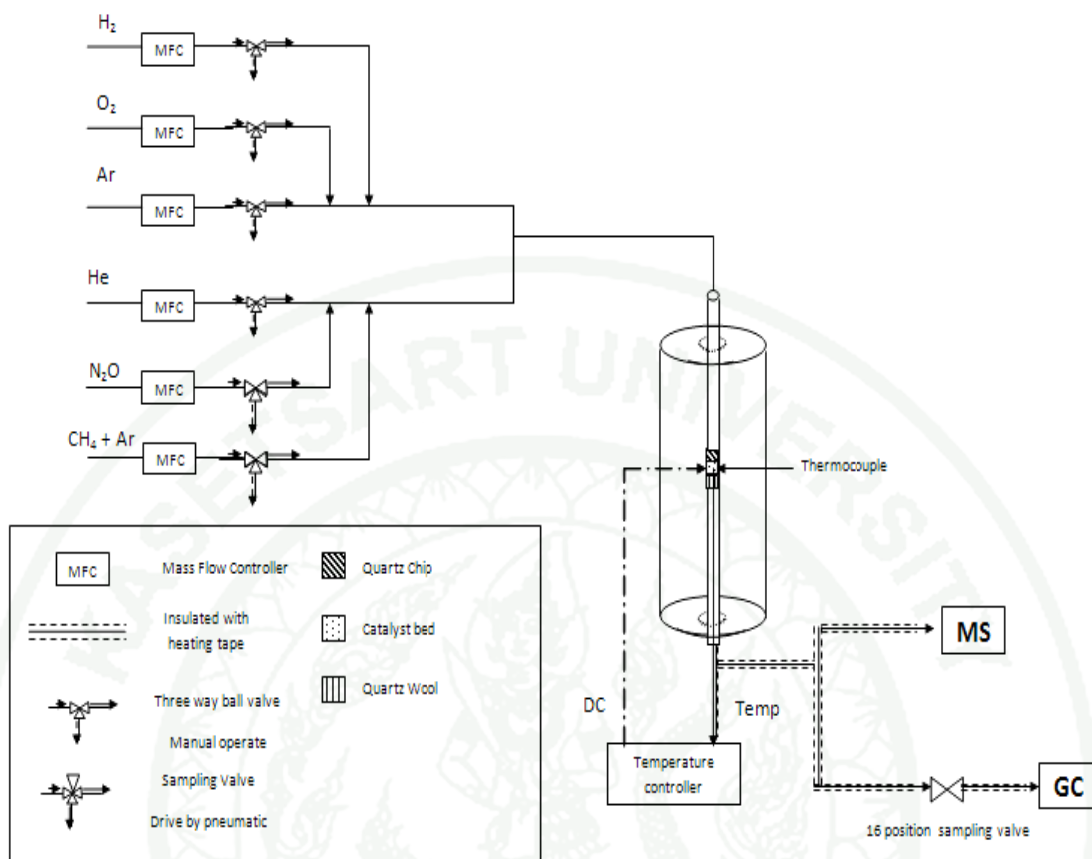


Figure 3 Set up diagram for test the reaction of N_2O with CH_4 or C_2H_6

The catalytic activity of each sample was started by pretreatment 0.100 g zeolite (240-425 μm) with 10 % O_2 in Ar (total flow 60 cm^3/min) at 600 $^\circ\text{C}$ for 2 hour following by treated with 10 % H_2 in Ar (total flow 60 cm^3/min) at 550 $^\circ\text{C}$ for 1 hour as will defined as the conventional pretreatment. After that, the treated catalyst was cooling down to 500 $^\circ\text{C}$ and kept catalysts under He 50 cm^3/min . for 30 min. The reaction studies were started by replacing He gas with the mixing of 2.5 % N_2O , 5 % CH_4 and 5 % Ar with He balance ($\text{N}_2\text{O}:\text{CH}_4:\text{Ar}:\text{He} = 2.5:5:5:87.5$, v/v/v/v) within the total flow rate of 50 cm^3/min into the reactor. The effluent gases were simultaneously characterized by MS. The MS detected the signals at mass numbers 15, 18, 28, 30, 32, 40, 44, 78, 91, 106. Signal at $m/e=40$ corresponds to the composition of Ar which was used as a reference (internal standard) for quantitative characterization.

In the same time, about 1 cm^3 of the sample was collected at specific time by multi-position looping valves for further gas chromatography (GC)

characterization. A GC (Trace GC) with a flame ionization detector (FID) was used here. The sample was injected to HayeSep® D column (100/120 10 ft x 1/8" OD). The experimental condition for GC experiment is given in Table 1. The first peak from GC is the reference signal of CH₄ for quantitative characterization. Amount of the products is determined by the calculation shown in Appendix B.

Table 1 The condition of GC (FID) for characterize the product composition from the reaction of CH₄ and N₂O

Parameter	Set value
Carrier gas, He	30 cm ³ /min
H ₂	40 cm ³ /min
Air	450 cm ³ /min
Block temperature	250 °C
Gas inlet temperature	150 °C
Oven temperature	Programmed between 80-260 °C
	Details:
	1) Keep the temperature at 80 °C for 1.5 min
	2) Increase the temperature to 260 °C at the heating rate of 20 °C/min
	3) Keep the temperature at 260 °C for 17.5 min

3.4 Catalytic activity on the oxidative dehydrogenation of ethane

Ethylene (C₂H₄) production via the oxidative dehydrogenation reaction was studied over petrochemical zeolites catalyst. Previous study (Perez-Ramirez and Gallardo-Llamas, 2004; Sun *et al.*, 2008) showed that nitrous oxide is an effective oxidant. For this reason, nitrous oxide was chosen to be oxidative reagent in this study. For the reactivity test, the catalyst was first activated by steam pretreatment for 2 hours. After that, it was oxidized and reduced before flushed with He gas at 500 °C.

Generally, reactant gas was a mixture of 3.0% N₂O, 3.0% C₂H₆ in He (He:N₂O:C₂H₆ = 94:3:3, v/v/v). This ratio was varied when optimized the reactant gas ratio. The total flow rate was 100 cm³/min. The gas product obtained after the reactant passed through the catalyst bed at 500 °C was characterized by GC with TCD detector. About 1 cm³ of gas product was injected to HayeSep® D (100/120 10 ft x 1/8" OD) in GC detector. The GC condition was set as Table 1, except oven temperature. The oven temperature was programmed between 40-260 °C, to improving the resolution between N₂ and CO.

4. Computational study

4.1 Fe-zeolites for N₂O decomposition

The structures of the zeolite clusters were obtained from the crystal structures of ZSM-5 (van Koningsveld *et al.*, 1987), FER (Morris *et al.*, 1994), BEA (Newsam *et al.*, 1988) and FAU (Olson *et al.*, 1969) zeolites, represented by clusters of 144T, 114T, 176T and 84T, respectively (T = tetrahedral Si or Al atom). The iron cation [FeO]⁺ was exchanged or replaced at the highly accessible Brønsted acid site of each zeolite.

The validations of models were test on Fe-ZSM-5. It was modeled by 5T, 96T, 128T and 144T framework structures. The smallest zeolites model, 5T cluster, consists of 4 Si-atoms, 1 Al-atom, 4 O-atoms, and terminated the dragging bond with 12 H-atoms (Si₄AlO₄H₁₂). All atoms in this model were optimized with the DFT methods. For 96T, 128T and 144T were used ONIOM method by treated 12T cluster cover the active center with DFT methods and treated the rest with UFF force field. Only 5T atoms around active region were relaxed, while the rest were fixed at their crystalline position. All atoms were treated with 6-31G** basis set, except Fe which was treated by Effective Core Potential (ECP) of Stuttgart. The system was considered at sextet state.

The 144T cluster of Fe-ZSM-5 covers the channel intersection cavity, the straight pore channel and the zigzag pore channel. A silicon atom was substituted with

an aluminum atom at the most favorable position (T12) and the iron cation was exchanged with an acidic proton (Figure 4). The 114T cluster of Fe-FER comprises

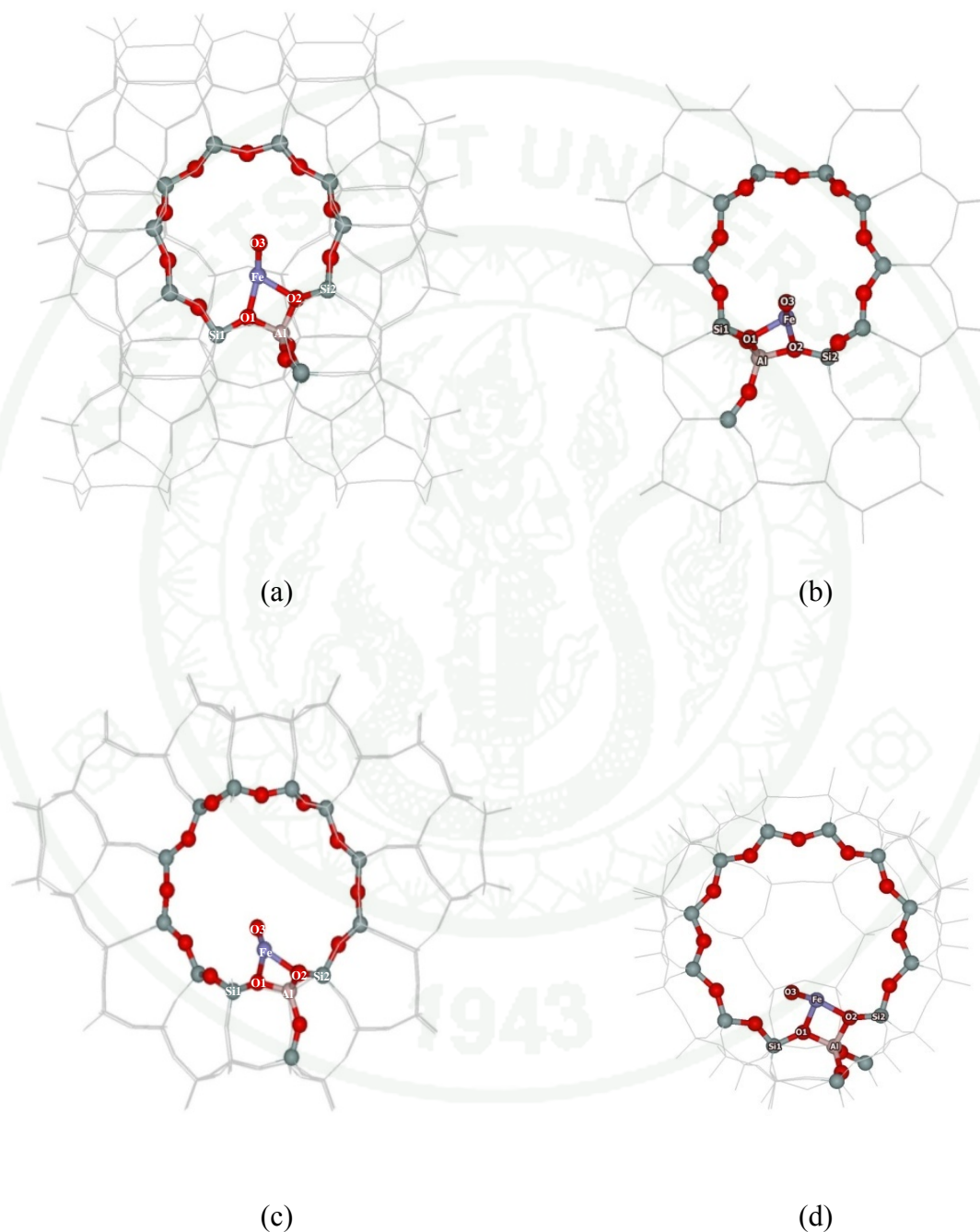


Figure 4 ONIOM model of nitrous dioxide on the Fe-Zeolite: (a) Fe-ZSM-5 12T/144T, (b) Fe-FER 12T/114T, (c) Fe-BEA 14T/176T and (d) Fe-FAU 14T/84T

the three different channels (10T-membered channel, 8T-membered cage, and 6T-membered channel). The ion exchange site is located, with similar arguments as above, at the T2 position in the 10T straight channel. The 176T cluster of the Fe-BEA includes the main gateway intersection of two perpendicular 12-membered channels. The ion exchange site is located at the T1 position on the 12-membered ring. The 84T cluster of the Fe-FAU represents the two connecting supercage structures of the faujasite zeolite. The active site is placed at site III on the 12T-membered ring window of the supercage.

The two layer of ONIOM model, called ONIOM2, which has previously been successfully employed, was adopted for computational efficiency (Jansang et al., 2006; Namuangruk et al., 2006; Namuangruk et al., 2005; Pantu et al., 2004; Kasuriya et al., 2003; Namuangruk et al., 2004). The clusters were divided into 2 regions: the inner active region was treated with the quantum mechanical density functional approach (here at the B3LYP/6-31G (d,p) level). The iron atom was treated with the energy-consistent pseudo-potential (ECP) of Stuttgart and Born (Stuttgart RSC 1997 ECP). The total spin of the system was kept constant at the sextet state throughout all calculations. The energies for the surrounding region were computed with the much simpler Universal Force Field (UFF). During the structure optimization, only the 5T portion of the active site region and the adsorbates were allowed to relax while the rest was fixed at the crystallographic coordinates. Normal mode analyses were carried out to verify that the transition states had only one imaginary frequency whose mode corresponds to the designated reaction. All calculations have been performed using the Gaussian 03 code (Gaussian, Inc., Pittsburgh).

Above methodology was applied to optimize all proposed reaction geometry following the reaction mechanism of N₂O decomposition. The mechanism of N₂O decomposition over single exchange metal iron over zeolites framework was proposed as Figure 5. The initial active site is metal oxo species which reported as the active sites for isolated Fe monodentate in ZSM-5 (Heyden *et al.*, 2005). The similar initial iron oxo species ([FeO]⁺) was placed at the exchanged position described above

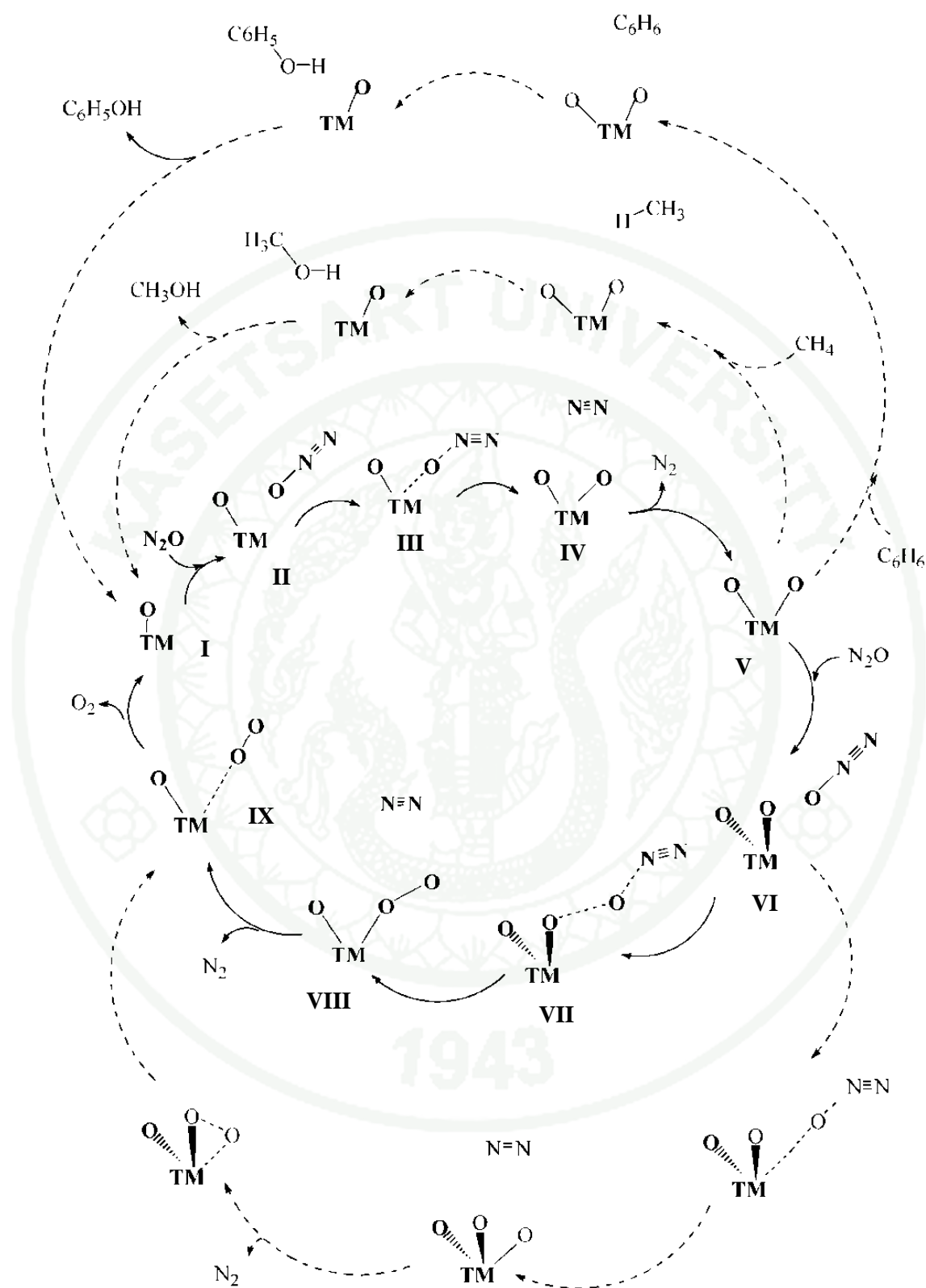


Figure 5 The proposed mechanism for N_2O decompositions over TM-ZSM-5 (TM= Fe, Co, Ni).

in all zeolites framework as showing at step 1 in the Figure 5. The next step was the coming N_2O adsorbed through its O-end to the $([\text{FeO}]^+)$ site in catalyst framework. This adsorbing N_2O was decomposed through the transition state structure at step 3 in Figure 5, which had only one imaginary frequency. Then this complex was changed to be the N_2 molecule adsorbed on iron dioxo species ($([\text{OFeO}]^+)$) as shown in step 4 in the Figure 5. After N_2 was desorbed, this produced iron dioxo species was the active species for many reactions, e.g., partial oxidation of CH_4 to CH_3OH or oxidation of C_6H_6 to $\text{C}_6\text{H}_5\text{OH}$ as showing as dot line arrows in the upper part of Figure 5. However, only the reactivity to produce this extremely active site will be investigated in this study. The activity in different zeolite framework will be compared in terms of energy and geometric parameters.

4.2 TM-ZSM-5 for N_2O decomposition

Transition metal (TM) ion exchanged zeolites show the different in catalytic reactivity in N_2O decomposition reaction. The affect of TM species on the N_2O decomposition was investigated over TM-ZSM-5. The TM (Fe, Co, or Ni) ion was replaced at the same position of substituted Fe as mention above. The structure of ZSM-5 was modeled with 96T cluster, since it big enough to represent this reaction which concerned only small probing species. The two layer of ONIOM model were also applied to optimize the proposed structures. The 12T active region was treated with new density function theory, M06 (6-31G (d,p) level). This density functional has been proven to give the reasonable structure and energy within smaller computational effort than B3LYP method in many systems (Zhao and Truhlar, 2008). The Fe, Co and Ni atom were treated with the ECP of Stuttgart and Born. The total spin of the systems were kept constant at high spin as sextet, quintet, and quartet for Fe-ZSM-5, Co-ZSM-5, and Ni-ZSM-5, respectively. During optimization, the probing atom, TM atom, O atom in TM-O structure, and 5T around TM atom was relaxed while the rest was fixed at the crystal position.

The reaction cycle of N_2O decomposition over TM-ZSM-5 were proposed through the 9 elementary steps as shown in Figure 5. The initial catalyst

structures for N_2O decomposition in this studied were TM-O/ZSM-5. The first elementary step was the first N_2O molecule came to adsorb over the active site (metal oxo species). The second step was decomposed the adsorbed N_2O through a transition state geometry and produced a metal dioxo species with adsorbed N_2 . This generated N_2 was then desorbed. After that, the second N_2O molecule came to adsorb over the metal dioxo site as step 6 in Figure 5. The adsorbed N_2O molecule decomposed again through the second transition state geometry and then forms the second N_2 molecule and 3 O-atoms bound to TM atom. Finally, 2 O-atoms were desorbed in the form of O_2 molecule and the starting active oxo species was regenerated. Moreover, the second adsorbed N_2O can decomposed through the another transition geometry as the dot line arrows in the lower part of Figure 5. This reaction mechanism was applied to all metal species to make the comparable reaction structures. The activities of each TM will compared in terms of structure and energy.

The produced dioxo iron by the decomposition of the first N_2O over Fe-O species is the reactive species for selective oxidation of hydrocarbon (Panov *et al.*, 1998; Kuchеров *et al.*, 2002; Wood *et al.*, 2004b; Parmon *et al.*, 2005). Methane and benzene can be oxidized to methanol and phenol following the dot arrow cycles presented in the upper part of figure 5. Finally, the produced CH_3OH or $\text{C}_6\text{H}_5\text{OH}$ is eliminated from the catalyst and produces the oxo iron species. The active species, dioxo iron, will regenerate by the decomposition of new N_2O over oxo iron following the line arrows through species 1 to 5 in figure 5.

1943

RESULTS AND DISCUSSIONS

In this work, the catalytic properties of transition metals in zeolite catalysts were studied. The reactivities of iron (Fe), cobalt (Co), copper (Cu) in zeolites were studied for nitrous oxide decomposition, methane conversion, and ethane oxidative dehydrogenation.

Characterization of Catalysts

1. Acidic Zeolites

Zeolite samples were obtained from Al-Si-Penta Zeolite GmbH and Zeolysts International. The commercial samples were obtained in either H-form or NH_4^+ -form. They were calcined in air at 550 °C before being used. Sample names, notations and properties are listed in Table 2. The zeolite samples were named by the framework type and the silica to alumina molar ratio ($\text{SiO}_2/\text{Al}_2\text{O}_3$) in parenthesis.

The chemical compositions of zeolite samples were characterized by the ICP-AES elemental analyzer. The $\text{SiO}_2/\text{Al}_2\text{O}_3$ ratios obtained from XRF analysis are agreement with those reported by the producers. Most of zeolite samples have Si/Al ratio in a range of 15 to 32 except for the Y(6) sample with a Si/Al ratio of 6. The USY zeolite is the ultrastable form prepared by dealumination the Y zeolite which increases the $\text{SiO}_2/\text{Al}_2\text{O}_3$ ratio to 32.

All zeolite samples contain a trace amount of iron (Fe) in a range of 100-500 ppm. The Fe content in zeolites can also be presented in term of Fe to Al molar ratio (Fe/Al), which is in a range of 0.004-0.011. It is noted that the ZSM-5(25) sample has the highest amount Fe content of 502 ppm and the zeolite Y(6) and USY(32) have a very low Fe content of 123 and 156 ppm, respectively. Because of the low content of iron, the iron species in all these samples are presumably to be highly dispersed.

1.1 Ion-exchanged zeolites

The amount of metal content in the ion exchanged zeolite is indicated in the sample name by adding a prefix indicating the metal type and the amount in ppm in parenthesis. Iron contents found in samples of ion-exchanged zeolites are listed in Table 3.

Table 2 Physicochemical characteristics commercial zeolites used in this study

Sample	Code ^a	Crystal structure	SiO ₂ / Al ₂ O ₃ ^d	Fe Contents (ppm)	Fe/Al ^e
BEA(26)	CP814E ^b	Ammonium-Beta (BEA)	26.5	293	0.004
BEA(51)	CP814Q ^b	Ammonium-Beta (BEA)	51.3	237	0.007
FER(20)	CP914C ^b	Ammonium ferrierite (FER)	19.5	299	0.004
MOR(15)	MSM-15 ^c	Mordenite (MOR)	15.2	411	0.004
USY(32)	CBV720 ^b	H-SDUSY(FUA)	32.5	156	0.001
Y(6)	CBV400 ^b	HY (FUA)	6.6	123	0.002
ZSM-5(25)	SH27 ^c	Pentasil (MFI)	25.4	502	0.007
ZSM-5(42)	SH55 ^c	Pentasil (MFI)	42.3	472	0.011

^a Commercial code name

^b zeolites from Zeolysts International

^c zeolites from Al-Si-Penta Zeolite GmbH

^d the value from XRF

^e the value from ICP-AES

By varying concentrations of metal ion in solutions, the ion-exchange degree (Fe/Al) can be obtained from 0.013 to 0.438. It is also noted that for small and medium pore zeolite (FER and ZSM-5) the obtained ion-exchange degrees are quite low (less than 0.1). This is due to the limiting pore dimension and the use of acidic iron solution. The iron solutions were prepared at a pH=1.0 to prevent the precipitation of iron hydroxide.

Table 3 Metal content in modified zeolites by FeCl₂ ion exchange characterized by ICP-AES

Zeolites	Fe concentration (ppm)	Fe/Al
Fe(598)BEA(26)	598	0.013
Fe(954)BEA(26)	954	0.017
Fe(1,861)BEA(26)	1,861	0.038
Fe(6,358)BEA(26)	6,358	0.108
Fe(9,639)BEA(26)	9,639	0.170
Fe(10,734)BEA(26)	10,734	0.189
Fe(14,787)BEA(26)	14,787	0.265
Fe(7,143)BEA(51)	7,143	0.212
Fe(10,387)BEA(51)	10,387	0.438
Fe(667)FER(20)	667	0.009
Fe(8,592)MOR(15)	8,592	0.085
Fe(6,382)USY(32)	6,382	0.173
Fe(7,143)USY(32)	7,143	0.212
Fe(10,230)Y(6)	10,230	0.051
Fe(11,293)Y(6)	11,293	0.061
Fe(5,241)ZSM-5(25)	5,241	0.081
Fe(502)ZSM-5(42)	502	0.012
Fe(739)ZSM-5(42)	739	0.019

Co and Cu were also exchanged on samples of zeolite BEA and ZSM-5. The obtained metal contents are listed in Table 4. The TM/Al ratio in exchange samples were about 0.15-0.25.

Table 4 Transition metal content in the zeolites exchanged with 0.10 M of transition metal in aqueous solution for 30 min that characterized by ICP-AES

Sample	Metal content in zeolites		TM/Al	Fe/Al
	Fe (%)	TM (%)		
Co(17,487)BEA(26)	0.0322	1.7487	0.257	0.005
Cu(16,500)BEA(26)	0.0220	0.8878	0.150	0.003
Co(11,584)ZSM-5(25)	0.0500	1.1584	0.161	0.007
Cu(15,878)ZSM-5(25)	0.0492	1.5878	0.217	0.007

1.2 XRD patterns of zeolites

The zeolite framework species were confirmed by the XRD patterns as shown in Figure 6. The number and peak position of each zeolites similar to the XRD pattern of the standard zeolites (<http://izasc.ethz.ch/fmi/xsl/IZA-SC/xrd.xsl>). However, the XRD peak of BEA(26) and BEA(51) are very broad peak that can be the effect of the small particle size of these samples. The ZSM-5(25) and ZSM-5(42) samples have sharp peaks and the peak position and shapes do not change significantly after steam treatment (Figure 7). It is indicated that the steam treatment for 2-4 hours has no significant effect on the structure and crystallinity of ZSM-5.

1.3 N₂ adsorption/desorption isotherm

Surface area and porosity of zeolite catalysts were characterized by the N₂ adsorption/desorption isotherms. The adsorption isotherms of the zeolite samples are shown in Figure 8. The adsorption quantity in all adsorption isotherms rise sharply and reach a plateau at low relative pressure (P/P_0) that corresponding to a Type I of IUPAC isotherm. This narrow range of P/P_0 to attain the plateau is an indication of a limited range of pore size of the micro porous materials. The isotherm of USY(30) shows a hysteresis loop at $P/P_0 > 0.4$ indicating that this sample contains pore in the range of mesopore. The specific surface area and pore volumes of nitrogen adsorption are presented in Table 5.

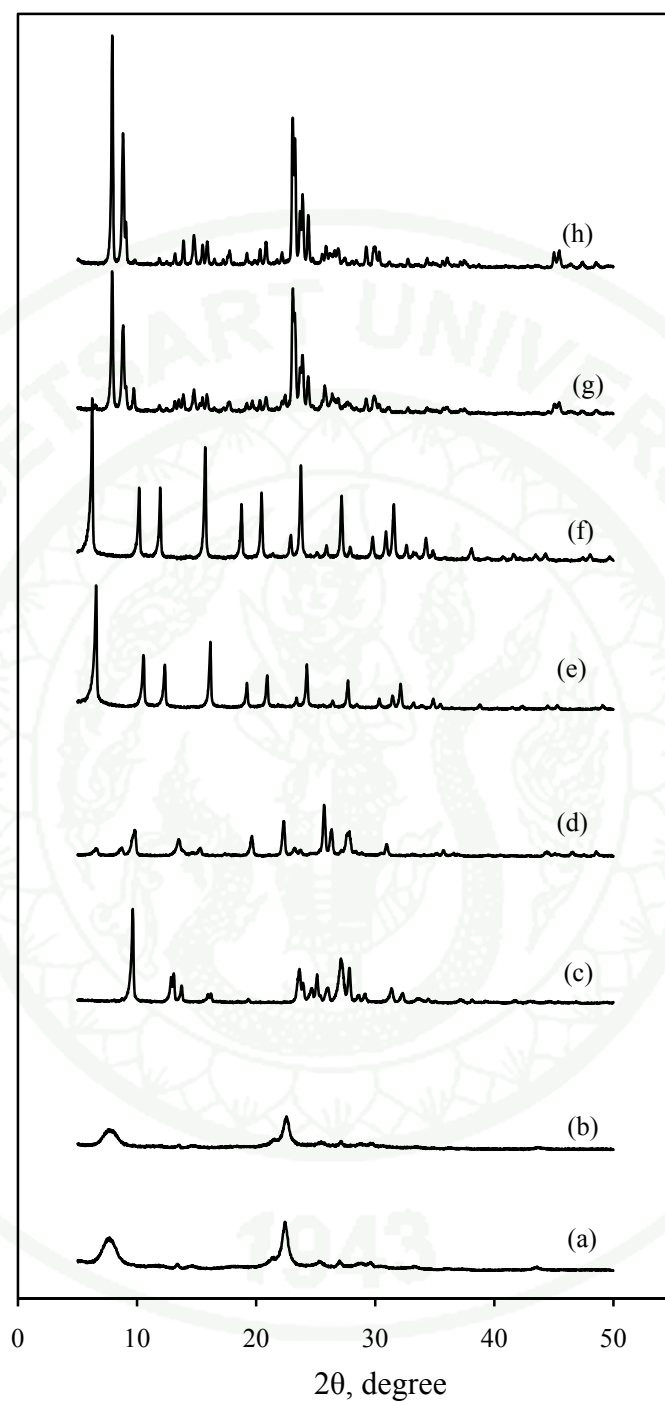


Figure 6 XRD patterns of the commercial zeolites (a) BEA(26), (b) BEA(51) (c) FER(20), (d) MOR(15), (e) USY(30), (f) Y(6), (g) ZSM-5(25) and (h) ZSM-5(42)

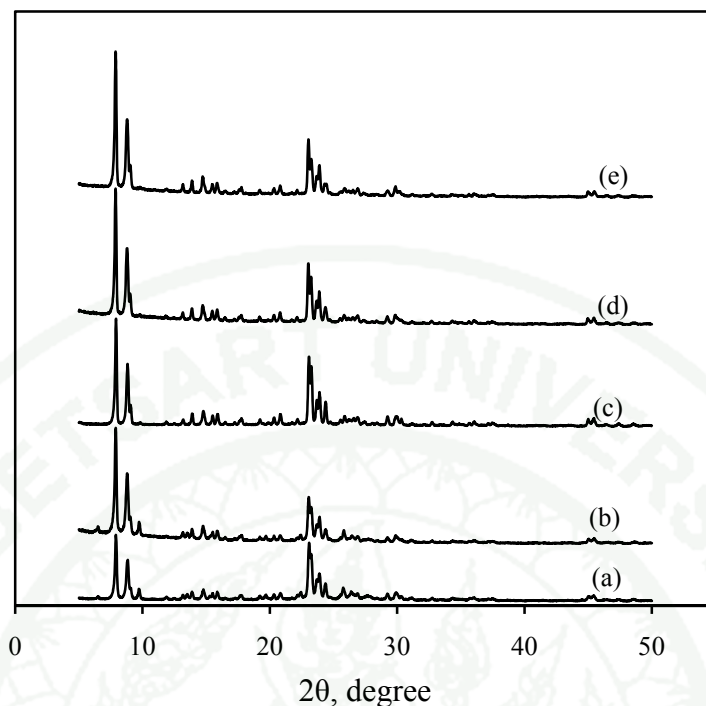


Figure 7 XRD patterns of the ZSM-5 zeolites (a) ZSM-5(25), (b) ZSM-5(25) st2h, (c) ZSM-5(42), (d) ZSM-5(42) st2h and (e) ZSM-5(42) st4h

The BEA(26), BEA(51), Y(6), and USY(30) have high BET surface areas in a range of 700-900 m²/g. The USY(30) sample also have highest amount of external surface area (244 m²/g). On the other hand Y(6) has small external surface area of 63 m²/g. BEA(26) and BEA(51) have similar isotherm and micropore quantity. The specific surface area of ZSM-5 and FER are around 360-400 m²/g. The ratios of micropore to the total surface area of every sample are ranging from 65 to 90%. The high external surface area in some zeolites samples may be a result of the small crystal size and/or the presence of mesopore and macropore.

The surface area and porosity of the transition metal ion exchanged zeolites shown in Table 6 are in the range with the starting zeolites. It indicates that pore blockage does not happen in the modified zeolites.

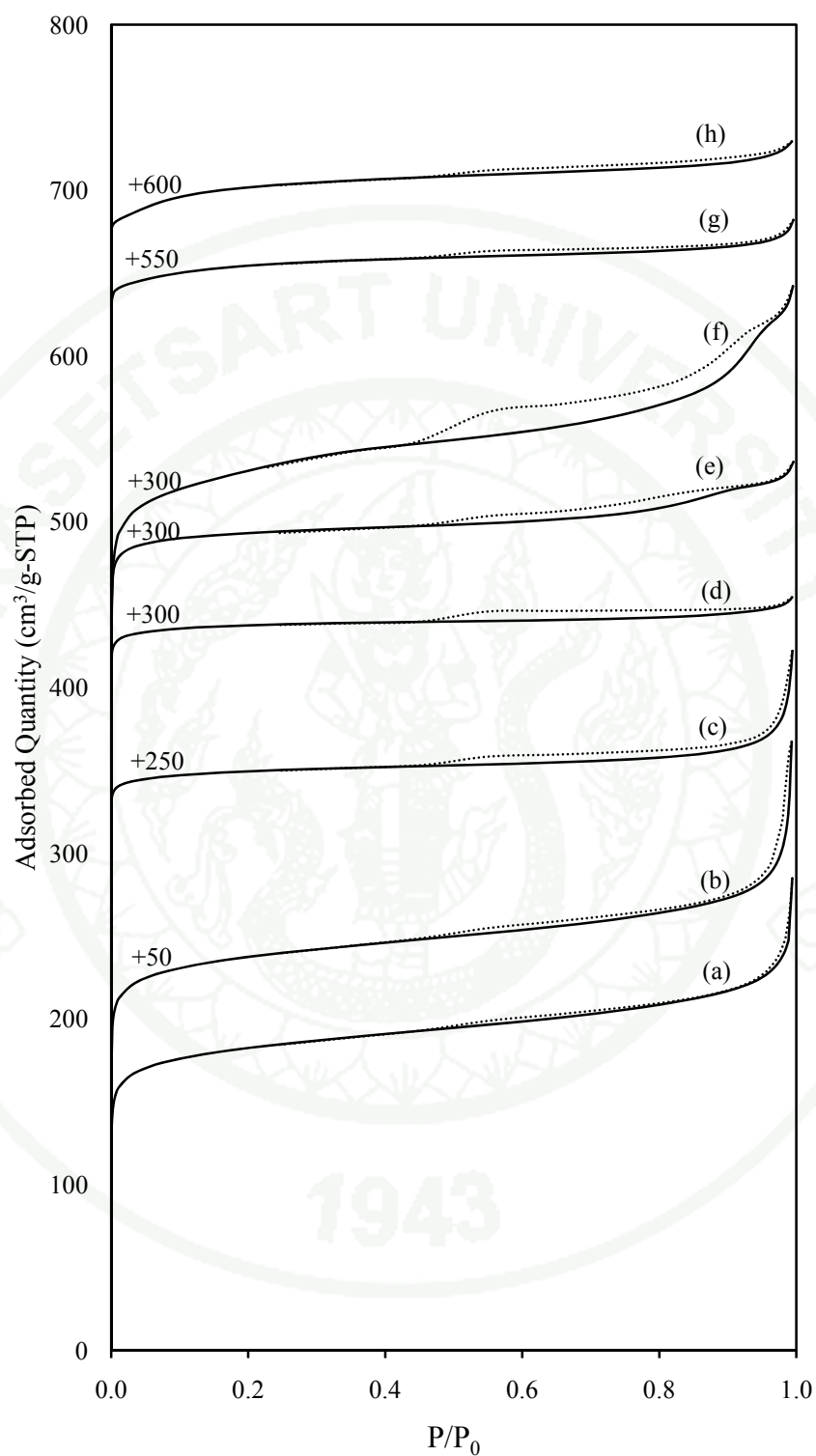


Figure 8 N_2 adsorption isotherms (—) and desorption isotherms (.....) of commercial zeolites: (a) ZSM-5(25), (b) ZSM-5(42), (c) BEA(26), (d) BEA(51), (e) Y(6), (f) USY(30), (g) FER(20), and (h) MOR(15)

Table 5 Surface area and porosity of commercial zeolites

Sample	$S_{\text{BET}}^{\text{a}}$ (m^2/g)	$S_{\text{micro}}^{\text{b}}$ (m^2/g)	$S_{\text{ext}}^{\text{c}}$ (m^2/g)	$V_{\text{total}}^{\text{d}}$ (cm^3/g)	$V_{\text{micro}}^{\text{e}}$ (cm^3/g)
BEA(26)	680	544	136	0.36	0.21
BEA(51)	696	562	134	0.36	0.22
FER(20)	378	338	40	0.18	0.13
MOR(15)	557	517	40	0.23	0.19
Y(6)	770	707	63	0.49	0.27
USY(30)	867	623	244	0.35	0.25
ZSM-5(25)	395	304	91	0.18	0.12
ZSM-5(42)	361	274	87	0.17	0.11

^a Surface area by BET method^b micropore surface area by *t*-plot method^c external surface area by *t*-plot method^d total pore volume at $P/P_0=0.99$ ^e micropore volume by *t*-plot method**Table 6** Surface area and porosity of transition metal exchanged zeolites

Sample	$S_{\text{BET}}^{\text{a}}$ (m^2/g)	$S_{\text{micro}}^{\text{b}}$ (m^2/g)	$S_{\text{ext}}^{\text{c}}$ (m^2/g)	$V_{\text{total}}^{\text{d}}$ (cm^3/g)	$V_{\text{micro}}^{\text{e}}$ (cm^3/g)
Fe(5,241) ZSM-5(25)	398	308	90	0.19	0.12
Fe(739) ZSM-5(42)	364	227	97	0.17	0.11
Fe(10,734) BEA(26)	650	410	240	0.56	0.17
Fe(1,861) BEA(26)	612	381	230	0.54	0.17
Fe(598) BEA(26)	616	411	205	0.53	0.16
Fe(7,143) BEA(51)	657	535	122	0.33	0.22
Fe(11,293) Y(6)	779	707	72	0.36	0.27
Fe(7,143) Y(30)	881	620	261	0.50	0.25
Fe(667) FER(20)	386	342	44	0.18	0.13
Fe(8,592) MOR(15)	531	503	28	0.21	0.19
Co(17,487) BEA(26)	634	419	215	0.54	0.17
Cu(16,500) BEA(26)	623	380	243	0.69	0.16
Co(11,584) ZSM-5(25)	390	301	89	0.19	0.12
Cu(15,878) ZSM-5(25)	389	301	88	0.19	0.12

^a Surface area by BET method^b micropore surface area by *t*-plot method^c external surface area by *t*-plot method^d total pore volume at $P/P_0=0.99$ ^e micropore volume by *t*-plot method

The isotherms of steam treated ZSM-5 were shown in Figure 9. The isotherms show the micropore character and hysteresis loop which indicates the presence of mesopore. The results in Table 7 are show that, when applied the steam treatment, the external surface area of ZSM-5 zeolites are increased while the micro-pore surface area and micropore volume are decreased. This result is similar to the report by Perez-Ramirez and coworker that a small fraction of micropores are converted to mesopores due to the extraction of framework Al to extra framework position (Perez-Ramirez *et. al.* 2003). They support this postulation with the results of MAS-NMR which found the decreasing of tetrahedrally coordinated Al in zeolite framework concentration in the steamed ZSM-5. Simultaneously, with the appearance of hexacoordinate Al in octahedral position and petacoordinated Al species in non framework position after treated ZSM-5 with steam.

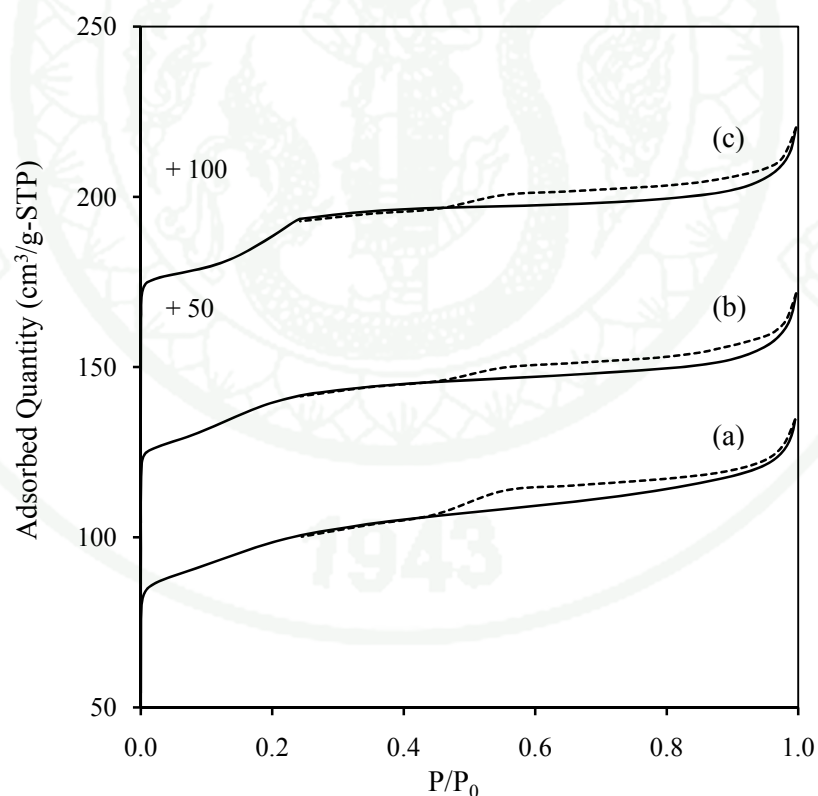


Figure 9 N₂ sorption isotherm over steam treatment zeolites: ZSM-5(25) st2h (a), ZSM-5(42) st2h (b), ZSM-5(42) st4h (c)

Table 7 Surface area and porosity of steam treatment zeolites

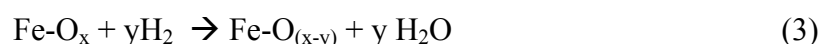
Sample	$S_{\text{BET}}^{\text{a}}$ (m^2/g)	$S_{\text{micro}}^{\text{b}}$ (m^2/g)	$S_{\text{ext}}^{\text{c}}$ (m^2/g)	$V_{\text{total}}^{\text{d}}$ (cm^3/g)	$V_{\text{micro}}^{\text{e}}$ (cm^3/g)
ZSM-5(25) st2h	366	225	141	0.19	0.09
ZSM-5(42) st2h	325	163	162	0.16	0.07
ZSM-5(42) st4h	323	117	206	0.16	0.04
BEA(26) st2h	542	357	185	0.52	0.15
FER(20) st2h	390	335	55	0.18	0.13

^a Surface area by BET method^b micropore surface area by *t*-plot method^c external surface area by *t*-plot method^d total pore volume at $P/P_0=0.99$ ^e micropore volume by *t*-plot method

The external surface area of BEA zeolite is also increased after pretreatment in 30% steam at 650 °C for 2h. However, for the FER zeolite, the external surface area did not change after the steam treatment. This result is in agreement with the work of Peixoto *et al.* that the steam treatment did not affect the textural properties of FER zeolite (Peixoto *et al.*, 2003). Moreover, the studied about the framework stability of Fe-FER for N₂O decomposition under the water contaminated system also shown that, FER matrix is much more stable in the presence of water for more than 50 h (Melian-Cabrera *et al.*, 2005).

1.4 Temperature program reduction (TPR)

The H₂-TPR of commercial zeolites are shown in Figure 10. The TPR measurements showed the main region of hydrogen consumption between 400-600 °C due to the reduction of trace amount of metal present in the samples. The reduction process can be simplified as equation 3:



The Fe in zeolite can be reduced at lower temperature than the reduction temperature of cluster FeO_x at 630 °C (Melian-Cabrera *et al.*, 2006). Figure 11 shows the results of temperature programmed reduction on the Fe-exchange zeolites.

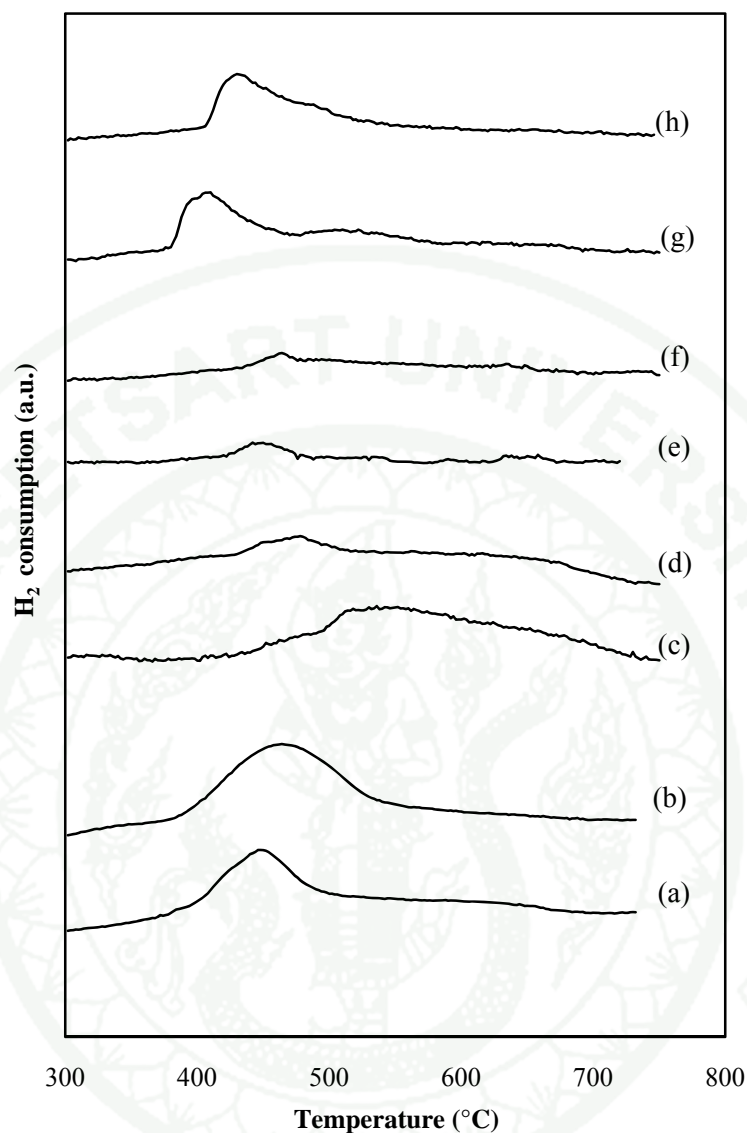


Figure 10 H₂-TPR profile of 2 vol.% H₂ in Ar (total flow 30 cm³/min) and heating rate 10 °C /min over commercial zeolites: (a) BEA(26), (b) BEA(51), (c) FER(20), (d) MOR(15), (e) USY(30), (f) Y(6), (g) ZSM-5(25), and (h) ZSM-5(42)

The TPR spectra of Fe-exchange zeolites in Figure 11 also shows reduction peak in region of 400-500 °C similar to the TPR of their starting samples. This result indicates that the Fe-exchange samples generally have a good metal dispersion. The TPR are similar to the TPR profiles reported by Lobree and coworker

that reported about the samples with a low Fe cations exchange (e.g. $\text{Fe}/\text{Al} \leq 0.56$) with had high dispersion of metal (Lobree *et al.*, 1999).

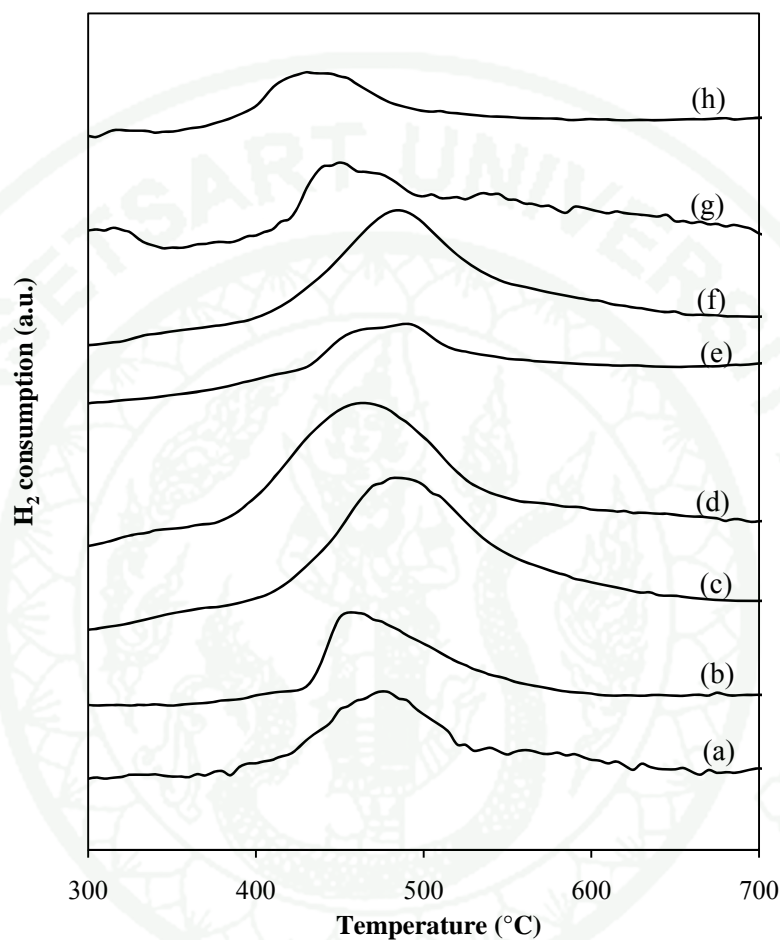


Figure 11 H₂-TPR profile of Fe zeolites (a) Fe(5,241) ZSM-5(25), (b) Fe(739) ZSM-5(48), (c) Fe(10,734) BEA(26), (d) Fe(7,143) BEA(52), (e) Fe(11,293) Y(6), (f) Fe(7,143) USY(32), (g) Fe(667) FER(20), and (h) Fe(8,592) MOR(15)

It can be observed that TPR of Fe-exchanged Y and USY zeolites which originally have very low Fe content shows reduction peaks at about 500°C. These reduction peaks suggest that iron clusters in these samples may be larger than those in others zeolites.

1.5 SEM

Visualizations of the samples morphology was done by SEM. Figure 12 show the surface characteristic of ZSM-5(25) before (a) and after (b) steam treatment from SEM instrument. It is showing the crystal sizes of zeolites before steam treatment are around 1-2 μm . After steam treatment, the zeolite crystals are broken into smaller size. This is correlated to the external surface quantity which increasing in the external surface area.

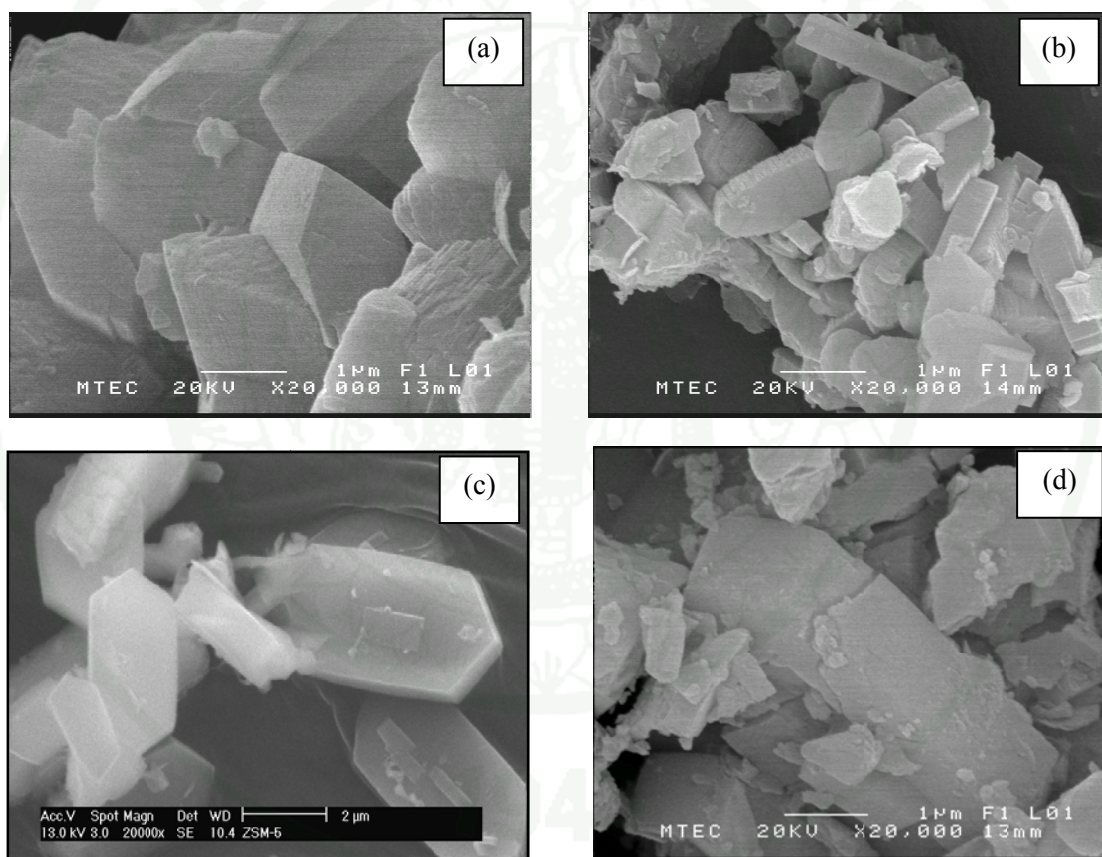


Figure 12 Morphology of starting (a) ZSM-5(25) and (c) ZSM-5(42) and the morphology after steam treatment for 2 h of (b) ZSM-5(25) and (d) ZSM-5(42) characterized by SEM

Nitrous oxide decomposition over zeolite catalysts

The reactivity of zeolites on N_2O decomposition were studied by temperature programmed reaction. The reaction feed of 5% N_2O at $100 \text{ cm}^3/\text{min}$ was passed through 0.05 g of zeolite sample in a fixed bed reactor. The thermal decomposition of N_2O was carried out through the same fixed bed reactor but was packed with the inert quartz chips.

1. Temperature programmed reaction of nitrous oxide decomposition over different zeolite framework

In the blank run, N_2O decomposition was carried out in a reactor packed with the 0.05 g inert quartz chips (particle size 250-425 μm). The reaction profile is shown in Figure 13. The result shows that the thermal decomposition of N_2O occurs above 750 $^\circ\text{C}$.

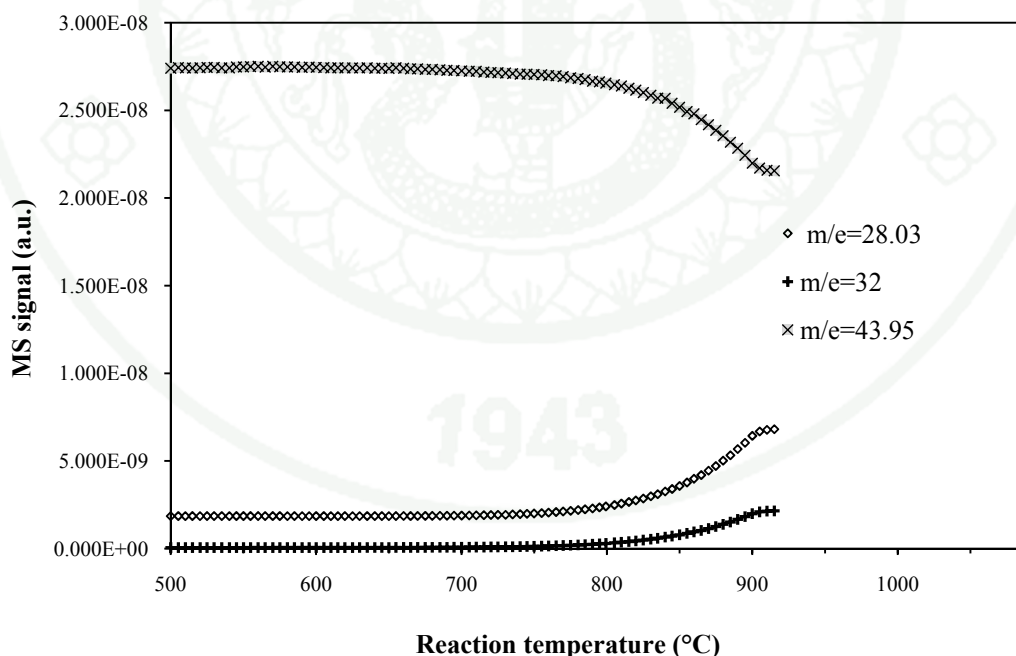


Figure 13 Reaction profile of N_2O decomposition in the reactor packed with quartz chips. Signal at $m/e=28.03$, 32 and 43.95 are corresponding to N_2 , O_2 , and N_2O , respectively.

When the reactor was packed with about 0.05 g of FER(55) sample, the N_2O decomposition took place at temperature about 500 °C. The reaction profile as is shown in Figure 14. The MS signals of N_2 and O_2 are simultaneously increased when N_2O was consumed indicating that N_2O was decomposed to N_2 and O_2 . Over this sample, N_2O was completely consumed at approximately 700 °C which lower than the temperature for N_2O thermal decomposition to start.

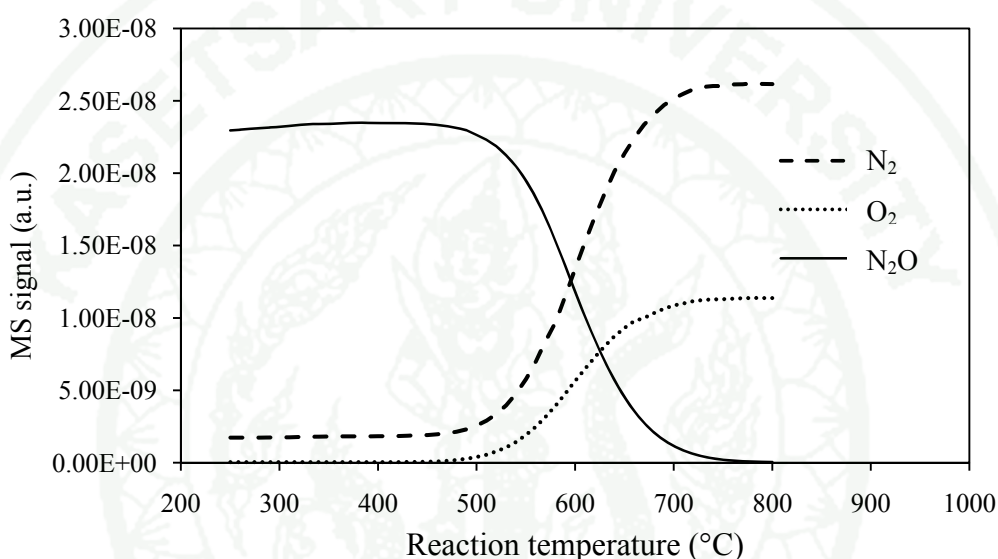


Figure 14 MS signal profiles of N_2O decomposition over FER(55) [N_2 (---), O_2 (.....) and N_2O (—)].

The temperature programmed catalytic decomposition of N_2O over zeolite samples were tested. The N_2O conversions over various samples were plotted against temperature in Figure 15. To compare activities of zeolite samples, we define an on-set temperature as a temperature that 10% N_2O is consumed. The on-set temperatures are at 470, 505, 520, 550, 550, 610, 640, and 640 °C for FER(20), BEA(26), BEA(51), ZSM-5(25), ZSM-5(42), Y(6), USY(30) and MOR(15), respectively. We can also look at the light-off temperature which is defined as the temperature that 50% N_2O was consumed. The light-off temperatures are 527, 555, 567, 605, 610, 710, 730 and 720 °C for FER(20), BEA(26), BEA(51), ZSM-5(25), ZSM-5(42), Y(6), USY(30) and MOR(15), respectively. The same activity trends are obtained from both the on-set temperature and light-off temperature. The activities for N_2O

decomposition on zeolite samples decrease in the following order, FER > BEA > ZSM-5 > FAU~MOR.

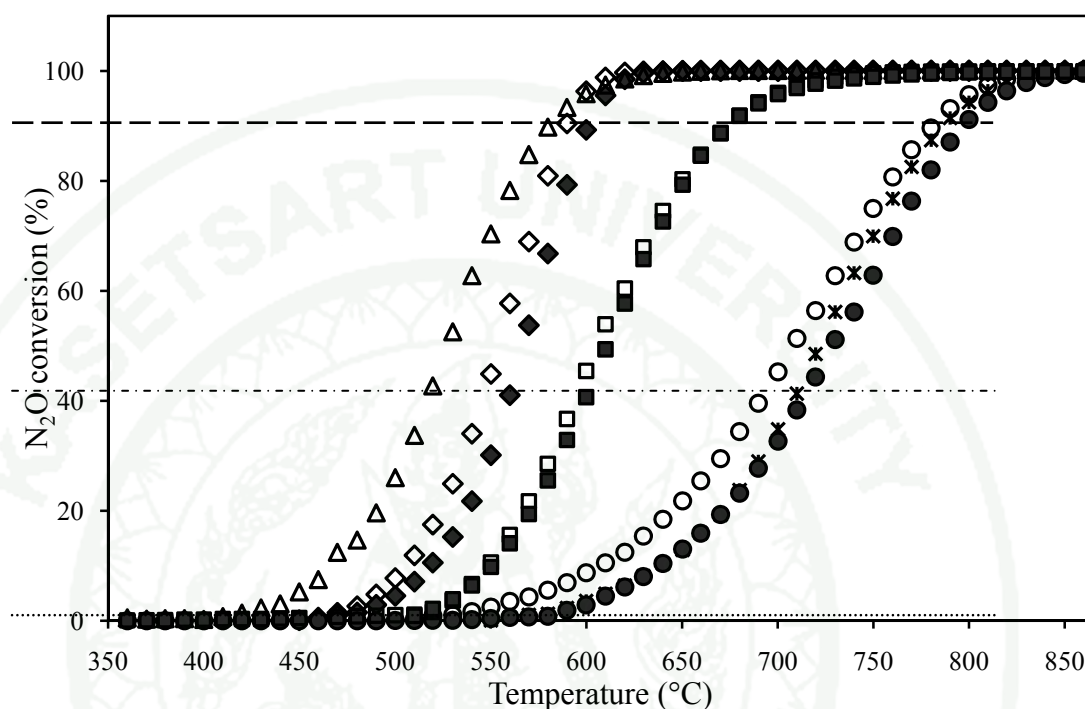


Figure 15 Reaction profile of N_2O temperature programmed decomposition over commercial zeolites [BEA (26) (\diamond), BEA (51) (\blacklozenge), FER (20) (Δ), MOR (15) (\times), Y (6) (\circ), USY (30) (\bullet), ZSM-5(25) (\square), and ZSM-5(42) (\blacksquare)] ; 10% conversion (.....), 50 % conversion (— · —) and 100% conversion (— — —)

The results of N_2O decomposition by trace Fe contain zeolites studied by Øygarden *et al.* showed the reactivity trend at 10% conversion from the static study as FER ~ BEA > ZSM-5 ~ MOR > USY with the onset temperature about 500, 550 and 640 °C for each group (Øygarden *et al.*, 2006). The reactivity trend in this study is generally in agreement with the report of Øygarden *et al.*, except that in MOR zeolite. In this study the MOR zeolite appears to be much less active than the ZSM-5 sample. The Fe content in MOR(15) is lower than ZSM-5 but it is higher than BEA and FER. Therefore, the low activity of MOR should not be due to the amount of Fe content but it should be due to the nature of Fe species on the framework surface.

2. Nitrous oxide decomposition on Fe-exchanged zeolites

The effect of metal content on this reaction was investigated from the reaction over the metal exchanged zeolites. The reactivity of N_2O decomposition on Fe-exchange zeolites was tested on Fe-exchange BEA(26). The decreasing of on-set temperature and light-off temperature was observed to decrease with the increase of Fe content BEA(26) as seen in Figure 16. On-set temperatures decrease from 505 °C on the starting BEA(26) sample to 465, 437, 443, and 440 °C, on samples which Fe content at 1861, 6358, 10734 and 14787 ppm, respectively. The observed activity from the light-off temperature is also in a similar trend. It can be pointed out that the increase activity with the increase Fe content in BEA(26) reaches the maximum activity at the Fe content of about 10,000 ppm or Fe/Al about 0.18.

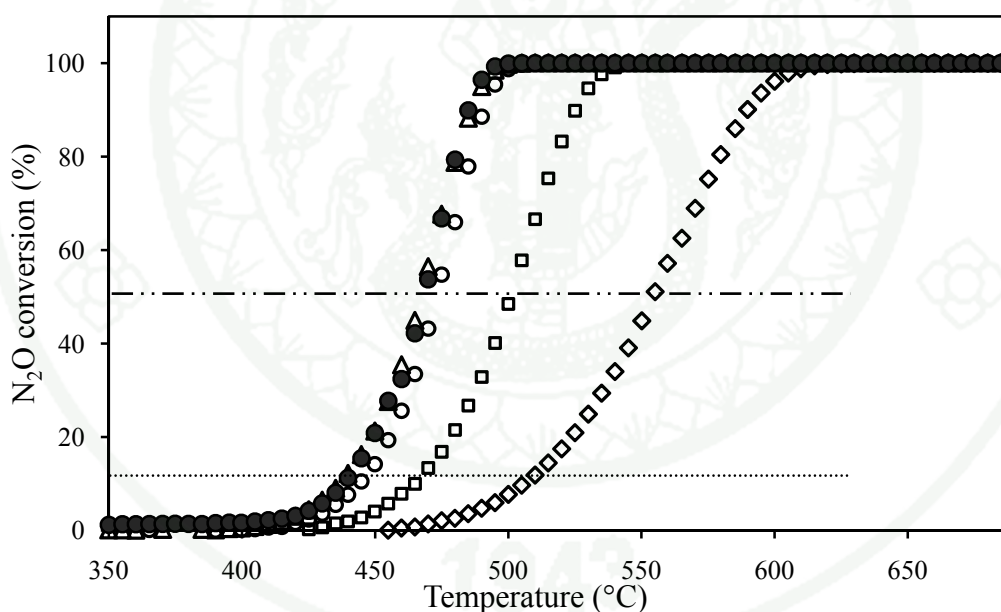


Figure 16 Reaction profile of N_2O temperature programmed decomposition over Fe exchanged BEA(26) [BEA(26) (\diamond), Fe(1,861)BEA(26) (\square), Fe(6,358)BEA(26) (\triangle), Fe(10,734)BEA(26) (\circ), Fe(14,787)BEA(26) (\bullet)]; 10% conversion (.....) and 50 % conversion (— . . —)

The reaction profiles of N_2O decomposition over various Fe-exchanged zeolite samples are shown in Figure 17. The on-set temperatures are 440, 440, 455, 465, 475,

and 505 °C for Fe(6,358)BEA(26), Fe(667)FER(20), Fe(5,241)ZSM-5(25), Fe(7,143)USY(30), Fe(11,293)Y(6) and Fe(8,592)MOR(15), respectively. The light-off temperature are present the similar trend which are 470, 495, 500, 520, 545 and 555 °C for Fe-BEA, -FER, -ZSM-5, -USY, -Y and -MOR, respectively. The light-off temperatures give a better indication of active trend. The activity trend for N₂O decomposition on Fe-exchanged zeolite is Fe-BEA > Fe-ZSM-5 ~ Fe-FER > Fe-USY ~ Fe-Y ~ Fe-MOR.

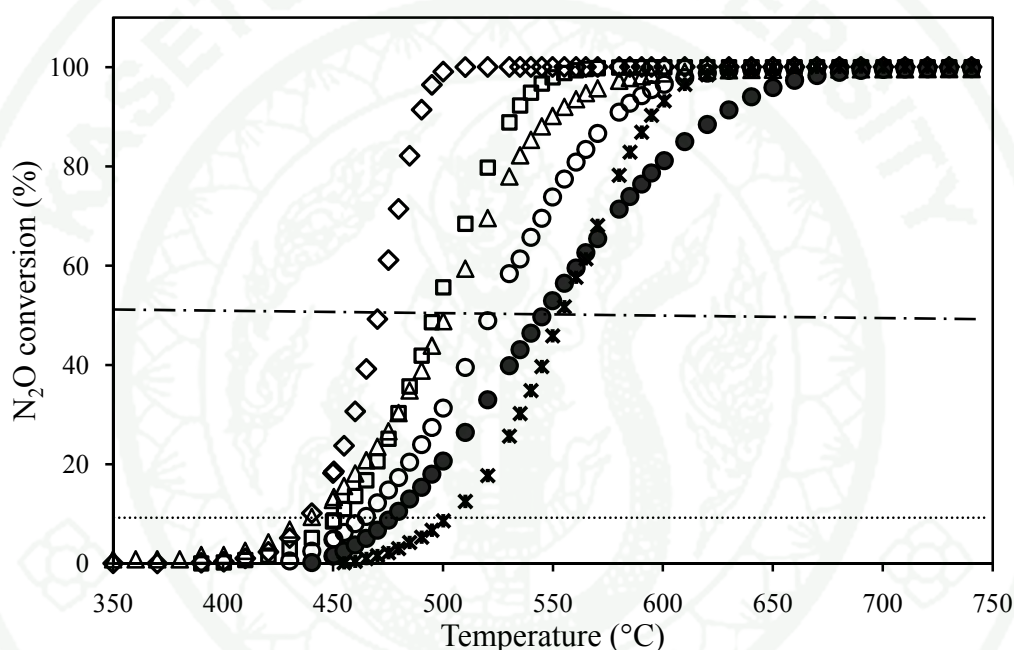


Figure 17 Temperature profile of N₂O temperature programmed decomposition over the same Fe content over different zeolites species[Fe(6,358)BEA(26) (◇), Fe(667)FER(20) (Δ), Fe(8,592)MOR(15) (✱), Fe(7,143)USY(30) (●), Fe(11,293)Y(6) (○), and Fe(5,241)ZSM-5(25) (□)] at 10% conversion; (— . . .) and 50% conversion (.....)

Jíša *et al.* reported the N₂O conversion over Fe-BEA and Fe-ZSM-5 that on-set temperature were about 450 °C (Jíša *et al.* 2009) similar to what observed in this study. These results were also correlated well with the study of Melian-Cabrera and co-worker. They has been found that, Fe-ZSM-5 and Fe-BEA had comparable activity, while Fe-FER had higher activity than the others zeolite catalyst (Melian-Cabrera *et al.*, 2005). Moreover, Guzmán-Vargas *et al.* had reported the reactivity

trend for Fe-exchanged zeolites for N_2O decomposition was $\text{Fe-FER} > \text{Fe-BEA} > \text{Fe-ZSM-5}$ (Guzmán-Vargas *et al.*, 2003). The report shows the similar trend as the trend of starting zeolites which the Fe content is in a range of 200-500 ppm, in this study. However, in the Fe-exchanged samples, we observed the activity of Fe-FER to be lower than Fe-BEA because the Fe content in Fe-FER is at 667 ppm which is approximately one tenth of the Fe content in Fe-BEA and Fe-ZSM-5.

The addition of Fe by ion-exchange into the starting MOR (15) and Y(6), which are less active for N_2O decomposition, can improve their activities significantly. The on-set temperature of Y(6), USY(30) and MOR(15) were decreased about 175, 135, and 135 °C, respectively. Nevertheless, activities of this zeolites group are still significantly lower than those of Fe-FER, Fe-BEA and Fe-ZSM-5 samples.

3. Catalytic reactivity of CH_4 and N_2O over zeolites

The blank test for the reaction of CH_4 with N_2O is shown in Figure 18. At temperature approximately 750 °C, the signals of CH_4 (at $m/e = 15.09$) and N_2O (at $m/e = 43.95$ and 30.02) started to decrease with the increasing of signal of N_2 (at $m/e = 28$). This result shows that the reaction of N_2O with CH_4 cannot occur at a temperature lower than 700 °C without a catalyst. It was observed that the thermal decomposition of N_2O in the presences of CH_4 started at approximately the same as in the case without methane. The presence of CH_4 did not facilitate the activity for N_2O thermal decomposition.

The N_2O conversions over zeolite samples in the presence of CH_4 are shown in Figure 19. The BEA(26), FER(20) and ZSM-5(25) have the lowest on-set temperature at about 390 °C. The marked decrease of the on-set temperature from 550 °C (without CH_4) to 390 °C (in the presence of CH_4) is observed on the ZSM-5(25). The catalytic activities for N_2O decomposition with the presence of CH_4 of ZSM-5, BEA and FER are similar. The on-set temperature for MOR(15) is 400 °C which is slightly lower than that of the most active group (BEA, FER, ZSM-5). From the light-

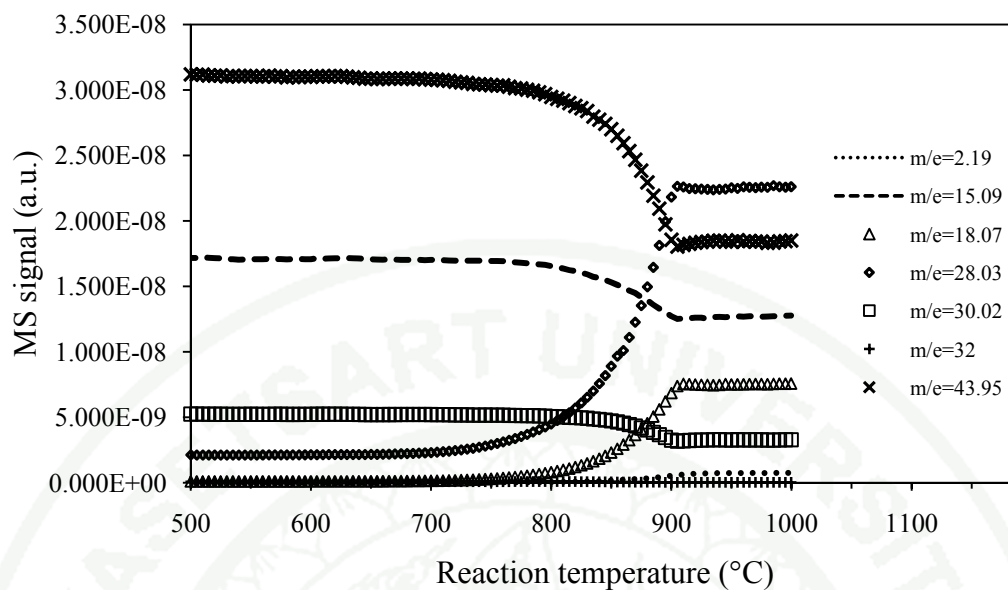


Figure 18 MS signal of 5%vol. CH_4 and 5%vol. N_2O temperature programmed reaction in the blank reactor (packed with quartz).

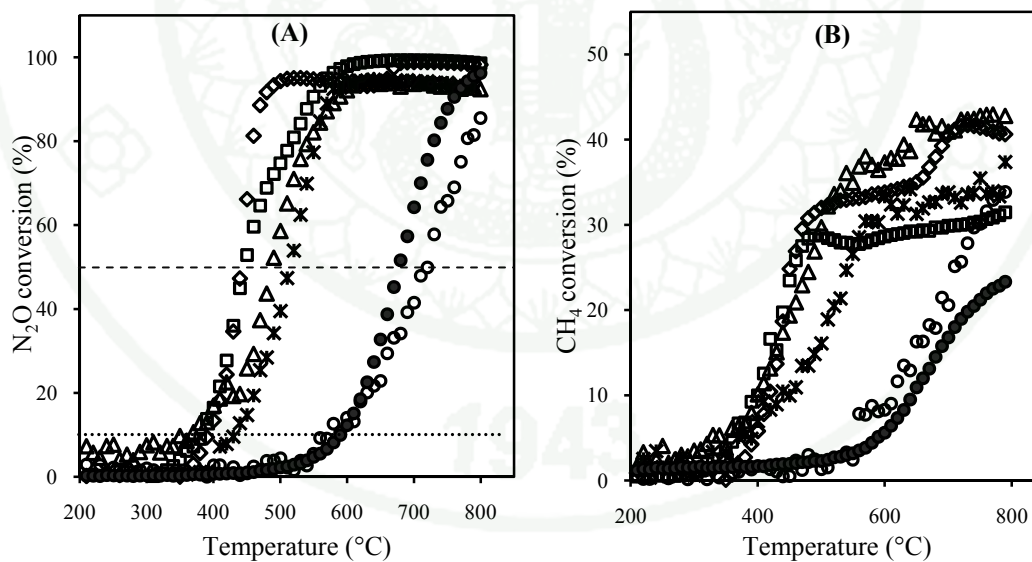


Figure 19 Conversion of N_2O (A) and CH_4 (B) studied by temperature programmed reaction of N_2O and CH_4 over commercial zeolites [BEA(26) (\diamond), FER(20) (Δ), MOR(15) (\times), USY(30) (\circ), Y(6) (\bullet), ZSM-5(25) (\square)] at 10% conversion; (— . . .) and 50% conversion (.....)

off temperature, it is confirmed that MOR(15) has a comparable activity to BEA, FER, and ZSM-5 for the N_2O decomposition in the presence of CH_4 . However, much lower activities were observed over USY(30) and Y(6). These results suggested that, ZSM-5, BEA, FER and MOR samples contain the active species for N_2O decomposition in the presence of CH_4 as reducing agent. The low activities of zeolite Y and USY, may be due to the very low Fe content in these samples.

The results of CH_4 on N_2O decomposition in Fe exchanged zeolites are shown in Figure 20. The on-set temperature of Fe(14,787)BEA(26), Fe(8,592)MOR(15), Fe(5,241)ZSM-5(25), Fe(7,143)USY(32), Fe(11,293)Y(6) and Fe(667)FER(20), are 290, 335, 345 °C, 370, 370 and 390, respectively. Addition of Fe content by ion exchange significantly increases the activities in all samples. The marked improvement can be observed on Fe(11,293)Y(6) and Fe(7,143)USY(32) with the decrease of on-set temperature from 600°C to 370 °C upon adding Fe content by ion-exchange. It is appeared that the amount of iron loading is strongly affected the catalytic activity for N_2O decomposition in the presence of CH_4 for the BEA, FER, MOR and ZSM-5 zeolites. The Fe(14,787)BEA(26) is the most active sample and it contained the highest Fe amount. On the other hand, the Y and USY samples showed the lower reactivity even though they contained high Fe loading. Therefore, zeolites framework still plays an important role on the formation of active species and the activity for N_2O decomposition.

The results of others transition metal studied in BEA(26) are showing in Figure 21. Fe(14,787)BEA(26) has the lowest on-set temperature following by Co(17,487)BEA(26) and Cu(16,500)BEA(26), respectively. The exchanged amount of Fe, Co and Cu are comparable in these samples. Therefore, Fe is more active than Co and Cu for N_2O decomposition in the presence of CH_4 .

Similarly, the activities of Fe, Co, and Cu on ZSM-5(25) are showed in Figure 22. The on-set temperature of Fe(5,241)ZSM-5(25), Co(11,584)ZSM-5(25), Cu(15,878)ZSM-5(25) and V(5,691)ZSM-5(25) are 340, 365, 355 and 390 °C, (25)

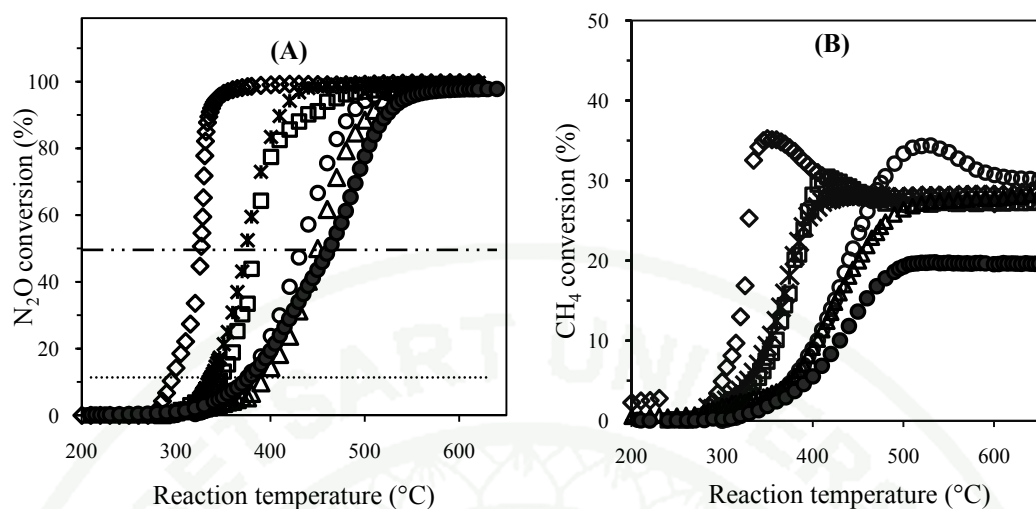


Figure 20 Conversion of N_2O (A) and CH_4 (B) studied by temperature programmed reaction of N_2O and CH_4 over Fe exchanged zeolites [Fe(14,787)BEA(26) (◇), Fe(667)FER(20) (Δ), Fe(8,592) MOR(15) (✕), Fe(7,143) USY(32) (○), Fe(11,293)Y(6) (●), Fe(5,241)ZSM-5(25) (□)] at 10% conversion; (.....) and 50% conversion (— . .).

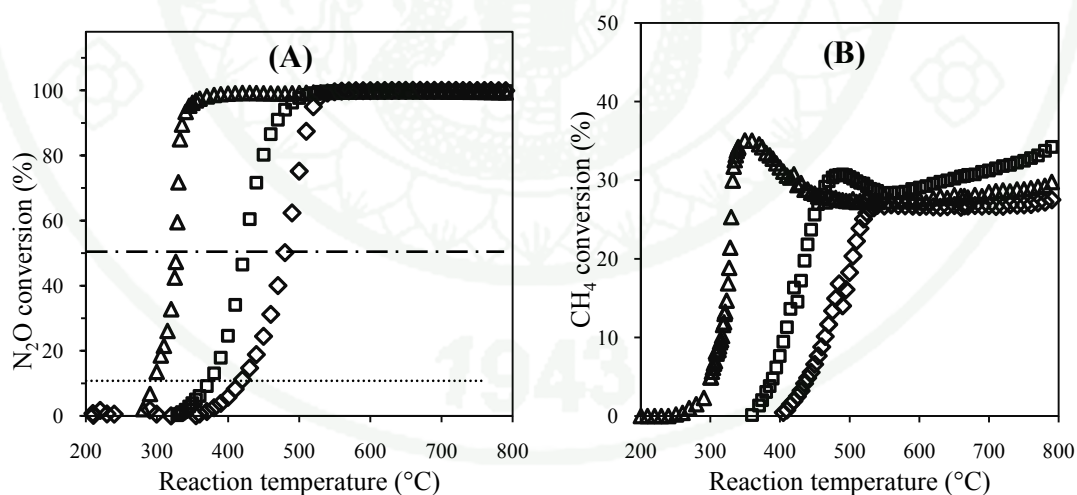


Figure 21 Conversion of N_2O (A) and CH_4 (B) studied by temperature programmed reaction of N_2O and CH_4 over TM exchanged BEA(26) [Fe(14,787)BEA(26) (Δ), Co(17,487)BEA(26) (□), Cu(16,500)BEA(26) (◇)] at 10% conversion; (.....) and 50% conversion (— . .)

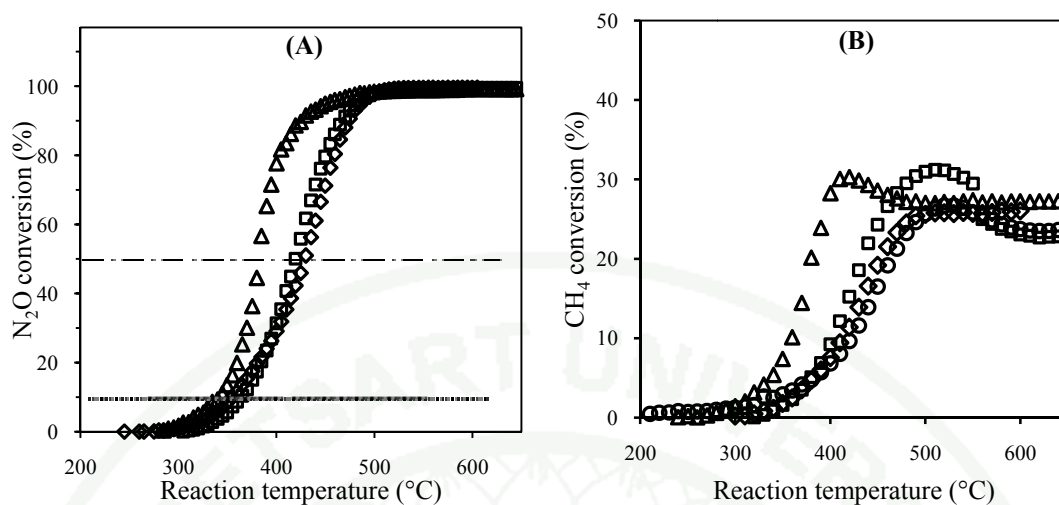
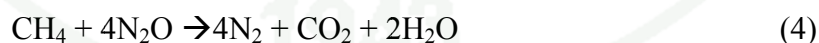


Figure 22 Conversion of N₂O (A) and CH₄ (B) studied by temperature programmed reaction of N₂O and CH₄ over TM exchanged ZSM-5(25) [Fe(5,241)ZSM-5(25) (Δ), Co(11,584)ZSM-5(25) (□), Cu(15,878)ZSM-5(25) (◇)] at 10% conversion; (.....) and 50% conversion (— . .)

respectively. The light-off temperature of Fe(5,241)ZSM-5(25), Co(11,584)ZSM-5(25), and Cu(15,878)ZSM-5(25) are 380, 420, and 430 °C, respectively. Notice that, the Co and Cu loading are much higher than the Fe loading. Therefore, it is appeared that, Fe is much more active for N₂O decomposition than Co and Cu.

Look at the CH₄ conversion in the presence of N₂O. If the reaction goes to the complete oxidation, for one molecule of CH₄, it needed 4 molecules of N₂O as equation 4:



Therefore, if the reaction takes place stoichiometrically to complete oxidation, CH₄ conversion should be at 25%. However, the CH₄ conversion in Figure 19(B), 20(B), 21(B) and 22 (B) are 25-35%. Therefore, there might be other hydrocarbons produced in a significant amount.

4. Carbon products distribution from the reaction of CH₄ and N₂O

The catalytic conversions of CH₄ and N₂O (CH₄:N₂O = 2:1) on zeolite samples are shown in Figure 23. Over the BEA, FER, and MOR samples, the conversions of CH₄ are high at early time on stream and rapidly decrease within 1 hour. Over the ZSM-5 sample, CH₄ conversion is relatively stable with time on stream in the first hour. CH₄ conversion was slightly changed from the initial value of 28% to 25% at 1 hour. Within the first hour of time on stream, N₂O stayed close to 100% conversion over BEA and ZSM-5 zeolites while the N₂O conversion was significantly decreased from 100% to 70% in FER and MOR.

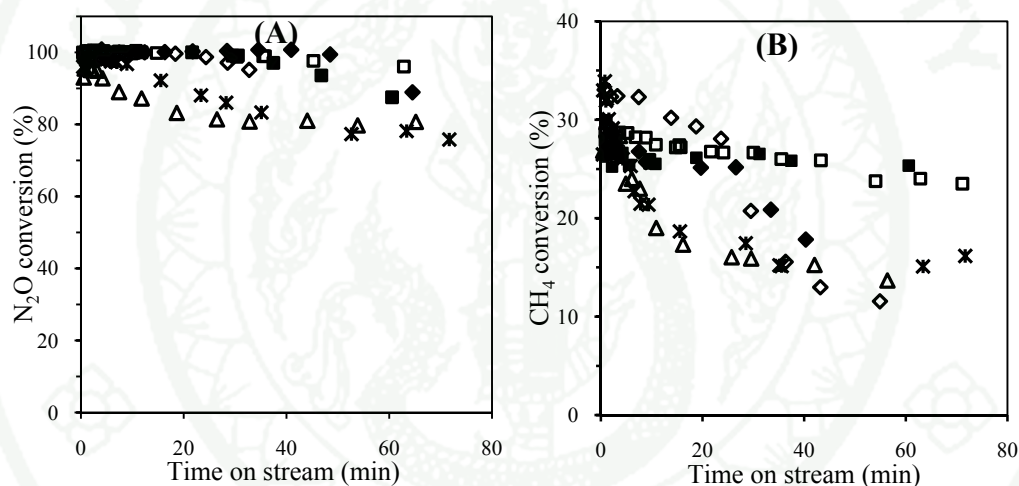


Figure 23 N₂O conversion (A) and CH₄ conversion (B) from the reaction of 5% CH₄ and 2.5 % N₂O (in total flow rate 50 cm³/min) over 0.100 g commercial zeolites at 500 °C: BEA(26) (◇), BEA(51) (◆), ZSM-5(25) (□), ZSM-5(42) (■), MOR(15) (×), and FER(20) (Δ)

At 500 °C, the CH₄ cannot convert over Y(6) and USY(30) due to the low activities of these samples. Even at the reaction temperature of 550 °C, the N₂O conversion was only 25-10% over Y(6) and 10-2% over USY(30) as shown in Figure 24. The CH₄ conversions were lower than 5% over both Y(6) and USY(30).

Products distribution from the reaction over FER, MOR catalysts consist of C₂-C₃ hydrocarbon (ethane, ethylene, propane, and propylene). The C₂-C₃ products

rapidly decrease with time on stream as shown in Figure 25. Over BEA zeolites hydrocarbon products are very low as shown in Figure 26. BEA zeolites were more stable than MOR and FER.

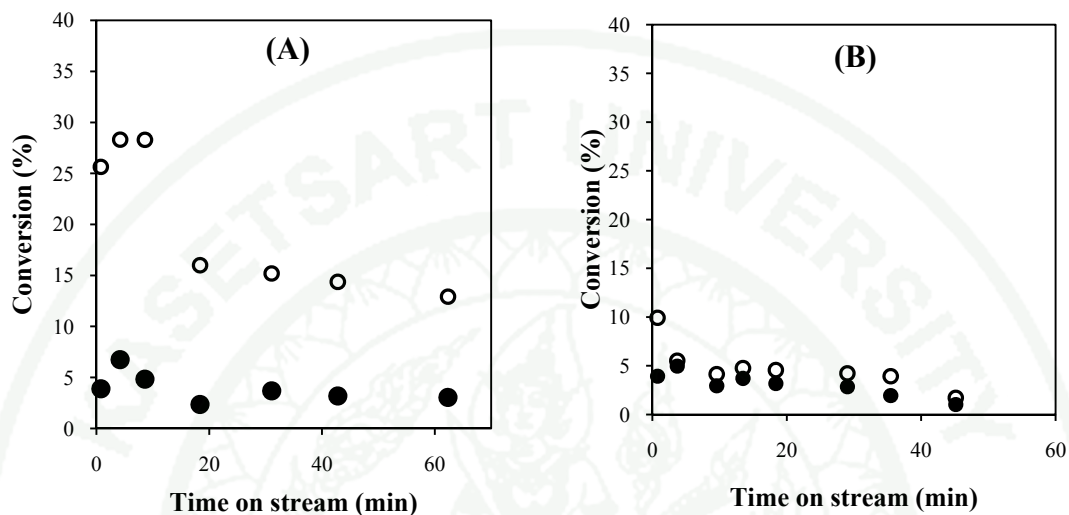


Figure 24 CH₄ and N₂O conversion from the reaction of 5% CH₄ and 2.5 % N₂O (in total flow rate 50 cm³/min) over 100 mg of Y(6) (A) and USY(30) (B) at 550 °C. ((●) methane conversion, (○) nitrous conversion)

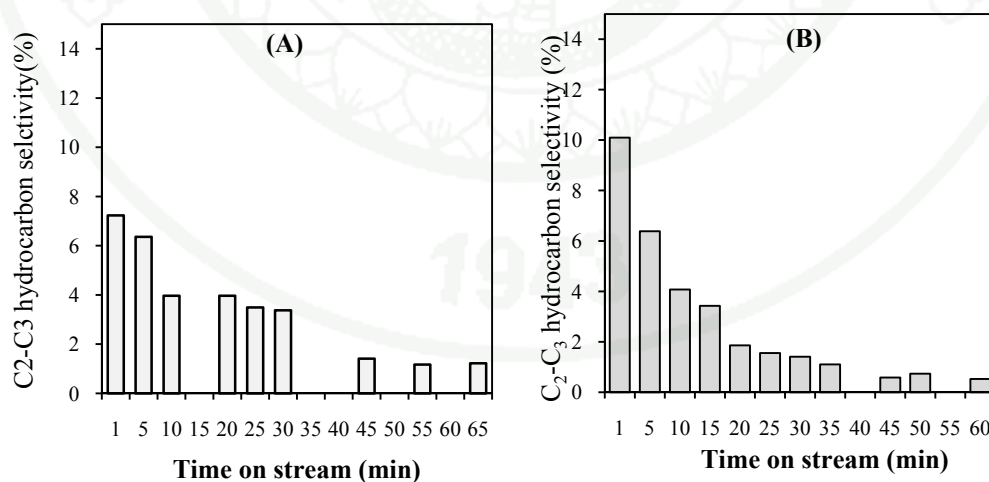


Figure 25 C₂ and C₃ hydrocarbon selectivity from the reaction of 5% CH₄ and 2.5 % N₂O (in total flow rate 100 cm³/min) over 100 mg of FER zeolites at 500°C; (A) FER and (B) MOR

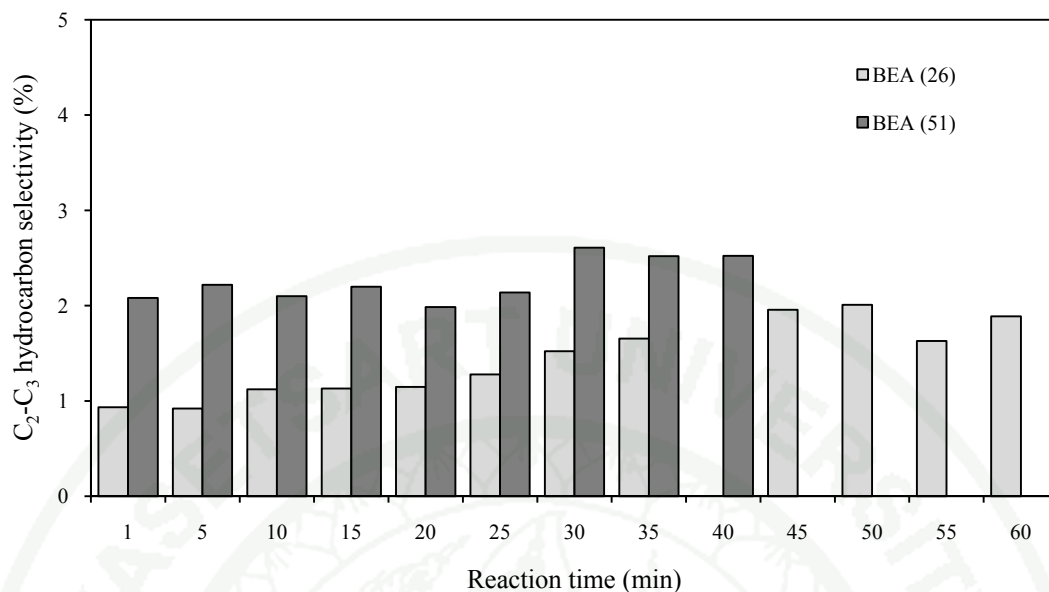


Figure 26 C₂ and C₃ hydrocarbon selectivity from the reaction of 5% CH₄ and 2.5 % N₂O (in total flow rate 50 cm³/min) over 100 mg of BEA zeolites at 500°C.

The hydrocarbon product over ZSM-5(25) and ZSM-5(42) are showed in Figure 27. The main hydrocarbon products of this reaction were aromatic hydrocarbons; benzene, toluene and xylene. This zeolite also produces C₂-C₃ hydrocarbon with the lower selectivity. The C₂-C₃ selectivity was range between 3-5 % while the total aromatic products were about 20 % selectivity. The about 25% of CH₄ conversion was lost via others species such as deposit coke. The color of used catalysts changed from white to black indicating carbon deposit on the zeolites surface as coke. The coke formation is the results of side reaction of methane such as dehydrogenation and polymerization, etc.

To improve the catalytic stability, zeolite samples were treated with steam at 650 °C for 2 hours. The steam treated ZSM-5 showed the more stable activity as shown in Figure 28. The activity was stable for 4 hours time on stream. Product distributions over ZSM-5(25) and ZSM-5(50) were similar. The products distributions over ZSM-5 were summarized in Figure 29.

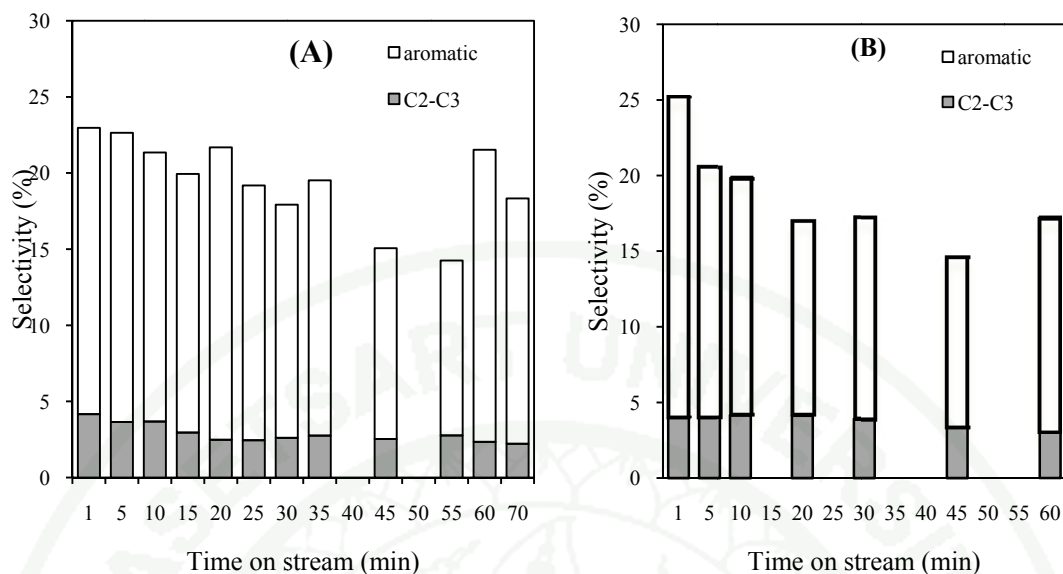


Figure 27 C₂ and C₃ hydrocarbon selectivity from the reaction of 5% CH₄ and 2.5 % N₂O (in total flow rate 50 cm³/min) over 100 mg of ZSM-5(25) (A) and ZSM-5(42) (B) at 500 °C.

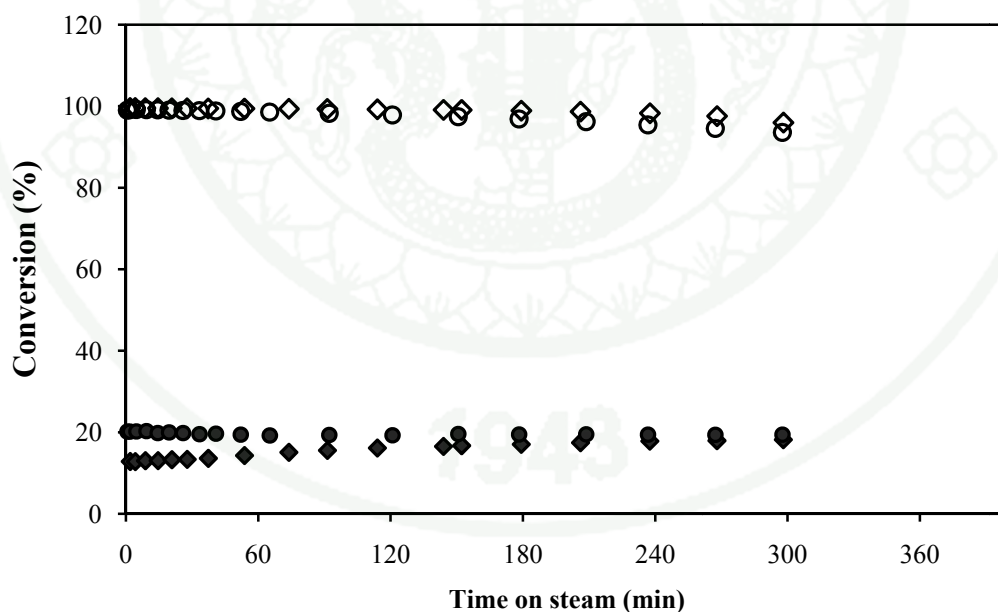


Figure 28 CH₄ conversion (filled symbol) and N₂O conversion (blank symbol) from the reaction of 6% CH₄ and 3 % N₂O (in total flow rate 50 cm³/min) over 0.100 g of steam treatment ZSM-5(25) (◆,◇) ZSM-5(42) (●,○) at 500 °C

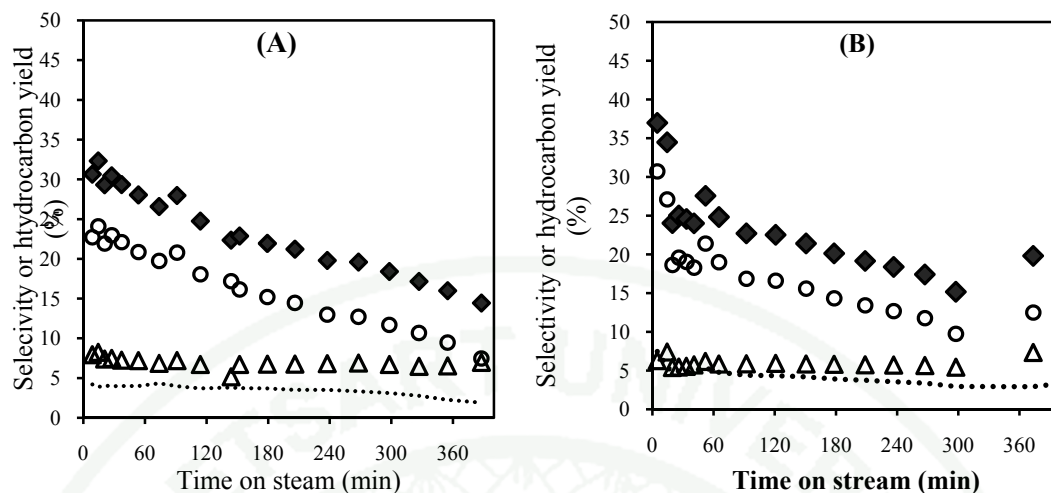


Figure 29 C₂-C₃ hydrocarbon (Δ), aromatic hydrocarbon (○), and total hydrocarbon selectivity (◆) and hydrocarbon yield (.....) from the reaction of 6% CH₄ and 3 % N₂O (in total flow rate 50 cm³/min) over 100 mg of steam treatment ZSM-5(25) (A) and ZSM-5(42) (B) at 500 °C

The amount of coke formation during the reaction over the reaction was studied from TGA analysis. The amounts of deposit coke from the used zeolite were plotted in Figure 30. The result shows that, coke was rapidly deposited over non-steam treated sample to about 8%wt in 1 hour. For steam treated zeolite, coke formation was observed at a lower rate. For 3 hours time on stream, the coke formation was about 3% wt which is approximately equivalent to the quantity that accumulated within the first 10 min. over the non steam-treatment ZSM-5.

Surface area and porosity of used ZSM-5 samples were shown in Table 8. BET surface area of non steam treatment ZSM-5(42) decreases to lower than 150 m²/g after the contacted with the reactant only 20 min time on stream. Both micro- and external-surface areas are simultaneously decrease. Moreover, pore volume of this sample is decreased from 0.19 to 0.07 cm³/g. Over steamed sample, even after 180 min time on stream, surface area and pore volume are higher than the non-steam treated sample that used 20 min. After treated with steam, the coke formation rate on ZSM-5 is decreased and the decreasing of surface area and pore volume are less than the non-steam treatment.

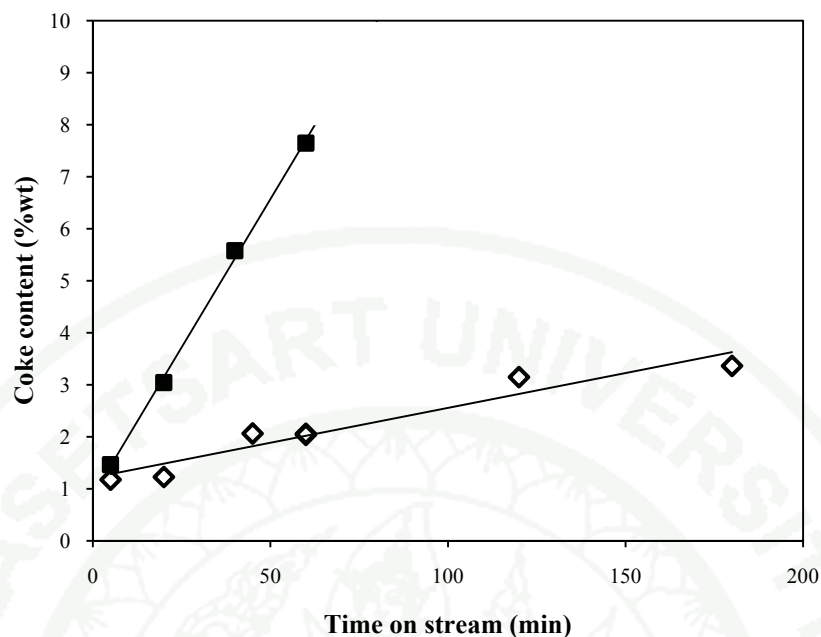


Figure 30 Coke content determined by TGA under N_2 atmosphere ($20 \text{ cm}^3/\text{min}$) and heating rate $10 \text{ }^\circ\text{C}/\text{min}$ ((■) non steam-treatment, (◇) steam-treatment)

The coke formation from the TGA result appears to linearly increase with the reaction time. On the non-steam treated zeolite, the coke formation rate was $133 \text{ } \mu\text{g}/\text{min}$ corresponding to 41% selectivity of the converted methane. The steam-treatment process is more resistant to coke deposition on ZSM-5 sample. The coke formation rate is $2.4 \text{ } \mu\text{g}/\text{min}$ and equivalent to about 7.5% selectivity.

The CO_2 selectivity was estimated from MS signal of CO_2 fragment at $m/e=22$ is range about 20-30%. The CO selectivity of GC measurement was about 38-43%. The carbon balances from this study were 82 to 110%.

Oxidative dehydrogenation of ethane over zeolites

Generally, ethene (C_2H_4) can be produced from ethane (C_2H_6) in the cracking unit at temperature above $800 \text{ }^\circ\text{C}$ (Olah and Molnar, 2001). This industrial process requires high temperature. With the aim to working at lower the reaction temperature,

Table 8 Surface area and porosity of coke zeolites

Sample	$S_{\text{BET}}^{\text{a}}$ (m^2/g)	S_{μ}^{b} (m^2/g)	$S_{\text{ext}}^{\text{c}}$ (m^2/g)	$V_{\text{total}}^{\text{d}}$ (cm^3/g)	V_{μ}^{e} (cm^3/g)
ZSM-5 (42)	361	274	87	0.19	0.11
ZSM-5(42) st2h	325	163	162	0.16	0.07
ZSM-5 (42) st4h	323	117	206	0.16	0.05
ZSM-5 (42) st2h used 5 min	315	192	123	0.15	0.08
ZSM-5 (42) st2h used 20 min	302	151	151	0.16	0.06
ZSM-5 (42) st2h used 45 min	290	183	107	0.14	0.08
ZSM-5 (42) st2h used 60 min	293	234	69	0.13	0.09
ZSM-5 (42) st2h used 120 min	273	164	109	0.13	0.07
ZSM-5 (42) st2h used 180 min	280	180	100	-	-
ZSM-5 (42) used 5 min	317	240	77	0.14	0.10
ZSM-5 (42) used 20 min	146	118	28	0.07	0.05
ZSM-5 (42) used 40 min	199	150	49	0.10	0.06
ZSM-5 (42) used 60 min	290	188	102	0.13	0.08

^a Surface area by BET method^b micropore surface area by *t*-plot method^c external surface area by *t*-plot method^d total pore volume at $P/P_0=0.95$ ^e micropore volume by *t*-plot method

an oxidative dehydrogenation of ethane has been extensively study (Heracleous *et al.*, 2004; Batholomew and Farrauto, 2006; Choudhary *et al.*, 2006). Addition of oxidant gas such as air, oxygen (O_2), carbon dioxide (CO_2), and nitrous oxide (N_2O), the dehydrogenation of ethane can be successively carried out at about 400-650°C (Blaneck *et al.*, 2002; Heracleous *et al.*, 2004; Choudhary *et al.*, 2006). Using of catalysts such as Cr supported on Al_2O_3 ($\text{Cr}/\text{Al}_2\text{O}_3$), Cr/ZrO_2 , $\text{Pt}/\text{Sn}/\text{Al}_2\text{O}_3$, $\text{Mo}/\text{Al}_2\text{O}_3$, Ag and Cu metals, Pt, Pd, and Ru supported on carbon or alumina, and zeolites can further make reaction favor at lower temperature (Batholomew and Farrauto, 2006).

Dehydrogenation of ethane with nitrous oxide

The oxidative dehydrogenation of C_2H_6 was first test by using N_2O as oxidant gas without any catalyst. The reactant gas was a mixture of 3.0 % N_2O and 3.0 % C_2H_6 . The reactions were carried out at reaction temperatures from 300°C to 800°C and the results are shown in Table 9.

Table 9 Products from the reaction of 3% C_2H_6 and 3% N_2O in the non-catalytic system

Temperature (°C)	% conversion ^a		% selectivity ^b				% Yield of C_2H_4 ^c
	C_2H_6	N_2O	C_2H_4	CH_4	CO and CO_2	Others	
300	0.0	0.0	-	-	-	-	-
600	0.0	0.0	-	-	-	-	-
650	2.4	0.8	98.2	-	-	1.8	2.3
675	5.9	1.1	96.1	0.6	2.4	0.9	5.5
700	13.0	2.7	94.7	0.8	2.0	2.5	12.3
725	25.5	6.4	93.2	1.2	2.8	2.8	23.8
750	43.0	13.6	91.5	1.7	4.3	2.5	39.4
775	61.7	29.4	87.5	2.5	7.7	2.3	54.0
800	78.0	59.0	79.6	3.5	13.9	3.0	62.7

$$^a \text{ Conversion (\%)} = \left(\frac{(\text{inlet concentration}) - (\text{outlet concentration})}{(\text{inlet concentration})} \right) \times 100$$

$$^b \text{ Selectivity (\%)} = \left(\frac{(\text{no. of C-atom convert}) - (\text{no. of C-atom in selected product})}{(\text{no. of C-atom convert})} \right) \times 100$$

where [no. of C – atom] is refers to a number of carbon atom in reaction species.

$$^c \text{ } C_2H_4 \text{ yield (\%)} = \left(\frac{(\text{number of C-atom in } C_2H_4)}{(\text{number of C-atom in the inlet})} \right) \times 100$$

Reaction occur at temperatures above 650°C. Ethylene (major products), methane (CH_4), carbon dioxide (CO_2) and carbon monoxide (CO) were produced. Side reactions such as cracking, combustion were also occurred. Nevertheless, the main

product of this experiment is C_2H_4 , with almost 100% selectivity at low conversion. At 650°C, % conversion of C_2H_6 and N_2O were very low (only 2.4 and 0.8 % respectively). Almost all amount of the converted C_2H_6 was changed to C_2H_4 (98.2 % selectivity).

Ethylene was produced at more than 90% selectivity at temperature below 750 °C. At the higher reaction temperature, the conversion of C_2H_6 and N_2O were increased simultaneously. The yield of C_2H_4 was also increased with reaction temperature. However, at the higher reaction temperature, the CO_x product selectivity was increased. The cracking reaction also occurred at higher temperature.

2. Ethane dehydrogenation over catalyst

The effect of zeolite, ZSM-5, on ethane dehydrogenation were also performed in the fixed bed reactor. The ZSM-5 samples used in this study were pretreated with steam at 650°C for 2 hr before performing any reaction. The fixed bed reactor was packed with 0.15 g ZSM-5(25) catalyst. After treated ZSM-5(25) with the conventional processes, a gas mixture of 3.0% C_2H_6 in He was introduced into the reactor. The catalytic activity was analyzed from the effluence gas composition at the reactor outlet by GC. The results at temperature 500°C – 700 °C were reported in Table 10.

Table 10 Products from the reaction of 3% C_2H_6 over ZSM-5(25) 0.15 g

Temperature (°C)	C_2H_6 Conversion (%)	Selectivity (%)			C_2H_4 yield (%)
		C_2H_4	CH_4	Others	
500	0.0	-	-	-	-
600	0.0	-	-	-	-
650	0.0	-	-	-	-
700	4.2	87.5	-	12.5	3.7

C_2H_6 conversion was only 4.2 % at 700 °C. At this condition C_2H_4 selectivity was 87.5 % which produced ethylene only 3.7% yield. This value is lower than the results from the reaction with oxidant, N_2O , in the non catalyst reactor at the same reaction temperature which could convert 13.0% C_2H_6 and produced about 12.3% C_2H_4 yield. The C_2H_4 selectivity over ZSM-5(25) catalyst at 700 °C without oxidant gas was only 87.5%, while the rest 12.5% was defined as others residue. From these results, the present of N_2O is an important parameter to achieve the higher C_2H_4 yield from the dehydrogenation of C_2H_6 at the lower reaction temperature.

3. The effects of N_2O concentration on ethane dehydrogenation over ZSM-5

The reactions were performed at 500 °C over about 0.15g of steam treatment ZSM-5(25). The quantities of C_2H_6 and N_2O in the reactant mixture were adjusted in the total flow rate 100 cm³/min with He balance. The concentrations of C_2H_6 and N_2O were varied from 1.5% to 4.0% and 0.0% to 3.0%, respectively. The gaseous product from the reaction at initial (collected at 5 min after feed the reactant gas though the reactor) and at 180 min time on stream were analyzed by GC. The reactant conversion and products selectivity are presented in Table 11.

It has been found that ethane conversion could not occur at 500 °C over ZSM-5(25) without the presence of N_2O . However, with the mixture of 3.0% C_2H_6 and 0.5% N_2O over ZSM-5(25) zeolite, 100% N_2O conversion and 13% C_2H_6 conversion were achieved throughout 180 min time on stream. Ethene selectivity was about 78% with trace amounts of CH_4 , C_2H_6 , CO_x , and other residue which was defined as deposited carbon. The yield of C_2H_4 product was constant at about 10 % for at least 3 hours at this reaction condition. Rate of C_2H_6 conversion, C_2H_4 production, N_2O conversion, and other residue were calculated respect to the weight of ZSM-5(25) (kg) in an hour as following equation 5:

$$\text{Consumption or Production rate } \left(\frac{\text{mole}}{\text{kg}\cdot\text{h}} \right) = \frac{\text{mole of species consumed (mol)}}{\text{weight of catalyst (kg)}/\text{h}} \quad (5)$$

Table 11 Gas composition from the reaction of C₂H₆ over 0.150g ZSM-5(25) at 500 °C in the total flow rate 100 cm³/min

Gas inlet (%)		Time on stream (min)	Conversion (%)		Selectivity (%)						C ₂ H ₄ yield (%)	Consumption or Production rate (mole/kg·h)		
C ₂ H ₆	N ₂ O		C ₂ H ₆	N ₂ O	C ₂ H ₄	CH ₄	C ₃ H ₆	C ₄ H ₈	COx ^b	Deposit ^c		N ₂ O	C ₂ H ₆	C ₂ H ₄
3.0	0.0	5	0.0	-	-	-	-	-	-	-	-	-	-	-
		30	0.0	-	-	-	-	-	-	-	-	-	-	-
3.0	0.5	5	13.1	100	78.0	1.05	2.99	0.00	4.73	13.0	10.2	8.93	7.00	5.45
		180	13.8	100	78.3	0.54	4.07	0.00	4.95	14.9	10.2	8.93	7.43	5.44
3.0	1.5	5	33.3	100	52.6	1.65	5.79	0.00	9.90	26.1	17.5	26.78	17.8	9.37
		180	32.8	96.1	55.9	1.94	7.12	3.22	10.0	17.6	18.3	25.74	17.8	9.87
3.0	3.0	5	51.8	100	41.3	2.81	9.59	0.00	16.5	21.4	21.4	53.57	27.7	11.4
		180	48.1	90.0	45.2	3.22	8.34	8.65	16.5	15.6	21.7	48.21	25.8	11.6
1.5	1.5	5	46.9	100	45.4	3.78	9.09	0.00	19.9	18.9	21.3	26.78	12.4	5.71
		180	51.2	100	39.7	3.95	9.07	0.00	20.6	17.6	20.4	26.78	13.8	5.45
1.5	3.0	5	76.8	100	21.5	3.87	10.6	0.00	31.8	25.6	16.5	53.56	20.57	4.42
		180	65.0	78.0	30.3	5.24	12.4	17.4	28.5	8.90	19.2	41.78	17.40	5.51
2.0	4.0	5	74.8	100	22.0	4.60	8.86	0.00	35.6	17.8	16.4	71.41	26.70	5.87
		180	74.3	100	25.0	6.30	13.3	0.00	39.1	5.97	18.6	71.41	26.53	6.64

^a conversion^b Selectivity to CO and CO₂ as the carbon basis^c The loss carbon defined as coke

The molar production of C_2H_4 with this reaction condition was about 5.45 mole/kg·h. The molar conversion of N_2O and C_2H_6 are 8.93 and 7.43 mole/kg·h, respectively. The comparable conversion rates suggest that reactions occur mostly oxidative dehydrogenation. The selectivity is constant at 78% for 3 h.

When the molar ratio of N_2O to C_2H_6 (N_2O/C_2H_6) was increased to 3.0 % C_2H_6 and 1.5 % N_2O , the conversion of C_2H_6 increased to be about 33 %. However, the selectivity of C_2H_4 reduced to 45 %. At the initial time on stream, N_2O was totally converted and decreased to be about 96 % after 180 min time on stream while C_2H_6 conversion showed a little decreased. The conversion of ethane was increased by changing the mixture of inlet gas to 3.0 % C_2H_6 and 3.0 % N_2O in He balance. At this N_2O/C_2H_6 molar ratio, C_2H_6 was more converted to CO_x products. At the initial time on stream, C_2H_6 conversion and N_2O conversion were about 51.8 % and 100 %, respectively. The catalyst deactivation was pronounced than the previous condition. The conversions of both C_2H_6 and N_2O were more decreased at 180 min time on stream.

The catalytic deactivation of ZSM-5(25) was the results of coke formation during the reaction took place. This deactivation can affect the active site environment and also the reaction mechanism over the catalytic surface. The effect of inlet concentration and N_2O/C_2H_6 molar ratio are investigated in this study. The lower gas mixture concentration at 1.5% C_2H_6 and 1.5 % N_2O was used at the same reaction contact time. The reactant conversion and C_2H_4 productivity are in the similar range as the 3% C_2H_6 : 3% N_2O inlet concentrations which produced about 21% C_2H_4 yield. The highest yield of C_2H_4 was about 21% which is comparable to the similar range of the previous literature report (Silberona *et al.*, 2004; Heracleous, *et al.*, 2004). It can be concluded that the N_2O/C_2H_6 molar ratio of inlet gas was function on the product distribution while the inlet concentration will effect on the catalyst stability.

When increase the N_2O/C_2H_6 molar ratio to two (3.0/1.5 and 4.0/2.0), the C_2H_6 conversion was about 75% and the % C_2H_4 yield was about 16 %. The yield of C_2H_4 was less than when the N_2O/C_2H_6 molar ratio of one was used. It was found that N_2O

concentration had strong effect on the C_2H_6 conversion and C_2H_4 selectivity. The excess N_2O feed would lead to side reactions to produce other compounds such as C_2H_4 , CH_4 , and CO . The stability of the main product, C_2H_4 , under the N_2O gas was tested under the same reactor condition. The results of C_2H_4 stability from this reaction was then presented in Table 12.

It was found that C_2H_4 can be converted in the presence of N_2O at $500^\circ C$ over ZSM-5(25) catalyst. The products mainly compose of CO_x , C_3H_8 , and carbon deposit. However, without N_2O gas, the C_2H_4 conversion was only 1.1% and 5.10 % at $500^\circ C$ and $600^\circ C$, respectively. Ethylene is as active as ethane to react with N_2O . Therefore, when increase the ratio of N_2O/C_2H_6 the selectivity to ethylene decrease. The maximum production rate and the highest C_2H_4 yield were obtained at the feed N_2O/C_2H_6 molar ratio equal to one.

4. Effects of zeolite framework species

The effect of zeolite species (BEA(26), FER(20), MOR(15), USY(30) and ZSM-5(25)) on the C_2H_6 dehydrogenation was investigated. The reaction results were summarized in Table 13.

The results from Table 13 show that ZSM-5(25) is the most active catalyst for C_2H_6 dehydrogenation and for the N_2O decomposition. BEA(26) is the second most active catalyst. It is very active for N_2O conversion which remains 100% throughout three hours of time on stream. However, the C_2H_6 % conversion and C_2H_4 % selectivity over BEA(26) are lower than over the ZSM-5(25) zeolite. The more stability can be the effect of a bigger pore sized on BEA(26) which can promoted the diffusion rate inside the zeolites framework.

FER(20) can convert about 31% of C_2H_6 at the initial time on stream as similar as BEA(26) but the lower % N_2O conversion. FER(20) is less stable than BEA(26) which may be due to the smaller pore size. The smaller pore can be slower diffusion rate which effect on the lower reactant conversion and the higher carbon condensation inside the pore. Moreover, the smaller pore is easier blocked by the deposited component.

Table 12 Gas composition from the reaction of C₂H₄ over 0.100 g ZSM-5(25) at 500 °C in the total flow rate 100 cm³/min

Gas inlet (%)		Temperature (°C)	Time on stream (min)	Conversion (%)		Selectivity (%)					Y _{C₂H₄} (%)	Consumption/ Production rate (mole/kg-h)		
C ₂ H ₄	N ₂ O			C ₂ H ₄	N ₂ O	C ₂ H ₆	CH ₄	C ₃ H ₆	CO _x ^b	Deposit ^c		N ₂ O	C ₂ H ₆	C ₂ H ₄
3.0	3.0	500	5	48.5	100.0	0.41	2.20	27.66	28.59	21.08	-48.5	77.69	0.15	37.68
			30	43.5	98.8	0.41	3.09	35.95	35.04	11.99	-43.5	76.79	0.14	33.81
3.0	0.0	500	5	1.14	-	-	-	-	-	-	-1.10	-	-	0.86
3.0	0.0	600	5	5.10	-	1.83	-	26.42	-	32.78	-5.10	-	-	3.99

^a conversion

^b Selectivity to CO and CO₂ as the carbon basis

^c The loss carbon defined as coke

^d Ethylene yield

Table 13 Products from the reaction of 3% C₂H₆ and 3% N₂O over 0.100g zeolites at 500 °C in the total flow rate 100 cm³/min.

Sample	Time on stream (min)	Conversion (%)		Selectivity (%)						Y _{C₂H₄} ^c (%)	Consumption/Production rate (mole/kg-h)		
		C ₂ H ₆	N ₂ O	C ₂ H ₄	CH ₄	C ₃ H ₆	C ₄ H ₈	CO _x ^a	Deposit ^b		N ₂ O	C ₂ H ₆	C ₂ H ₄
ZSM-5(25)	5	52.2	100	37.8	2.89	9.74	0.70	11.3	32.9	19.7	80.38	41.96	15.85
	180	31.0	51.2	59.4	3.24	7.43	0.85	11.6	6.12	18.4	41.08	24.87	14.76
BEA(26)	5	31.4	100	32.2	5.12	1.02	0.00	34.8	25.6	10.1	80.29	25.21	8.13
	180	28.5	100	36.4	10.7	9.98	0.00	41.9	0.32	10.4	80.32	22.89	8.33
FER(20)	5	31.2	78.8	41.2	0.58	11.2	0.26	24.6	19.1	12.8	63.32	25.07	10.32
	180	20.8	49.9	55.3	0.38	3.08	2.69	29.5	12.7	11.5	40.11	16.72	9.24
MOR(15)	5	23.4	44.8	48.2	1.20	3.06	6.16	13.7	28.9	11.3	35.99	18.80	9.06
	120	5.74	8.70	43.6	0.00	1.23	0.65	17.5	37.2	2.50	6.99	4.61	2.01
USY(30)	5	5.42	5.82	38.9	0.00	2.15	0.00	7.02	52.2	2.11	4.67	4.35	1.70
	60	4.32	3.12	37.4	0.00	1.57	0.00	5.49	55.8	1.62	2.71	3.47	1.30

^a Selectivity to CO and CO₂ as the carbon basis^b The loss carbon defined as coke^c Ethylene yield

MOR(15) is less active for N_2O conversion. The initial % C_2H_6 and N_2O conversions are only 23.4 and 44.8, respectively. MOR(15) is also less stable than ZSM-5(25), BEA(26), and FER(20). After 120 min time on stream the production rate over MOR(15) was decreased from 9.06 mol/kg·h to 2.01 mol/kg·h due to the high rate of carbon deposition. USY(30) is the less active for N_2O decomposition and C_2H_6 dehydrogenation were very low. The conversion of C_2H_6 and N_2O were only about 5%.

Computational study of N_2O decomposition over TMI zeolites

The N_2O decomposition over transition metal ion exchanged (TMI) zeolites has been studied extensively, but the detail mechanism over the metal is still in debate. The form of deposited metal is varied with the preparations and treatment processes (Joyner and Stockenhuber, 1999). The mononuclear ion sitting on the exchanged proton active site has been observed in a very dilute case (Choi, *et al.*, 2004; Schwider, *et al.*, 2005). In this section, the possible pathways for N_2O decomposition to form N_2 and O_2 over TM-ZSM-5 were studied. The complex structures, reaction energies profile and stability of the generated structures are discussed.

1. Methods and models selection

The TM-ZSM-5 structure was optimized by ab initio (HF and MP2) and DFT (B3LYP and new functional M06 series) methods using various basis functions. Compared to the popular B3LYP functional, the exchange-correlation functional term of M06 series is modified by adding a portion of the Hartree-Fock exchange energy to the total exchange-correlation energy with fraction of 0.00, 0.27 and 0.54 for M06-L, M06 and M06-2X, respectively (Zhao and Truhlar, 2009). Basis sets of 6-31G**, 6-311++G**, and aug-cc-pvtz were used.

The optimized geometries of N_2O calculated at various methods are shown in Table 14. The equilibrium N-N and N-O bond distances obtained from microwave spectroscopy and infrared spectroscopy are 1.128 and 1.184 Å, respectively (David,

2005). These bond distances calculated of by HF method and various basis sets are shorter than the experimental values. MP2, B3LYP and the new density functionals, M06 series, give results close to the experimental values.

Table 14 The optimized geometry of N₂O

Method	Basis set	Optimized structure		
		N-N (Å)	N-O (Å)	N-N-O angle (°)
HF	6-31G**	1.092	1.179	180.000
HF	6-311++G**	1.085	1.171	180.000
HF	Aug-cc-pvtz	1.082	1.169	180.000
MP2	6-31G**	1.154	1.176	179.735
MP2	6-311++G**	1.156	1.175	179.905
MP2	Aug-cc-pvtz	1.155	1.181	180.000
B3LYP	6-31G**	1.136	1.195	179.981
B3LYP	6-311++G**	1.125	1.185	180.000
B3LYP	Aug-cc-pvtz	1.121	1.184	180.000
M06	6-31G**	1.133	1.182	180.000
M06	6-311++G**	1.123	1.173	180.000
M06	Aug-cc-pvtz	1.118	1.172	180.000
M06L	6-31G**	1.142	1.188	179.880
M06L	6-311++G**	1.141	1.189	179.981
M06L	Aug-cc-pvtz	1.118	1.172	180.000
M062X	6-31G**	1.131	1.200	179.959
M062X	6-311++G**	1.115	1.180	180.000
M062X	Aug-cc-pvtz	1.111	1.180	180.00
Experiment		1.126 ^a	1.186 ^a	-

^a equilibrium value from IR spectroscopy and microwave spectroscopy

The validations of models were performed on Fe-ZSM-5 in order to find a suitable cluster size which can represent the whole ZSM-5 framework. The tested

models are 5T, 96T, 128T and 144T framework structures. General configurations of high level parts are shown in Figure 31. The optimized geometries parameters of Fe-O bond length and Fe-Al distance are summarized in Table 15.

The optimized structures were compared with the experimental data. The Fe-O and Fe-Al distances measured from EXAFS are about 1.6 and 2.5 Å, respectively (Choi, *et al.*, 2003). For all DFT functional, the Fe-O3 distance in the FeO-ZSM-5 is predicted to be 1.63-1.651 Å for all models. The Fe-O3 and Fe-O4 distances in FeO₂-ZSM-5 case are slightly longer (0.01-0.03 Å) than that in the FeO-ZSM-5. However, the predicted Fe-O bond length is in the range of experimental report. Moreover, the predicted Fe-Al distances are ranging between 2.80-2.87 Å which in the range of isolated Fe (Choi, *et al.* 2003; Pringruber, *et al.* 2006). Only M06-2X can predict two forms of FeO₂ structures as planar and tetrahedral structures. The tetrahedral form is more stable than the planar form by 10.86 kcal/mol.

The N₂O adsorption energy over Fe-ZSM-5 was also tested by various DFT methods. N₂O is adsorbed via its oxygen atom pointing to the Fe-atom. The adsorption energies obtained from various models and methods are presented in Table 16. Wood and coworkers were reported the adsorption energy of N₂O over Fe-ZSM-5 from experimental studied is -16.0 kcal/mol (Wood *et al.*, 2002). The microcalorimetry of

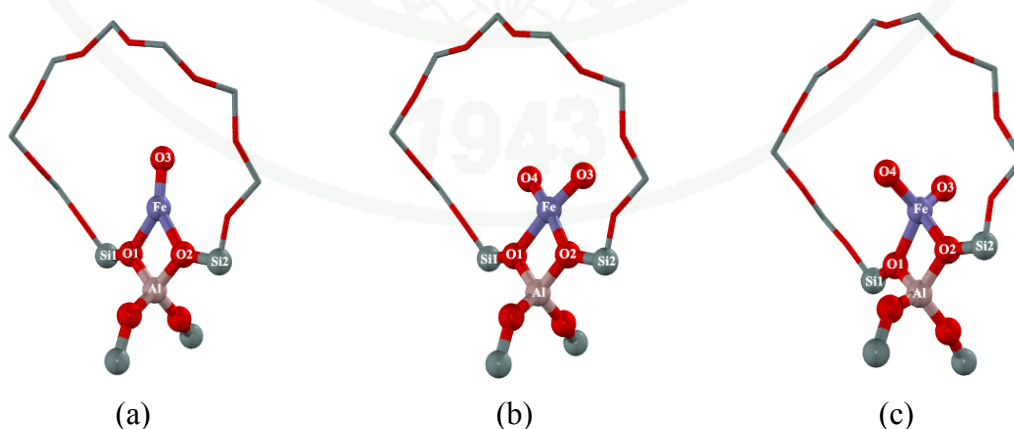


Figure 31 General configurations of high level parts in FeO_x-ZSM-5 (a) FeO-ZSM-5, (b) FeO₂-ZSM-5 and (c) FeO₂-ZSM-5 in tetrahedral form.

Table15 The optimized geometry of Fe-O and Fe-O₂ in ZSM-5 with various methods and models

Method	Zeolite Model	Form of FeOx	Bond length (Å)			Dihedral (°)
			Fe-O3	Fe-O4	Fe-Al	O4-O3-O2-O1
B3LYP	12T/144T	[FeO] ⁺	1.651	-	2.870	-
		[OFeO] ⁺	1.663	1.667	2.836	163.343
	12T/128T	[FeO] ⁺	1.651	-	2.870	-
		[OFeO] ⁺	1.664	1.665	2.831	148.314
	12T/96T	[FeO] ⁺	1.651	-	2.870	-
		[OFeO] ⁺	1.662	1.668	2.834	148.693
M06	5T	[FeO] ⁺	1.638	-	2.832	-
		[OFeO] ⁺	1.667	1.667	2.836	155.090
	12T/128T	[FeO] ⁺	1.637	-	2.842	-
		[OFeO] ⁺	1.662	1.661	2.814	170.680
	12T/96T	[FeO] ⁺	1.638	-	2.840	-
		[OFeO] ⁺	1.658	1.663	2.808	158.705
M06-L	5T	[FeO] ⁺	1.634	-	2.826	-
		[OFeO] ⁺	1.663	1.664	2.806	147.603
	12T/128T	[FeO] ⁺	1.651	-	2.871	-
		[OFeO] ⁺	1.673	1.673	2.828	173.892
	12T/96T	[FeO] ⁺	1.651	-	2.867	-
		[OFeO] ⁺	1.673	1.673	2.829	174.621
M06-2X	5T	[FeO] ⁺	-	-	-	-
		[OFeO] ⁺	1.676	1.675	2.831	165.767
	12T/128T	[FeO] ⁺	1.639	-	2.860	-
		[OFeO] ⁺	1.664	1.664	2.838	172.857
	12T/96T	[FeO] ⁺	1.639	-	2.859	-
		[OFeO] ⁺	1.662	1.666	2.838	172.623
		[OFeO] ⁺ *	1.662	1.851	1.794	77.940

* Tetrahedral structure

Table 16 N₂O adsorption Energy over FeO_x/ZSM-5 optimized by ONIOM2 model

Zeolites model	Adsorption energy of N ₂ O (kcal/mol)							
	B3LYP		M06		M06L		M06-2X	
	[FeO] ⁺	[OFeO] ⁺	[FeO] ⁺	[OFeO] ⁺	[FeO] ⁺	[OFeO] ⁺	[FeO] ⁺	[OFeO] ⁺
12T/128T	-10.74	-8.17	-16.90	-14.57	-15.84	-13.18	-21.36	-18.90
12T/96T	-10.70	-8.61	-16.65	-14.90	-15.74	-13.85	-21.09	-20.09
Experiment	-16 kcal/mol							

N₂O adsorption on Fe-ZSM-5 reported the adsorption energy of 16.3 kcal/mol at low N₂O loading and the adsorption energy decreasing with N₂O adsorbed amount (Rakic *et al.*, 2005). In the ONIOM model using B3LYP method, the adsorption energy is calculated to be -11.1 kcal/mol. Whereas, in the case of 5T bare cluster, the computed adsorption energy is only about -6 kcal/mol (Ryder *et al.*, 2002). Therefore, the addition of the van der Waals interactions with the zeolite pore increases the interaction energy about two fold. The adsorption energies from ONIOM calculation with M06 and M06-L are in the range of -13.2 to -16.9 kcal/mol over [FeO]⁺- and [OFeO]⁺-ZSM-5. M06-2X predicted the overestimated adsorption energy. This can be the effect of the high Hartree Fock exchange energy. It should be concluded that B3LYP, and M06 series are suitable for the system of N₂O and FeO_x-ZSM-5. Moreover, ZSM-5 model with 96T or more are proper to this study.

2. N₂O decomposition over various Fe-zeolites

In this study, the effect of the intra-crystalline nanostructured pore network on the activity of Fe exchanged zeolites (ZSM-5, BEA, FER and FAU) for N₂O decomposition. Since the intention was to study theoretically the intrinsic activity of the iron species located in the frameworks of different zeolites, the iron species were placed on top of the highly accessible ion-exchange site of each zeolite. The zeolite frameworks were modeled by 12T/144T for FER and ZSM-5, 14T/176T for BEA, and 14T/84T for FAU, respectively. All structures were optimized by ONIOM

(B3LYP:UFF). The structure of the N_2O adsorption on iron species at the active sites inside the different zeolite morphologies was presented in Figure 32. The geometric parameters for all structures are summarized in Table 17.

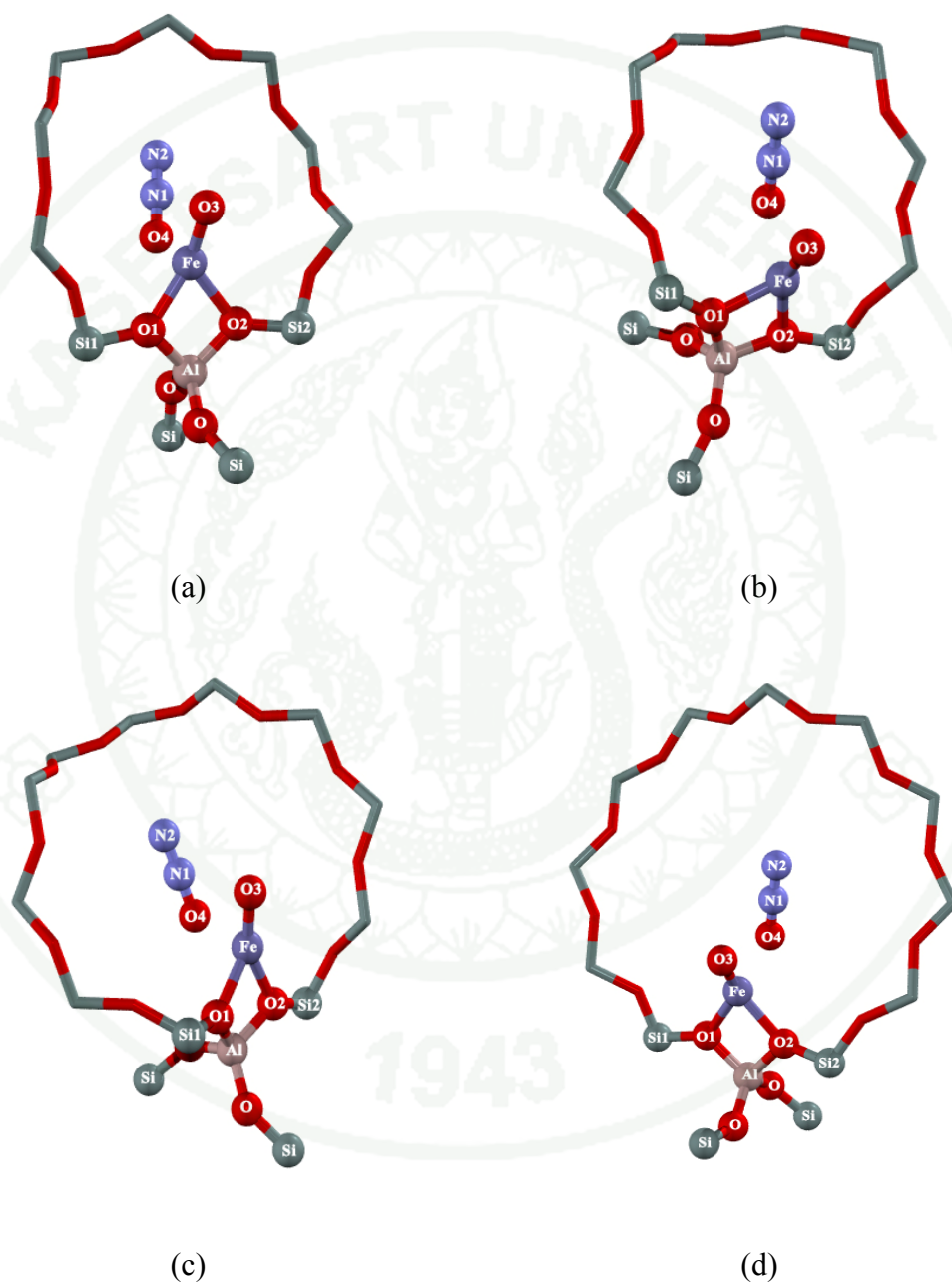


Figure 32 ONIOM model of nitrous dioxide on the Fe-Zeolite: (a) Fe-ZSM-5 12T/144T, (b) Fe-FER 12T/114T, (c) Fe-BEA 14T/176T and (d) Fe-FAU 14T/84T

Table 17 The optimized geometric parameters of the isolated zeolite cluster, adsorption intermediates and transition states (TS) for nitrous oxide decomposition over Fe-Zeolite by ONIOM (B3LYP:UFF)

	Fe-ZSM-5				Fe-FER				Fe-BEA				Fe-FAU			
	N ₂ O+ [FeO]	N ₂ O/ [FeO]	TS	N ₂ + [FeO ₂]	N ₂ O+ [FeO]	N ₂ O/ [FeO]	TS	N ₂ + [FeO ₂]	N ₂ O+ [FeO]	N ₂ O/ [FeO]	TS	N ₂ + [FeO ₂]	N ₂ O+ [FeO]	N ₂ O/ [FeO]	TS	N ₂ + [FeO ₂]
Fe-Al	2.870	2.876	2.832	2.836	2.863	2.872	2.836	2.787	2.863	2.848	2.812	2.789	2.847	2.854	2.844	2.825
Fe-O1	2.065	2.083	2.085	1.999	2.041	2.052	2.042	1.996	2.050	2.082	2.033	2.017	2.055	2.067	2.059	2.010
Fe-O2	1.999	2.026	1.968	1.974	2.060	2.076	2.009	2.002	2.061	2.069	2.053	2.000	2.053	2.070	2.030	2.020
Fe-O3	1.651	1.663	1.622	1.663	1.658	1.671	1.621	1.659	1.650	1.662	1.619	1.658	1.648	1.664	1.619	1.663
Fe-O4	-	2.268	1.816	1.667	-	2.308	1.826	1.673	-	2.284	1.817	1.665	-	2.263	1.812	1.660
Fe-N1	-	3.116	3.021	-	-	3.015	2.996	-	-	3.023	3.011	-	-	3.002	3.018	-
N1-O2	1.193	1.212	1.555	-	1.193	1.211	1.546	-	1.193	1.213	1.534	-	1.193	1.215	1.555	-
N1-N2	1.134	1.125	1.133	1.106	1.134	1.125	1.137	1.106	1.134	1.125	1.134	1.106	1.134	1.124	1.134	1.106
O1-O2	-	3.124	2.722	2.268	-	2.949	2.703	2.314	-	2.920	2.647	2.284	-	2.974	2.701	2.287
O1-Fe-O2	-	104.2	104.6	85.9	-	94.3	103.1	88.0	-	94.2	100.6	86.8	-	97.2	103.7	87.0
Si1-O3-Al	125.8	125.7	125.9	124.3	141.0	141.6	140.7	140.4	127.6	127.4	127.0	126.9	124.5	129.8	124.6	125.0
Si2-O4-Al	129.9	130.2	129.3	130.6	150.9	150.9	150.1	149.4	131.1	131.5	130.0	131.0	129.6	124.8	129.5	128.7
Fe-O2-N1	-	124.3	127.2	-	-	114.2	125.2	-	-	116.3	127.7	-	-	116.1	127.2	-

In BEA and FAU zeolites, the iron cation is located at the ion-exchange site of the 12-membered ring pore channel with ellipsoidal and circular openings of 0.66 x 0.67, and 0.74 nm for BEA and FAU zeolites, respectively. Moreover, the Fe-FAU site is accessible from the supercage, which is a large cavity with an approximate size of 1.12 x 1.22 nm. Despite the different pore sizes and geometries, the local structures around the iron are not much different. In all cases, the iron cation is coordinated by two oxygen bridging atoms (O3 and O4) of the zeolite. The Fe-O bond distances are in the range of 2.00-2.07 Å and the Fe-Al distances are in the range of 2.85-2.87 Å. The iron atom (Fe^{II}) is covalent bonded to the O- radical anion (O1) with a bond distance of 1.65-1.66 Å. In ZSM-5 framework these bonds are about 2 Å which well correlated with EXAFS reported (Park, *et al.*, 2008; Choi *et al.*, 2004; Jia *et al.*, 2002). In others framework, these bonds are optimized to be similar range.

The geometries of the iron species slightly change upon the adsorption of a nitrous oxide molecule. In all cases, the Fe-O1 bond distance is slightly increased, by ~0.01 Å, and the distance between the iron and the oxygen atom of the adsorbed nitrous oxide (O2) ranges from 2.26-2.31 Å. The adsorbed N_2O configurations in each zeolites framework are also shown in Figure 33. The adsorption energy is computed to be -11.4, -11.1, -9.7, and -10.0 kcal/mol for Fe-FER, Fe-ZSM-5, Fe-BEA, and Fe-FAU, respectively. It can be concluded that the different types of zeolite framework do not affect the adsorption energy of small molecule like N_2O .

Then the N-O bond of adsorbed nitrous oxide molecule breaks to give an oxygen atom attached to the iron site and a nitrogen molecule. The structure of the transition state in Fe-FER is shown for this case in Figure 33 and it similar to other zeolites. At the transition state, the N-O bond of the nitrous oxide is breaking and a new Fe-O bond is forming. The relative energies of the transition states are computed to be 24.9, 28.0, 28.0, and 27.3 kcal/mol for Fe-FER, Fe-ZSM-5, Fe-BEA and Fe-FAU, respectively. The ONIOM method has shown the important effect of zeolite framework that is included by the UFF force field. Only quantum cluster calculations would give the activation energies to be 28.0, 30.3, 29.5, and 28.0 kcal/mol for Fe-FER, Fe-ZSM-5, Fe-BEA and Fe-FAU, respectively. The van der Waals interactions with the zeolite framework stabilize the transition state complexes by 3.1, 2.3, 1.5, and

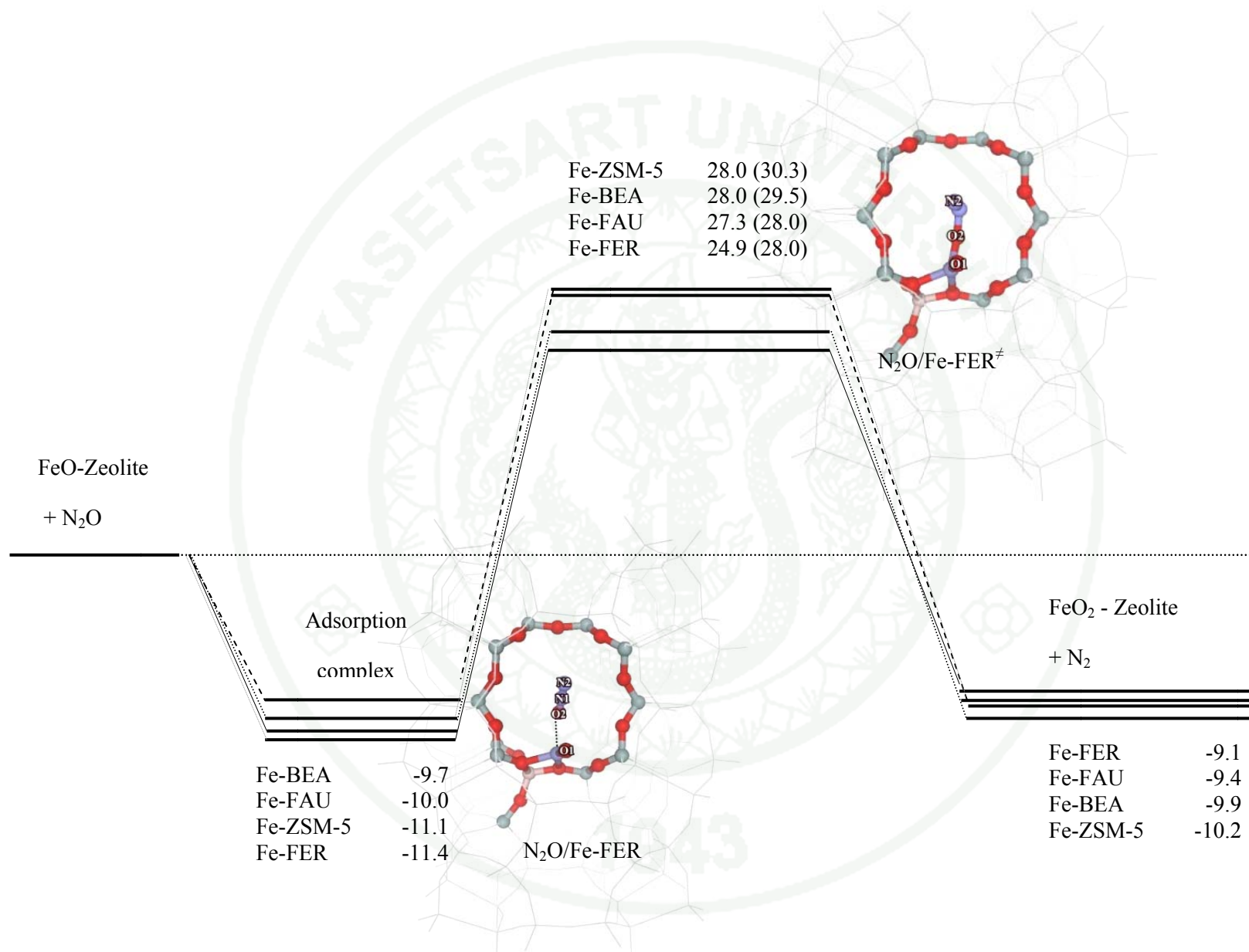


Figure 33 Energy Profile (kcal/mol) for nitrous decomposition over Fe-Zeolite. The uncertainties are discussed in the text.

0.7 kcal/mol, respectively. While the uncertainties in the absolute values of the energies, essentially due to the computational method, can be estimated to be about ± 2 kcal/mol, the uncertainties in the energy differences are of the order of ± 0.5 kcal/mol. The transition state in the Fe-FER can thus be said to be significantly lower than in other zeolites since the smallest pore in Fe-FER exerts the strongest confinement effect. In other zeolites (Fe-ZSM-5, Fe-BEA, and Fe-FAU), the reaction takes place inside relatively large pores or large cavities and there is thus not much difference in the confinements. Therefore, the intrinsic activity trend for the nitrous oxide decomposition is Fe-FER > Fe-BEA \sim Fe-ZSM-5 \sim Fe-FAU. The observed activity trend from temperature programmed reaction is Fe-FER > Fe-BEA > Fe-ZSM-5 \gg Fe-FAU. This trend is in agreement with the result of Mauvezin *et al.* (Mauvezin *et al.*, 2001). The high activity of the Fe-FER can be explained by the high intrinsic activity observed in the computational model. Although the intrinsic activity of Fe-BEA and Fe-ZSM-5 are comparable, the observed higher activity of Fe-BEA could result from the faster transport of reactants and products in the larger pore network of the beta zeolite.

The observed activity of Fe-FAU disagrees with the model of intrinsic activity because the model catalytic site might not be present in real Fe-FAU. Faujasite contains many ion-exchange sites. In the model, we took the most accessible site to avoid mass transfer limitations. However, in the real faujasite, cations such as Fe^{II}, Fe^{III} and Cu^{II} are known to be preferentially exchanged at the sites I and I', where they are stabilized by coordinating with three bridging oxygen atoms of the 6-membered ring face of the sodalite unit (Fowkes *et al.*, 2002; Drake *et al.*, 2006). The cations at these sites (I and I') are thus located inside the sodalite cage and are very difficult to access by any reactants. If these sites were relevant, the nitrous oxide decomposition in Fe-FAU would suffer from severe transport limitation. As reflected by the low catalytic activity, this could be the case.

The intrinsic activity of iron oxide-exchanged zeolites for the decomposition of nitrous oxide by the ONIOM2 scheme shows the effect of pore network. The confinement effect of nanostructure pore network stabilizes the adsorbed species, intermediates, and transition states inside the zeolites. This confinement effect is more

pronounced in a small pore zeolite, Fe-FER, and causes the highest activity for N_2O decomposition. For medium- and large-pore zeolites, there is no substantial difference since the nitrous oxide molecule is much smaller than the pore sizes. Therefore, the predicted intrinsic activity trend is $\text{Fe-FER} > \text{Fe-ZSM-5} \sim \text{Fe-BEA} \sim \text{Fe-FAU}$. The experimentally observed activity trend is in agreement with the intrinsic activity for Fe-FER, Fe-ZSM-5, and Fe-BEA but not for Fe-FAU. In Fe-FAU, the decomposition of nitrous oxide seems to be under severe transport limitation because the iron cations could be preferentially located at six-membered ring of sodalite unit, which has a very small pore opening.

3. N_2O decomposition over TM-ZSM-5 zeolites

Theoretical study of N_2O decomposition over Fe-ZSM-5, Co-ZSM-5 and Ni-ZSM-5 exchanged at Brønsted site over ZSM-5 were performed with ONIOM method. 96T cluster of ZSM-5 was chosen as the studied model and it was divided into two parts. The active region (12T and the active Fe site) is treated with new functional M06 method, while the rest is treated with UFF force field. The 96T model of ZSM-5 with various transition metals (TMs) is presented in Figure 34.



Figure 34 Parameter and atomic label defined for TM-ZSM-5 (TM=Fe, Co, and Ni) gases optimized structures [structure (I): TM-O-ZSM-5 straight channel (a) and TM-O-ZSM-5 zigzag channel (b); structure (IV): TM-O2-ZSM-5 straight channel (c) and TM-O2-ZSM-5 zigzag (d); and structure (VIII) TM-O2-ZSM-5 straight channel (e) and TM-O2-ZSM-5 zigzag channel (f)]

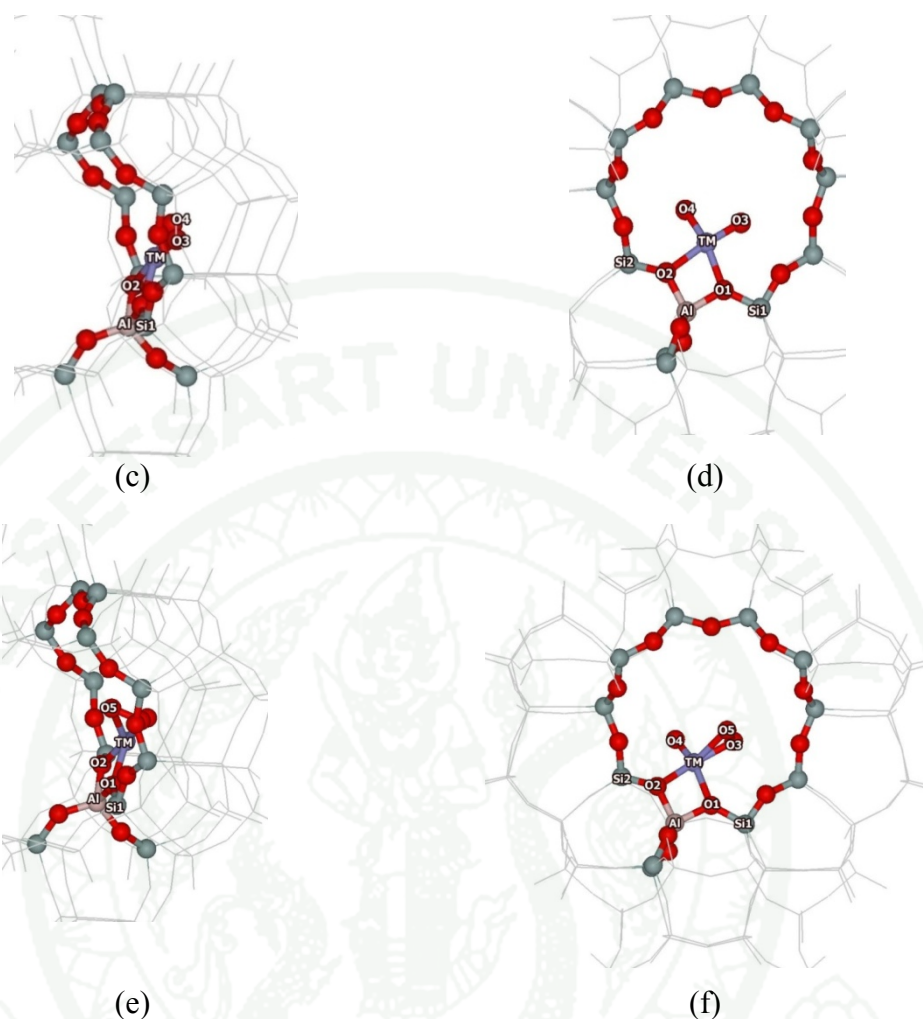


Figure 34 Continued

The isolated TM-O bond lengths in TMO-ZSM-5 were optimized to be 1.638, 1.621, and 1.614 Å for Fe-, Co-, and Ni-ZSM-5, respectively. Bond distances are correlated with metal ion size which decreases across the row, which metal size of Fe>Co>Ni. Distances from transition metal atom to framework oxygen are about 2 Å and bond length of Fe-O>Co-O>Ni-O. The Fe-O distance in Fe-ZSM-5 had been discussed in previous topic. Co-O distances that of 1.950 Å to 2.018 Å are also correlated with the literature reported. Bell group reported the Co-O bond distance in Co-ZSM-5 optimized by fitting EXAFS signal with DFT calculation to be 2.08 Å (Rice *et al.*, 1998). Later, they using B3LYP method the optimized Fe-O distance in 5T cluster was reported as 1.68 Å for FeO- and FeO₂-ZSM-5 which are in similar

range as this calculation (Heyden *et al.*, 2005). Ni-ZSM-5 is also show the same value around 2 Å. This similar starting metal structure can further directly compare.

When the first N₂O molecule adsorbed over TM-ZSM-5, the N-O bond was increased from 1.182 Å (isolated N₂O) to 1.198, 1.197, and 1.193 Å after adsorbed on FeO-, CoO-, and NiO-ZSM-5, respectively. While the N-N bond decrease from 1.133Å in isolated N₂O to 1.125, 1.126, and 1.128 Å after form the adsorption complexes with FeO-, CoO-, and NiO-ZSM-5, respectively. It can see that the increasing of N-O bond and decreasing of N-N bond distance obey the metal size. This N₂O structural change is similar to the study of Heyden and coworkers (Heyden *et al.*, 2005). The adsorbed N₂O is still a linear molecule. After N₂O adsorption, distance between TM atom and framework oxygen (TM-O1 and TM-O2) and TM and Al atom are slightly increased. Structural parameter and atomic label for N₂O decompositions over TM-O ZSM-5 are defined in Figure 35. The optimized distances and bond angles are present in Table 18, 19, and 20 for Fe-, Co-, and Ni- ZSM-5, respectively.

The calculated adsorption energy of N₂O molecule over Fe-ZSM-5, Co-ZSM5, and Ni-ZSM-5 are -16.7, -14.9, and -10.8, respectively. Ryder and coworker were reported the adsorption energy of N₂O on FeO- and CoO-ZSM5 optimized by B3LYP as -6.6 and -5.2 kcal/mol, respectively (Ryder *et al.*, 2002). The adsorption energy over Fe-ZSM-5 was also higher than over Co-ZSM-5 as found in this work. However, the calculation of Fellah and coworker, report the higher adsorption energies over CoO-ZSM-5 than FeO-ZSM-5 about 5 kcal/mol. They reported the adsorption energy of -19.9 and -24.8 for FeO-and CoO-ZSM-5, respectively. The adsorption energy of N₂O over Fe-ZSM-5 and Co-ZSM-5 by microcalorimetry are in similar as about -16 kcal/mol (Rakic *et al.* 2005). Moreover, they found that the amounts of N₂O molecule chemisorptions are also equal. It can be estimate that the adsorption structure should be in similar form. The calculation result in this study can predict the well correlated value to the experimental study.

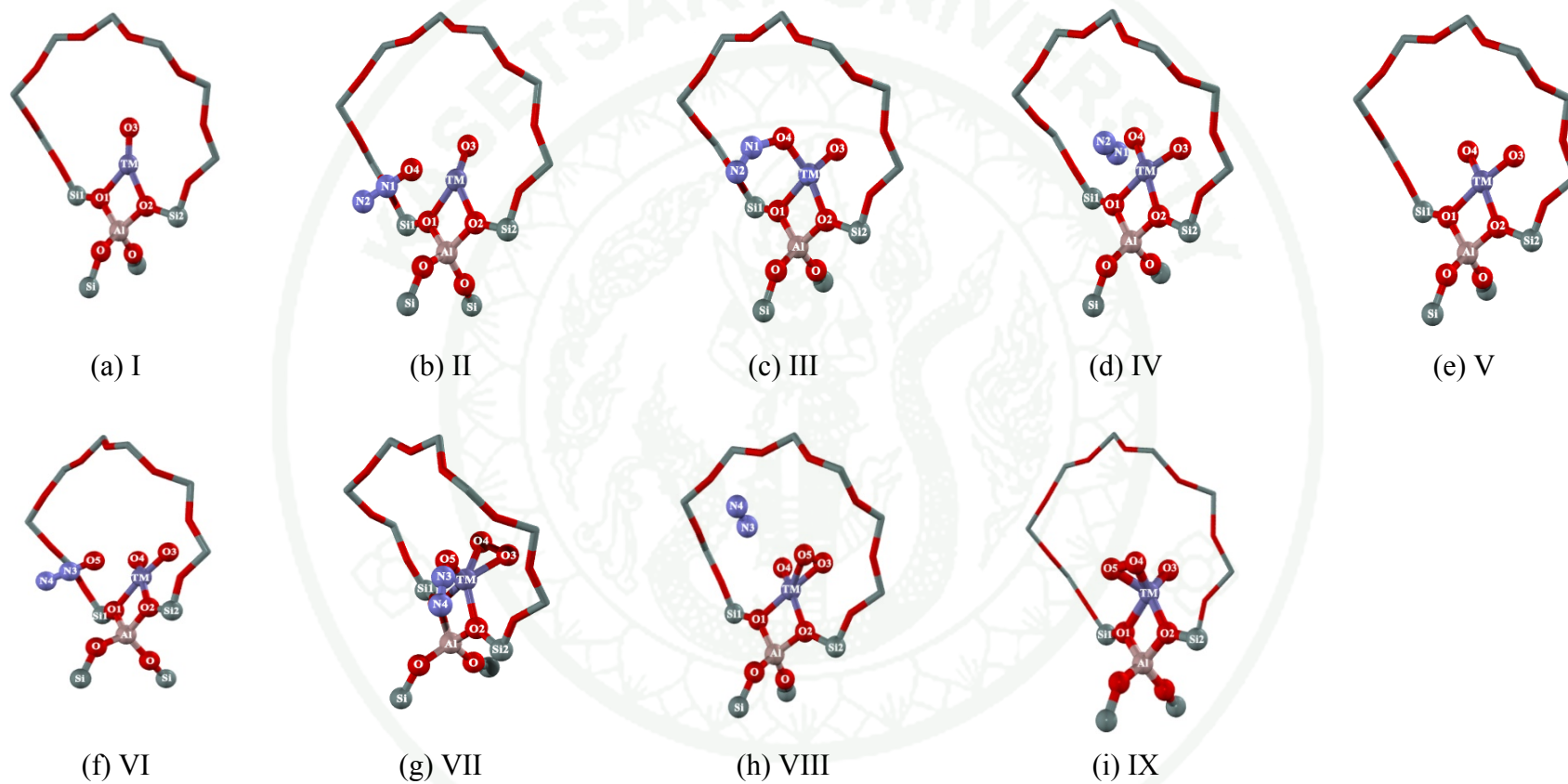


Figure 35 Parameter and atomic label defined for N_2O decompositions over TM-O ZSM-5 (TM=Fe, Co, and Ni) gases optimized structures (a) I, (b) II, (c) III, (d) IV, (e) V, (f) VI (g) VII, (h) VIII, and (i) IX

Table 18 Optimized geometric parameters of the isolated zeolite cluster, adsorption intermediates and transition states for nitrous oxide decomposition over Fe-ZSM-5

Parameter	Structure								
	I	II	III	IV	V	VI	VII	VIII	IX
Fe-Al	2.840	2.858	2.818	2.809	2.808	2.840	2.837	2.809	2.807
Fe-O1	2.045	2.083	2.038	1.983	1.954	2.020	2.064	2.015	2.017
Fe-O2	1.984	2.010	1.942	1.959	1.988	1.984	1.946	1.962	1.959
Fe-O3	1.638	1.643	1.620	1.667	1.658	1.663	1.658	1.610	1.889
Fe-O4	-	2.280	1.809	1.657	1.663	1.667	1.746	1.889	1.610
Fe-O5	-	-	-	-	-	2.307	1.922	2.047	2.045
Fe-N1	-	3.067	2.935	4.850	-	-	-	-	-
Fe-N3	-	-	-	-	-	3.076	3.132	-	-
N1-O4	-	1.198	1.596	5.524	-	-	-	-	-
N3-O5	-	-	-	-	-	1.197	1.704	3.358	-
O3-O4	-	3.334	2.700	2.283	-	2.281	2.407	2.778	2.783
O3-O5	-	-	-	-	-	3.130	1.915	3.469	1.290
O4-O5	-	-	-	-	-	3.115	3.267	1.290	3.470
O1-Al-O2	89.121	89.993	88.654	87.358	87.376	88.078	88.399	89.046	89.117
O1-Fe-O2	73.970	72.983	74.687	74.635	74.604	73.626	73.723	75.073	75.162
O3-Fe-O4	-	115.447	103.727	86.769	87.172	86.457	89.995	104.862	105.116
O3-Fe-O5	-	-	-	-	-	102.159	64.203	142.833	38.019
O4-Fe-O5	-	-	-	-	-	102.709	125.871	37.989	143.130
N1-N2	-	1.125	1.132	1.105	-	-	-	-	-
O4-N1-N2	-	178.904	123.546	122.120	-	-	-	-	-
N3-N4	-	-	-	-	-	1.126	1.106	1.105	-
O5-N3-N4	-	-	-	-	-	178.889	170.673	134.348	-

Table 19 The optimized geometric parameters of the isolated zeolite cluster, adsorption intermediates and transition states for nitrous oxide decomposition over Co-ZSM-5

Parameter	Structure								
	I	II	III	IV	V	VI	VII	VIII	IX
Co-Al	2.805	2.838	2.801	2.767	2.762	2.773	2.856	2.780	2.800
Co-O1	2.018	2.097	2.038	1.952	1.942	1.958	2.070	1.942	2.010
Co-O2	1.950	1.961	1.952	1.920	1.915	1.924	1.972	1.965	1.956
Co-O3	1.621	1.626	1.650	1.652	1.651	1.650	1.695	1.840	1.843
Co-O4	-	2.242	1.790	1.651	1.650	1.650	1.638	1.616	1.610
Co-O5	-	-	-	-	-	2.872	1.787	2.143	2.015
Co-N1	-	3.036	2.934	2.903	-	-	-	-	-
Co-N3	-	-	-	-	-	3.526	2.979	4.903	-
N1-O4	-	1.197	1.623	3.321	-	-	-	-	-
N3-O5	-	-	-	-	-	1.186	1.672	3.360	-
O3-O4	-	3.190	2.876	2.295	-	2.288	2.305	2.505	2.760
O3-O5	-	-	-	-	-	3.920	3.106	2.968	3.386
O4-O5	-	-	-	-	-	3.467	2.626	1.262	1.271
O1-Al-O2	89.903	89.938	89.594	87.320	87.004	87.636	88.539	87.828	89.131
O1-Co-O2	75.129	73.567	75.044	76.054	76.240	76.514	72.909	75.611	75.156
O3-Co-O4	-	110.064	113.382	88.032	87.991	87.775	87.518	92.699	105.950
O3-Co-O5	-	-	-	-	-	117.632	126.276	35.946	137.812
O4-Co-O5	-	-	-	-	-	96.379	100.038	103.440	38.135
N1-N2	-	1.125	1.117	1.104	-	-	-	-	-
N3-N4	-	-	-	-	-	1.130	1.114	1.105	-
O4-N1-N2	-	178.604	143.704	127.441	-	-	-	-	-
O5-N3-N4	-	-	-	-	-	179.714	142.312	136.282	-

Table 20 The optimized geometric parameters of the isolated zeolite cluster, adsorption intermediates and transition states for nitrous oxide decomposition over Ni-ZSM-5

Parameter	Structure								
	I	II	III	IV	V	VI	VII	VIII	IX
Ni-Al	2.781	2.810	2.818	2.735	2.730	2.830	2.825	2.806	2.744
Ni-O1	2.013	2.049	2.049	1.918	1.913	2.042	2.117	2.045	1.938
Ni-O2	1.917	1.952	1.967	1.914	1.910	1.982	1.912	1.929	1.928
Ni-O3	1.614	1.615	1.661	1.652	1.654	1.756	1.672	2.328	1.989
Ni-O4	-	2.378	1.763	1.712	1.704	1.739	1.756	3.119	2.739
Ni-O5	-	-	-	-	-	2.542	1.925	1.618	1.716
Ni-N1	-	3.114	2.958	2.900	-	-	-	-	-
Ni-N3	-	-	-	-	-	3.289	3.003	6.055	-
N1-O4	-	1.193	1.709	3.302	-	-	-	-	-
N3-O5	-	-	-	-	-	1.190	1.646	3.411	-
O3-O4	-	3.152	2.952	2.393	2.398	2.493	2.575	2.814	1.225
O3-O5	-	-	-	-	-	3.941	3.443	2.003	2.481
O4-O5	-	-	-	-	-	2.983	1.899	1.201	2.454
O1-Al-O2	88.915	89.489	89.691	87.689	87.455	89.316	89.776	89.036	110.921
O1-Ni-O2	75.853	74.097	74.229	77.205	77.283	73.825	73.760	74.775	770.72
O3-Ni-O4	-	102.569	119.097	90.698	91.120	91.044	97.307	89.109	23.940
O3-Ni-O5	-	-	-	-	-	132.067	146.267	70.379	82.601
O4-Ni-O5	-	-	-	-	-	86.199	61.926	19.311	62.830
N1-N2	-	1.128	1.110	1.104	-	-	-	-	-
O4-N1-N2	-	179.260	147.115	125.768	-	-	-	-	-
N3-N4	-	-	-	-	-	1.128	1.107	1.105	-
O5-N3-N4	-	-	-	-	-	179.498	172.864	135.673	-

At the transition states, the N-N bond in all complexes is contracted from the adsorption structure. The N1-O4 bond between N atom and O atom in N₂O molecule, are lengthening and ready to crack while the TM-O4 distances are contracted indicating the dissociation of the N-O bond. In Fe-ZSM-5 N1-O4 bond length increases from 1.198 to 1.596 Å similar to values calculated by Heyden *et al.* (Heyden *et al.*, 2005). The N1-O4 bond length in Co-ZSM-5 and Ni-ZSM-5 are also increase from 1.197 to 1.623 Å and 1.193 to 1.709 Å, respectively. In this state, the N2-N1-O4 bond angle is changed from 179° to 124°, 144°, and 147° for Fe-, Co-, and Ni-ZSM-5, respectively. Heyden *et al.* were also reported the bending N-N-O bond angle in transition state structure cover FeO-ZSM-5 as 143.6° (Heyden *et al.*, 2005). N-N-O bond angle predicted in this Fe-ZSM-5 is more bent than the literature reported. The longer N1-O4 distance can observe in the smaller bending N-N-O structure and related with the lower activation energy.

The relative energy of each complex is shown in Table 21. The apparent activation energies of N₂O decomposition are calculated to be 28.9, 34.5 and 49.5 kcal/mol for Fe-, Co-, Ni-ZSM-5, respectively. The reaction energy profile of N₂O decomposition over Fe-ZSM-5, CoZSM-5, and Ni-ZSM-5 were shown in Figure 36. These results are in the same range with the work of Ryder. They calculated the activation energy of N₂O over FeO- and CoO-ZSM-5 as 37.6 and 32.9 kcal/mol, respectively (Ryder *et al.*, 2002). Later reported by Fellah and coworkers, the activation energies are 58.1 and 48.6 for FeO- and CoO-ZSM-5, respectively (Fellah *et al.*, 2008). The reported values are very high since they optimized only the bond distance and constrain N₂O structure in linear form.

Activation energy of N₂O over Fe-ZSM-5 was reported in the wide range of energy. Pirutko and coworkers reported around 48-52 kcal/mol which vary to the Fe concentration. The lower Fe content is higher activation energy (Pirutko *et.al*, 2009). Wood *et al.* reported the activation energy over Fe-ZSM-5 in the same range as 44.2 kcal/mol (Wood *et al.*, 2004). Catalytic decomposition of N₂O over TMI-ZSM-5 has been reported by Abu-Zied and coworkers. The activity trend following on set temperature on metal species are Co>Fe>>Ni. However, at reaction temperature higher than 350 °C, Fe-ZSM-5 shows higher catalytic activity than Co-ZSM-5 (Abu-

Table 21 Relative energy for adsorption complex during N₂O decomposition over TM-ZSM-5

Structure	Relative energy (kcal/mol)		
	Fe-ZSM-5	Co-ZSM-5	Ni-ZSM-5
I + 2N ₂ O	0	0	0
II + N ₂ O	-16.7	-14.9	-10.8
III + N ₂ O	28.9	34.5	49.5
IV + N ₂ O	-3.8	6.2	23.4
V + N ₂ + N ₂ O	0.7	11.0	28.2
VI + N ₂	-14.2	2.9	16.9
VII + N ₂	42.8	56.0	75.8
VIII + N ₂	-23.2	-9.3	-10.8
IX + 2 N ₂	-17.7	-7.8	-0.4

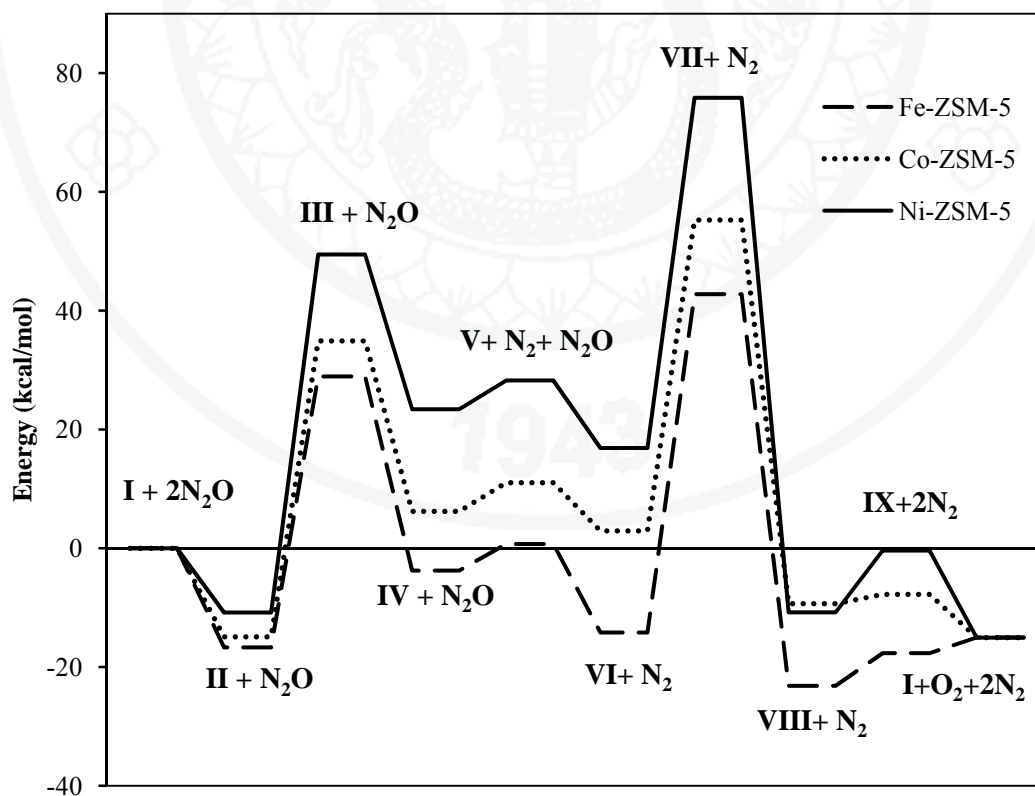


Figure 36 Energy profile of N₂O decomposition over TMO_x-ZSM-5

Zied *et al.*, 2008). Activation energy of N_2O decomposition over Co-ZSM-5 is about 35 kcal/mol for sample that Si/Al=50 and Co/Al=0.5. For the higher Co content, Si/Al=25-63, the activation energy was about 25 kcal/mol (Abu-Zied and Schwieger, 2009). Kapteijn *et al.* were reported activation energy for N_2O decomposition over Co-ZSM-5 and Fe-ZSM-5 as 25 and 40 kcal/mol, respectively (Kapteijn *et al.*, 1997). The activation energy over Co-ZSM-5 prepared by wet ion exchanged in the work of Smetts and coworker was about 29 kcal/mol (Smeets *et al.*, 2008). The activation energies in this calculation are close to the experimental results. N_2O decomposition over Ni-ZSM-5 used highest activation energy correlated with the lowest activity reported by Abu-Zeid and coworkers. However, the activation trend between Fe- and Co-ZSM-5 reverses the experimental reported because the rate determining step may be another step. The first N_2O prefers to decompose over Fe-ZSM-5 than Co-ZSM-5 and Ni-ZSM-5.

The produced N_2 molecule was desorbed with desorption energy 4.45, 4.84, and 4.84 kcal/mol for Fe-, Co-, and Ni-ZSM-5, respectively. The decomposition of N_2O over metal oxo produced the metal dioxo species. In Fe-ZSM-5, the Fe-O3 and Fe-O4 bond length are 1.67 Å which slightly increase from the FeO structure but is still in the values of isolated Fe from EXAFS (Choi, *et al.* 2003). The Fe-Al distance is still in the same range as the beginning structure. In Co-ZSM-5, the Co-O3 and Co-O4 are equal to 1.63 Å which equal to the Co-O3 distance in the CoO structure and in the range reported by Bell and coworker (Rice *et al.*, 1998). The structure of Ni-ZSM-5 structure was changed with the same trend as FeO_2 -ZSM-5.

After that, the second N_2O come to adsorb over the metal dioxo ZSM-5. N_2O adsorbed over dioxo species of TM-ZSM-5 through the oxygen atom with adsorption energies of -14.8, -8.1, and -11.4 kcal/mol for Fe-, Co-, Ni-ZSM-5, respectively. The adsorption forms over Fe- and Co-ZSM-5 are less exothermic than the adsorption over oxo metal. However, the adsorption on Ni-ZSM-5 shows the similar adsorption energy over oxo and dioxo species. The TM-Al distance and TM-O distance in all structures are increasing after this second N_2O came to adsorbed. This adsorbed N_2O can be decomposing through the transition structure. The apparent activation energies for the

second N_2O decomposition over TM-ZSM-5 are 42.8, 56.0, and 75.8 kcal/mol for Fe-, Co-, Ni-ZSM-5, respectively. The intrinsic activation energy of N_2O decomposition over different metal structures are in the same range. The second N_2 desorption were 5.5, 1.6 and 10.4 kcal/mol from FeO_3^- , CoO_3^- , and NiO_3^- -ZSM-5, respectively.

The finally step was the release of O_2 molecule from the TM-ZSM-5 and reproduced the initial active oxo species. The O_2 molecule was formed the strong adsorption complex with the metal oxo species. To eliminate this O_2 molecule from FeO-ZSM-5 required the energy only 2.6 kcal/mol. For the Co-ZSM-5 and Ni-ZSM-5, the O_2 desorption is stabilized the catalyst structures. So that, the rate limiting step over TM-ZSM-5 in this study is the decomposition of second N_2O . The activation energy of N_2O decomposition over transition Fe-ZSM-5 and Co-ZSM-5 from experimental were reported as 40 and 28 kcal/mol (Kapteijn *et al.*, 1997). The activation energy of this ONIOM2 (M06:UFF) on N_2O decomposition over transition Fe-ZSM-5, Co-ZSM-5, and Ni-ZSM-5 were calculated to be 42.8, 56.0, and 75.8 kcal/mol, respectively. The activity trend by the activation energy is Fe-ZSM-5 > Co-ZSM-5 > Ni-ZSM-5.

The stability of each TMO_x form in TM-ZSM-5 is compared in term of energy change along the reaction mechanism. Set the referent energy as TMO-ZSM-5 structure and other structures are comparing with this structure. Fe-ZSM-5 shows the most easiest change between $[\text{FeO}]^+ \rightarrow [\text{FeO}_2]^+ \rightarrow [\text{FeO}_3]^+ \rightarrow [\text{FeO}]^+$ structure due to they are smallest energy different between each structure. All propose $[\text{FeO}_x]^+$ structures are able to change between each form because the activation energy and the relative energy of each structure are not too high. The energy requirement for changing the oxidation state of $[\text{CoO}_x]^+$ in Co-ZSM-5 is between Fe-ZSM-5 and Ni-ZSM-5.

CONCLUSIONS

The catalytic activities of petrochemical zeolites with trace iron impurity were tested for nitrous oxide decomposition by temperature programmed reaction in the fixed bed reactor. Nitrous oxide was catalyzed by zeolites and can start at around 450°C in FER, BEA, and ZSM5. The catalytic activity trend was FER > BEA > ZSM5 >> MOR > FAU. Addition of methane into the feed gas were reduced the catalytic temperature to about 300°C in BEA, FER, ZSM5, and MOR but any improvement were observed in FAU. This result can propose that, the active species in FAU can not reach by methane atom which the reaction can occur under the diffusion control. The catalytic activities of these zeolites were improved by increase iron quantity with ion exchange. Fe-BEA showed the most active species and the starting temperature for Fe-BEA, Fe-FER, Fe-ZSM5, and Fe-MOR were shift to the same value.

Methane was oxidized at about 300°C by nitrous oxide over zeolites. The oxidizing products over BEA, FER, MOR, and ZSM5 at 500°C showed the trace amount of hydrocarbon. Reaction products of 5% methane and 2.5% nitrous oxide were selective to 20% aromatic and 5% of higher hydrocarbon (C₂-C₃). The catalytic activities of commercial zeolites were rapid deactivated by coke deposition. The steam treatment ZSM-5 was active for longer than 4 h but the product selectivity was not improved.

Ethane dehydrogenation reaction can activate by zeolites with the N₂O as oxidative reagent. The study at 500 °C was found that ZSM5 is the most reactive framework that produced ethylene about 21%. The suitable molar ratio of N₂O to C₂H₆ was also optimized to one. The excess N₂O molar ratio was reacted with the C₂H₄ through the side reaction and produced the lower C₂H₄ selectivity. ZSM-5 is also the most active zeolite for N₂O decomposition in the presence of C₂H₆.

The intrinsic activity of iron oxide exchanged zeolites for the decomposition of nitrous oxide has been studied by using the ONIOM2 scheme. The confinement effect of nanostructured pore network of zeolites stabilizes the adsorbed species,

intermediates, and transition states inside the zeolites. This confinement effect is more pronounced in a small pore zeolite, Fe-FER, and causes the highest activity for the nitrous oxide decomposition. For medium and large pore zeolites, there is no substantial difference since the nitrous oxide molecule is much smaller than the pore sizes. Therefore, the predicted intrinsic activity trend is Fe-FER > Fe-ZSM-5 ~ Fe-BEA ~ Fe-FAU which well correlated to the experimental results, except for the FUA zeolites. In Fe-FAU, the calculation model and the available sites in the starting zeolites can in different positions. The decomposition of nitrous oxide seems to be under severe transport limitation because the iron cations could be preferentially located at the six-membered ring of the sodalite unit, which has a very small pore opening.

The catalytic cycle of N₂O decomposition over Co-ZSM5 and Ni-ZSM5 were also comparative studied with the Fe-ZSM5. The proposed reaction mechanisms are base on the reaction mechanism over Fe-ZSM-5. Using M06 density functional calculation, the predicted activation energy of the first N₂O decomposition over Fe-, Co-, Ni-ZSM5 are 28.9, 34.9, and 49.6 kcal/mol, respectively. The rate determining step is the N-O bond braking in the second N₂O decomposition. The apparent activation energy for N₂O decompositions are 42.7, 56.0 and 75.8 kcal/mol for Fe-, Co-, Ni-ZSM5, respectively. Fe-ZSM-5 shows the most stable active species which easily change to concern species and recycle to initial active structure. Ni-ZSM-5 is hard to flow through this reaction mechanism because the energy different between each species are high. Co-ZSM-5 is better than Ni-ZSM-5 but less active than Fe-ZSM-5.

LITERATURE CITED

- Abu-Zeid, B.M. and W. Schwieger. 2009. Self oscillatory behavior in N_2O decomposition over Co-ZSM-5 catalysts. **App. Catal. B** 85: 120-130.
- _____, _____, and A. Unger 2008. Nitrous oxide decomposition over transition metal exchanged ZSM-5 zeolites prepared by the solid-state ion-exchange method. **App. Catal. B** 84: 277-288.
- Armor, J.N. 1998. Metal-exchanged zeolites as catalysts. **Micropor. Mesopor. Mater.** 22: 451-456.
- Ates, A. and A. Reitzmann. 2007. Experimental techniques for investigating the surface oxygen formation in the N_2O decomposition on Fe-ZSM-5 zeolites. **Chem. Eng. J.** 134: 218-227.
- Auroux, A. 1997. Acidity Characterization by microcalorimetry and relationship with relativity. **Top. Catal.** 4:71-89.
- Bartholomew, C.H. and R.J. Farrauto. 2005. **Fundamentals of Industrial Catalytic Processes**. John Wiley & Sons, Inc. New Jersey.
- Battiston, A.A., J.H. Bitter, F.M.F. de Groot, A.R. Overweg, O. Stephan, J.A. van Bokhoven, P.J. Kooyman, C. van der Spek, G. Vanko, and D.C. Koningsberger, 2003. Evolution of Fe species during the synthesis of over-exchanged Fe/ZSM-5 obtained by chemical vapor deposition of $FeCl_3$. **J. Catal.** 213; 251-271.
- Berlier, G., G. Spoto, P. Fisicar, S. Bor diga, A. Zecchina, E. Giamello, and C. Lamberti. 2002. Co-ordination and oxidation changes undergone by iron species in Fe-silicalite upon template removal, activation and interaction with N_2O : an in situ X-ray absorption study. **Microchem. J.** 71:101-116.

- Berthomieu, D., N. Jardillier, G. Delahay, B. Coq, and A. Goursot. 2005. Experimental and theoretical approaches to the study of TMI-zeolite (TMI=Fe, Co,Cu). **Catal Today**. 110: 294-302.
- Boissel, V., Tahir, S., and C.A. Koh. 2006. Catalytic decomposition of N₂O over monolithic supported noble metal-transition metal oxides. **App. Catal. B** 64:234-242.
- Bulanek, R., K. Novoveska, and B. Wichterlova. 2002. Oxidative dehydrogenation and ammoxidation of ethane and propane over pentasil ring Co-zeolites. **App. Catal. A** 235: 181-191.
- Busca, G. 1998. Spectroscopic characterization of the acid properties of metal oxide catalysts. **Catal. Today**. 41: 191-206.
- Campa, M.C., D. Pietrogiacomini, S. Tuti, G. Ferraries, and V. Indovina. 1998. The selective catalytic reduction of NO_x with CH₄ on Mn-ZSM-5: A comparison with Co-ZSM-5 and Cu-ZSM-5. **App. Catal. B** 18: 151-162.
- Clerici, M.G., 2000. Zeolites for fine chemicals production. **Top. Catal.** 13: 373–386.
- Chang, Y.-F and J.G. McCart. 1995. N₂O decomposition over [Fe]-ZSM-5 and Fe-HZSM-5 zeolites. **Catal. Lett.** 34: 163-177.
- Chernyavsky, V.S., L.V. Pirutko, A.K. Uriarte, A.S. Kharitonov, and G.I. Panov. 2007. On the involvement of radical oxygen species O[•] in catalytic oxidation of benzene to phenol by nitrous oxide. **J. Catal.** 245:466-469.
- Choudhary, V.R., Mondal, K., and Mulla, S.A.R. 2006. Non-catalytic pyrolysis of ethane to ethylene in the presence of CO₂ with or without limited O₂. **J. Chem. Sci.** 188: 261-267.

- Choi, S.H., B.R.Wood, J.A.Ryder, and A.T. Bell. 2003. X-ray Absorption Fine Structure characterization of the local structure of Fe in Fe-ZSM5. **J. Phys. Chem. B** 107: 11843-11851.
- Choi, S.H., B.R. Wood, A.T. Bell, M.T. Janicke, and C.O. Kevin. 2004. X-ray absorption fine structure analysis of the local environment of Fe in Fe/Al-MFI. **J. Phys. Chem. B** 108: 8970-8975.
- Chu, W. and F. Qiu. 2003. Remarkable promotion of benzene formation in methane aromatization with ethane addition. **Top. Catal** 22: 131-134.
- Connor, S. 2008a. **Exclusive: The methane time bomb**. The independent. Available source: <http://www.Independent.co.uk/news/science>. March 18, 2009.
- _____. 2008b. **Hundreds of methane 'plumes' discovered**. The independent. Available source: <http://www.Independent.co.uk/news/science>. March 18, 2009.
- Corma, A., 1995. Inorganics solid acids and their use in acid-catalyzed hydrocarbon reactions. **Chem. Rev.** 95: 559-614.
- Creyghton, E.J. and R.S. Dowing. 1998. Review: Shape-selective hydrogenation and hydrogen transfer reactions over zeolite catalysts. **J. Mol. Cat. A** 134: 47-61.
- Cruz, R.S, A.J.S. Mascarenhas, and H.M.C. Andrade. 1998. Co-ZSM-5 catalysts for N₂O decomposition. **App. Catal. B** 18:223-231.
- Cundy, C. S. and P. A. Cox. 2003. The hydrothermal synthesis of zeolites: history and development from the earliest days to the present time. **Chem. Rev.** 103: 663-701.
- David R. Lide, ed. 2005. **CRC Handbook of Chemistry and Physics**. 86th ed., CRC Press, Boca Raton, Florida, USA.

- Degnan, T. F. Jr. 2000. Applications of zeolites in petroleum refining. **Top. Catal.** 13: 349-256.
- _____. 20003. The implications of the fundamentals of shape selectivity for the development of catalysts for the petroleum and petrochemical industries. **J. Catal.** 216: 32-46.
- Degnan, T. F., G. K. Chitnis, and P. H. Schipper, 2000. History of ZSM-5 fluid catalytic cracking additive development at mobil. **Micropor. Mesopor. Mater.** 35-36: 245-252.
- Deka, R.C. and K. Hirao. 2000. Lewis acidity and basicity of cation-exchanged zeolites: QM/MM and density functional studies. **J. Mol. Catal. A** 181: 275-282.
- Drake, I.J., Y. Zhang, D. Briggs, B. Lim, T. Chau, and A.T. Bell. 2006. The Local Environment of Cu⁺ in Cu-Y Zeolite and Its Relationship to the Synthesis of Dimethyl Carbonate. **J. Phys. Chem. B** 110: 11654.
- Drozdova, L., R. Prins, J. Dedeczek, Z.Sobalik, and B. Wichterlova. 2002. Bonding of Co ions in ZSM-5, Ferrierite, and Mordenite: an X-ray absorption, UV-vis and IR study. **J. Phys. Chem B** 106:2240-2248.
- Dubkov, K.A., N.S. Ovanesyan, A.A. Shteinman, E.V. Starokon, and G.I. Panov. 2002. Evaluation of iron states and formation of α -sites up on activation of Fe-ZSM-5 zeolites. **J. Catal.** 207:341-352.
- Francoise, R., J. Rouquerol, and K. Sing. 1999. Adsorption by powders and poros solids principles, methodology and application. Acedemic Press, CA, USA.
- Fellah, F. M. and F.O., Onal. 2008. N₂O decomposition on Fe- and Co-ZSM-5: A density functional study. **Catal. Today** 137: 410-417.

- Ferretti, A.M., C. Oliva, L.Forni, G. Berlier, A.Zecchina, and C. Lamberti. 2002. Evaluation of extraframework iron species in Fe Silicalite 2. Effect of steaming. **J. Catal.** 208: 83-88.
- Fowkes, A.J., R.M. Ibberson, and F.J. Keil. 2002. Structural Characterization of the Redox Behavior in Copper-Exchanged Sodium Zeolite Y by High-Resolution Powder Neutron Diffraction. **Chem. Mater.** 14: 590-602.
- Garcia, H. and H. D. Roth. 2002. Generation and reaction of organic radical cations in zeolites **Chem. Rev.** 102: 3947-4007.
- Gardziella, A., L.A. Pilato, and A. Knop. 2000. Phenolic resins: chemistry, applications, standardization, safety, and ecology, 2nd ed. Springer-Verlag Berlin Heidelberg New York .NJ, USA.
- Ge, Xi., M. Zhu, and J. Shen. 2002. Catalytic performance of silica-supported chromium oxide catalysts in ethane dehydrogenation with carbon dioxide. **React.Kinet.Catal.Lett.** 77(1): 103-108.
- Godelitsas, Ath. and Th. Armbruster. 2003. HEU-type zeolites modified by transition elements and lead. **Micropor. Mesopor. Mater.** 61:3-24.
- Gorte, R.J. and D. White. 1997. Interactions of chemical species with acid zeolites in zeolites. **Top. Catal.** 4: 57-69.
- Gutierrez, L., E. Miro, and S. Irusta. 2008. Spectroscopic and catalytic characterization of Co-exchanged mordenites subject to CO/O₂ redox treatments. **Micropor. Mesopor. Mater.** 114: 281-292.
- Guzmán-Vargas, A., G. Delahey, and B. Coq. 2003. Catalytic decomposition of N₂O and catalytic reduction of N₂O and N₂O+NO by NH₃ in the presence of O₂ over Fe-zeolites. **App. Catal. B** 42: 369-379.

- Hadi, A., K. Inubushi, E. Purnomo, F. Razie, K. Yamakawa, and H. Tsuruta. 2000. Effect of land-use changes on nitrous oxide (N_2O) emission from tropical peatlands. **Chemosphere Global Change Sci.** 2: 347-358.
- Hasegawa, K., K. Hanaki, T. Matsuo, S. Hidaka. 2000. Nitrous oxide from the agricultural water system contaminated with high nitrogen. **Chemosphere Global Change Sci.** 2: 335-345.
- Hall, W.K. 1997. Characterization of Solid Catalysts; Acidity and basicity, pp. 689-698. In G. Ertl, H. Knozinger, and J. Weitkamp. **Handbook of Heterogeneous Catalysis**. A Wiley company, France
- Harris, C.C. 2003. **Quantitative Chemical Analysis**. 6th ed. W.H. Freeman and Company, New York.
- Heracleous, E. and A.A. Lemonidou. 2004. Homogeneous and heterogeneous pathways of ethane oxidative and non-oxidative dehydrogenation studied by temperature-programmed reaction. **App. Catal. A** 269:123-135.
- Heracleous, E., A.A. Lemonidou, and J.A. Lercher. 2004. Mechanistic features of ethane oxidative dehydrogenation by in situ FTIR spectroscopy over a $\text{MoO}_3/\text{Al}_2\text{O}_3$ catalyst. **App. Catal. A** 246: 73-80.
- Hiromi, M. and K. Arata. 2006. Adsorption and desorption of small molecules for the characterization of solid acids. **Catal. Surveys from Asia** 10:1-7.
- Hensen, E.J.M., Q. Zhu, R.A.J. Janssen, P.C.M.M. Magusin, P.J. Kooyman, R.A. van Santen. 2005. Selective oxidation of benzene to phenol with nitrous oxide over MFI zeolites. 1. On the role of iron and aluminum. **J. Catal.** 233: 123-135.
- Heyden, A., B. Peters, A.T. Bell, and F.J. Keli. 2005. Comprehensive DFT study of nitrous oxide decomposition over Fe-ZSM5. **J. Phys. Chem. B** 109: 1857-1873.

- Jane, R. 2009. Nitrous oxide fingered as monster ozone slayer. Thursday, August 27th, 2009. Available source: http://www.sciencenews.org/view/generic/id/46776/title/Nitrous_oxide_fingered_as_monster_ozone_slayer.
- Jansang, B. T. Nanok, and J. Limtrakul. 2006. Structures and Reaction Mechanisms of Cumene Formation via Benzene Alkylation with Propylene in a Newly Synthesized ITQ-24 Zeolite: An Embedded ONIOM Study. **J. Phys. Chem. B** 110(25): 12626- 12631.
- Jentoft, F.C. and B. C. Gates. 1997. Solid-acid-catalyzed alkane cracking mechanisms: evidence from reactions of small probe molecule **Top. Catal.** 4:1-13
- Jia, J. B. Wen, and W.M.H. Sachtler. 2002. Identification by isotopic exchange of oxygen deposited on Fe/MFI by decomposing N₂O. **J. Catal.** 210: 453-459.
- Jíša, K., Novakova, J., Schwarcz, M., Vondrova, A., Skenal, S., and Z. Sobalik. 2009. Role of Fe-zeolite structure and iron state in N₂O decomposition: Comparison of Fe-FER, Fe-BEA, and Fe-MFI catalysts **J. Catal.** 262: 27-34.
- Jule, A.R. and M.W. Schoonover. 2001. Early discoveries in zeolite chemistry and catalysis at Union Carbide, and follow-up in industrial catalysis **App. Catal. A** 222: 261-275.
- Joyner, R. and M., Stockenhuber. 1999. Preparation, characterization and performance of Fe-ZSM-5 catalysts. **J. Phys. Chem. B** 103: 5963-5976.
- Kachurovskaya, N.A., G.M. Zhidomirov, and R.A. van Santen. 2004. Computational study of benzene-to-phenol oxidation catalyzed by N₂O on iron-exchanged Ferrierite. **J. Phys. Chem. B** 108: 5944-5950.
- Kameoka, S., Kita, K., Tanaka, S., Nobukawa, T., Ito, S., Tomishige, K., Miyadera, T., and Kunimori, K. 2002. Enhancement of C₂H₆ oxidation by O₂ in the

presence of N_2O over Fe ion exchanged BEA zeolite catalyst. **Catal. Letter.** 79: 63-67.

Kapteijn, F., G. Marban, J. Rodriguez-Mirasol, and J.A. Moulijn. 1997. Kinetic analysis of the decomposition of nitrous oxide over ZSM-5 catalysts. **J. Catal.** 167: 256-265.

Kapteijn, F., J. Rodriguez-Mirasol, and J.A. Moulijn. 1996. Heterogeneous catalytic decomposition of nitrous oxide. **App. Catal. B.** 9:25-64.

Kasuriya, S., S. Namuangrak, P. Treesukol, M. Tirtowidjojo, and J. Limtrakul. 2003. Adsorption of ethylene, benzene, and ethyl benzene over faujasite zeolites investigated by the ONIOM method. **J. Catal.** 219: 320-328.

Kazansky, V.B. 2003. Location of bivalent transition metal ions in high-silica zeolites with the very broad range of Si/Al ratios in the framework probed by low-temperature H_2 adsorption. **J. Catal.** 216: 192-202.

Kiwi-Minsker, L., D.A. Bulushev, and A. Renken. 2003. Active sites in H-ZSN-5 with low Fe content for the formation of surface oxygen by decompositng N_2O : is every deposited oxygen active? **J. Catal.** 219: 273-285.

_____. 2005. Low temperature decomposition of nitrous oxide over Fe/ZSM-5: Modeling of the dynamic behavior. **Catal. Today.** 110: 191-198.

Kondratenko, E.V., M. Cherian, and M. Baerns. 2006. Oxidative dehydrogenation of propane over differently structured vanadia-based catalysts in the presence of O_2 and N_2O . **Catal. Today** 112: 60–63.

Kotrla, J., L. Kubelkova, C.-C. Lee, and R.J. Gorte. 1998. Calorimetric and FTIR Studies of acetonitrile on H-[Fe]ZSM-5 and H-[Al]ZSM-5. **J. Phys. Chem. B** 102: 1437-1443.

- Kuchеров, A.V., V.D. Nissenbaum, T.N. Kucheroва, and L.M.Kustov. 2002. Catalytic oxidation of methane by nitrous oxide on H[A]ZSM-5 zeolite, silicalite, and amorphous SiO₂ modified by iron, silver, and gadolinium ions. **Kinet. Catal.** 43(5) 711-723.
- Kupka, T., Branko Ruscic, and Robert E. Botto. 2003. Hatree-Fock and Density Functional Complete Basis-Set (CBS) predicted nuclear shielding anisotropy and shielding tensor components solid state. **Nucl. Magn. Reson.** 23: 145-167.
- Lesthaeghe, D., G. Delcore, V.V. Speybroeck, G.B. Marin, and M. Waroquier. 2006. Theoretical study on the alteration of fundamental zeolite properties by methylene functionalization. **Micro. Meso. Mater.** 96: 350–356.
- Li, L., Shen, Q., Yu, J., Li, J., Hoa, Z., and Xu, Z.P. 2008. Wet ion exchanged Fe-USY catalyst for effective N₂O decomposition. **Catal. Comm.** 9: 1745-1748.
- Limtrakul, J., T. Nanok, S. Jungsuttiwong, P. Kongpracha, and T. N. Truong. 2001. Adsorption of unsaturated hydrocarbons on zeolites: the effects of the zeolite framework on adsorption properties of ethylene. **Chem. Phys. Lett.** 349: 161-166.
- Lobree, L.J., I.C. Wang, J.A. Reimer, and A.T. Bell. 1999. Investigations of the State of Fe in H-ZSM-5. **J. Catal.** 186: 242-253.
- Majdan, M., S. Pikus, M. Kowalska-Ternes, A. Gladysz-Plaska, P. Staszczuk, L. Fuks, and H. Skrzypek. 2003. Equilibrium study of selected divalent *d*-electron metals adsorption on A-type zeolite. **J. Colloid and Interface Sci.** 262: 321-330.
- Marcilly, C.R. 2000. Where and How Shape Selectivity of Molecular Sieves Operated in Refining and Petrochemistry Catalytic Processes. **Top. Catal.** 13: 357-366.

- Matar, S. and L.F. Hatch. 2000. **Chemistry of petrochemical process 2nd ed** Gulf Publishing Company, Houston, Texas
- Marturano, P. L. Drozdova, A. Kogelbauer, and R. Prins. 2000. Fe/ZSM-5 Prepared by Sublimation of FeCl₃: The structure of the Fe species as determined by IR, 27Al MAS NMR, and EXAFS Spectroscopy. **J. Catal.** 192; 236-247 .
- Mauvezin, M., G. Delahay, B. Coq, S. Kieger, J.C. Jumas, and J. Olivier-Fourcade. 2001. Identification of iron species in Fe-BEA: influence of the exchange level. **J. Phys. Chem. B** 105: 928-935.
- Melian-Cabrera, I., F. Kapteijn, and J.A. Moulijn. 2005. Innovations in the synthesis of Fe-(exchanged)-zeolites. **Catal. Today** 110: 255–263.
- Melian-Cabrera, I., S. Espinosa., C. Mentrui, F. Kapteijn, and J.A. Moulijn. 2006. Alkaline leaching for synthesis of improved Fe-ZSM5 catalysts. **Catal. Commun.** 7: 100–103.
- Mohamed, M. M., I. O. Ali, and N. A. Eissa. 2005. Effect of thermal treatment on surface and bulk properties of Fe/ZSM-5 zeolites prepared by different methods. **Micropor. Mesopor. Mater.** 87: 93-102.
- Morris, R.E., S.J. Weigel, N.J. Henson, L.M. Bull, M.T. Janicke, B.F. Chmelka, and A.K. Cheetham. 1994. A Synchrotron X-ray Diffraction, Neutron Diffraction, 29Si MAS-NMR, and Computational Study of the Siliceous Form of Zeolite Ferrierite. **J. Am. Chem. Soc.** 116: 11849-11855.
- Mulla, S.A.R., O.V. Buyevskaya, and M. Baerns. 2002. A comparative study on non-catalytic and catalytic oxidative dehydrogenation of ethane to ethylene. **App. Catal. A.** 226: 73–78.

- Namuangruk, S., P. Pantu, and J. Limtrakul. 2004. Alkylation of benzene with ethylene over faujasite zeolite investigated by the ONIOM method. **J. Catal.** 225: 523- 530.
- Namuangruk, S., P. Pantu, and J. Limtrakul. 2005. Investigation of Ethylene Dimerization over Faujasite Zeolite by the ONIOM Method. **Chem. Phys. Chem.** 6: 1333-1339.
- Namuangruk, S., P. Khongpracha, P. Pantu, and J. Limtrakul. 2006. Structures and Reaction Mechanisms of Propene Oxide Isomerization on H-ZSM-5: An ONIOM Study. **J. Phys. Chem. B** 110: 25950-25957.
- Newsam, J.M., M.M.J. Treacy, W.T. Koetsier, and C.B. de Gruyter. 1988. **Proc. R. Soc. Lond. A**, 420(1859); 375.
- Niemantsverdriet, J. W. 2000. **Spectroscopy in Catalysis**. 2nded. Wiley-VCH Verlag GmbH, German.
- Niwa, M., Y. Habuta, K. Okumura, and N. Katada. 2003. Solid acidity of metal oxide monolayer and its role in catalytic reaction, **Catal. Today**. 87: 213-218.
- Nobukawa, T., K. Sugawara, K. Okumura, K. Tomishige, and K. Kunimori. 2007. Role of active oxygen transients in selective catalytic reduction of N₂O with CH₄ over Fe-zeolite catalysts. **App. Catal. B** 70: 342-352.
- Nobukawa, T., M. Yoshida, S. Kameoka, S. Ito. 2004. In-situ observation of reaction intermediate in the selective catalytic reduction of N₂O with CH₄ over Fe-ion-exchanged BEA zeolite catalysts for elucidation of it reaction mechanism using FTIR. **J. Phys. Chem. B** 108: 4071-4079.
- Nowinska, K., A. Waclaw, and A. Izbinska. 2003. Propane oxydehydrogenation over transition metal modified zeolite ZSM-5. **App. Catal. A** 243: 225-236.

- Öhman, L.O., B. Ganemi, E. Björnbo, K. Rahkamaa, R. L. Keiski, and J. Paul. 2002. Catalyst preparation through ion-exchange of zeolite Cu-, Ni-, Pd-, CuNi-, and CuPd-ZSM-5. **Mater. Chem. Phys.** 73: 263-267.
- Olah, G.A. and A. Molnar. 2001. **Hydrocarbon Chemistry**. 2nd ed., John Wiley & Sons, Inc. New Jersey
- Olson, D.H. and E. Dempsey. 1969. The crystal structure of the zeolite hydrogen faujasite. **J. Catal.** 13(2); 221-231.
- Ovanesyan, N. S., K. A. Dubkov, A. A. Pyalling, and A. A. Shteinman. 2000. The Fe active sites in Fe-ZSM-5 catalysts for the selective oxidation of CH₄ to CH₃OH at room temperature. **J. Radioanalytical and Nuclear Chem.** 246(1): 149-152.
- Øygarden, A.H. and J. Perez-Ramirez. 2006. Activity of commercial zeolites with iron impurities in direct N₂O decomposition. **App. Catal. B** 65: 163-167.
- Pabchanda, S., P. Pantu, and J., Limtrakul. 2005. Hydrolysis of methoxide species and regeneration of active site in Fe-ZSM-5 catalyst by the ONIOM method. **J. Mol. Catal.** 239: 103-110.
- Panjan, W. and J. Limtrakul. 2003. The influence of the framework on adsorption properties of ethylene/H-ZSM-5 system: an ONIOM study. **J. Mol. Struct.** 654: 35-45.
- Panov, G.I., V.I. Sobolev, K.A. Dubkov, V.N. Parmon, N.S. Ovanesyan, A.E. Shilov, and A.A. Shteinman. 1997. Iron complexes in zeolites as a new model of methane monooxygenase. **React.Kinet.Catal.Lett.** 61(2): 251-258.
- Panov, G.I., A.K. Uriarte, M.A. Rodkin, and V.I. Sobolev. 1998. Generation of active oxygen species on solid surfaces. Opportunity for novel oxidation technologies over zeolites. **Catal. Today** 41:365-385.

- Pantu, P., S. Pabchanda, and J. Limtrakul. 2004. Theoretical investigation of the selective oxidation of methane to methanol on nanostructured Fe-ZSM-5 by the ONIOM method. **Chem. Phys. Chem.** 5: 1-6 .
- Park, J.H., J.H. Choung, I.S. Nam, and S.W. Ham. 2008. N₂O decomposition over wet- and solid-exchanged Fe-ZEM-5 catalysts. **App. Catal. B** 78:342-354.
- Parmon, V.N., G.I.Panove, A. Uriarte, and A.S. Noskov. 2005. Nitrous oxide in oxidation chemistry and catalysis: application and production. **Catal. Today.** 100: 115-131.
- Paulat, F., T. Kuschel, C. Nather, V.K.K. Praneeth, O. Sander, and N. Lehnert. 2004. Spectroscopic properties and electronic structure of pentammineruthenium(II) dinitrogen oxide and corresponding nitrosyl complexes: Binding mode of N₂O and reactivity. **Inorg. Chem.** 43:6979-6994.
- Peixoto, D.P.B., S.M. Cabral de Menezes, and M. I. Pais da Silva. 2003. Influence of different processes of dealumination on acid properties of an H-ferrierite zeolite. **Mat. Lett.** 57: 3933-3942.
- Perez-Ramirez, J. 2004. Active iron sites associated with the reaction mechanism of N₂O conversions over steam-activated FeMFI zeolites. **J. Catal.** 227:512-522.
- Perez-Ramirez, J., F. Kapteijn, G. Mul, and J. A. Moulijn. 2002. NO-Assisted N₂O decomposition over Fe-Based catalysts: Effects of gas-phase composition and catalyst constitution. **J. Catal.** 208: 211-223.
- _____, _____, J.C. Groen, A. Domenech, G. Mul, and J. A. Molijn. 2003. Steam-activated FeMFI zeolites. Evolution of iron species and activity in direct N₂O decomposition. **J. Catal.** 214: 33-45.

- Perez-Ramirez, J., A.G. Llamas, C. Daniel, and C. Mirodatos. 2004. N₂O-mediated propane oxidative dehydrogenation over Fe-zeolites. TEOM studied for continuous propylene production in a cyclically-operated reactor. **Chem. Eng. Sci.** 59: 5535-5543.
- Perez-Ramirez, J. and A.G. Llamas. 2004. N₂O-mediated propane oxidative dehydrogenation over steam-activated iron zeolites. **J. Catal.** 223: 382-388.
- Pirngruber, G.D. and P.K. Roy. 2004. Themomechanism of N₂O decomposition on Fe-ZSM5: an isotope labeling study. **Catal. Lett.** 93:75-80.
- Pirngruber, G.D., P. K. Roy, and R. Prins. 2006. On determining the nuclearity of iron sites in Fe-ZSM-5-a critical evaluation. **Phys. Chem. Chem. Phys.** 8:3939-3950.
- Pirutko, L.V., V.S. Chernyavsky, E.V. Starokon, A.A. Ivanov, A.S. Kharitonov, and G.I. Panov. 2009. The role of α -sites in N₂O decomposition over Fe-ZSM-5. Comparison with the oxidation of benzene to phenol. *App. Catal B* 91: 174-179.
- Pyatnitskii, Y.I. 2003. Contempolary methods for the direct catalytic conversion of methane. **Theo. Exper. Chem.** 39(4): 201-218.
- Quincoces, C.E., A. Kikot, E. I. Basaldella, and M. G. Gonzalez. 1999. Effect of hydrothermal treatment on Cu-ZSM-5 catalyst in the selective reduction of NO. **Ind. Eng. Chem. Res.** 38: 4236-4240.
- Rakic, V., V. Rac, V. Dondur, and A. Auroux. 2005. Competitive adsorption of N₂O and CO on CuZSM-5, FeZSM5, CoZSM5 and bimetallic forms of ZSM-5 zeolite. **Catal. Today.** 110: 272-280.
- Raksakoon, C. and J. Limtrakul. 2003. Adsorption of aromatic hydrocarbon onto H-ZSM-5 zeolite investigated by ONIOM study. **J. Mol. Struct.** 631: 147-156.

- Ribera, A., I.W.C.E. Arends, S. de Vries, J. Perez-Ramirez and R.A. Sheldon. 2000. Preparation, characterization, and performance of FeZSM-5 for the selective oxidation of benzene to phenol with N_2O . **J. Catal.** 195: 287-297.
- Rice, A.J., A.K., Chakraborty, and A.T. Bell. 1998. A density functional theory study of the interactions of H_2O with H-ZSM-5, Cu-ZSM-5, and Co-ZSM-5. **J. Phys. Chem. A.** 102:7498-7504.
- Ryder, J., Chakraborty, A.K., and Bell, 2002. A.T. Density Functional Theory study of nitrous decomposition over Fe- and Co- ZSM5. **J. Phys. Chem. B** 106:7059-7064.
- Sanchez-Galofre, O. Y. Segura, and J. Perez-Ramirez. 2007. Deactivation and regeneration of iron-containing MFI zeolites in propane oxidative dehydrogenation by N_2O . **J. Catal.** 249:123-133.
- Sang, C. and C.R.F. Lund. 2000. Isothermal “light-off” during catalytic N_2O decomposition over Fe/ZSM-5. **Catal. Lett.** 70:165-173.
- Schwidder, M., M.S. Kumar, K. Klementiev, M. M. Pohl, A. Bruckner, and W. Grunert. 2005. Selective reduction of NO with Fe-ZSM-5 catalysts of low Fe content I. Relations between active sites structure and catalytic performance. **J. Catal.** 231:314-330.
- Sheldon, R.A., I. Arends, and U. Hanefeld. 2007. Green Chemistry and Catalysis. Wiley –VCH Verlag GmbH & Co., KGaA, Weinheim, Germany.
- Sheldon, R.A. and R.S. Downing, 1999. Heterogeneous Catalytic Transformation for Environmentally Friendly Production. **App.Catal. A** 189: 163-183.
- Shilov A.E. and G.B. Shulpin. 2000. **Activation and Catalytic Reactions of Saturated Hydrocarbons in the Presence of Metal Complexes.** Kluwer Academic Publishers, Netherlands.

- Silberova, B., M. Fathi1, and A. Holmen. 2004. Oxidative dehydrogenation of ethane and propane at short contact time. **App.Catal. A** 276: 17–28.
- Sinev, M. Y., et al., Z.T. Fattakhova, Y. P. Tulenin, P.S. Stennikov, and V.P. Vislovskii. 2003. Hydrogen formation during dehydrogenation of C2–C4 alkanes in the presence of oxygen: oxidative or non-oxidative? **Catal. Today** 81: 107–116.
- Smeets, P. J, Q. Meng, S. Corthals, H. Leeman, R.A. Schoonheydt. 2008. Co–ZSM-5 catalysts in the decomposition of N₂O and the SCR of NO with CH₄: Influence of preparation method and cobalt loading. **App. Catal. B** 84: 505–513.
- Smirnov, K.S. and F. Thibault-Starzyk. 1998. Confinement of acetonitrile molecules in Mordenite. A computer modeling study. **J. Phys. Chem. B** 103:8595-8610.
- Sobolev, V.I., G.I. Panov, A.S. Kharitonov, V.N. Romannikov, A.M. Volodin, and K.G. Ione. 1993. **J. Catal.**,139: 435- .
- Sobolev, V.I., K.A. Dubkov, O.V. Oanna, and G.I. Panov. 1995. Selective oxidation of methane to methanol on a Fe-ZSM-5 surface. **Catal. Today** 24: 251- 252.
- Somorjai, G.A. K. R. McCre, and J. Zhu. 2002. Active sites in heterogeneous catalysis: development of molecular concepts and future challenges. **Top. Catal.** 18: 157-166.
- Speight, J.G. 2006. The Chemistry and Technology of Petroleum. CRC Press Taylor and Francis Group, LLC. 4th ed. New York.
- Starokon, E.V., K.A. Dubkov, L.V. Pirutko, and G.I. Panov, 2003. Mechanisms of iron active on F-containing zeolites and the charge of α -oxygen. **Top. Catal.** 23: 137-143.

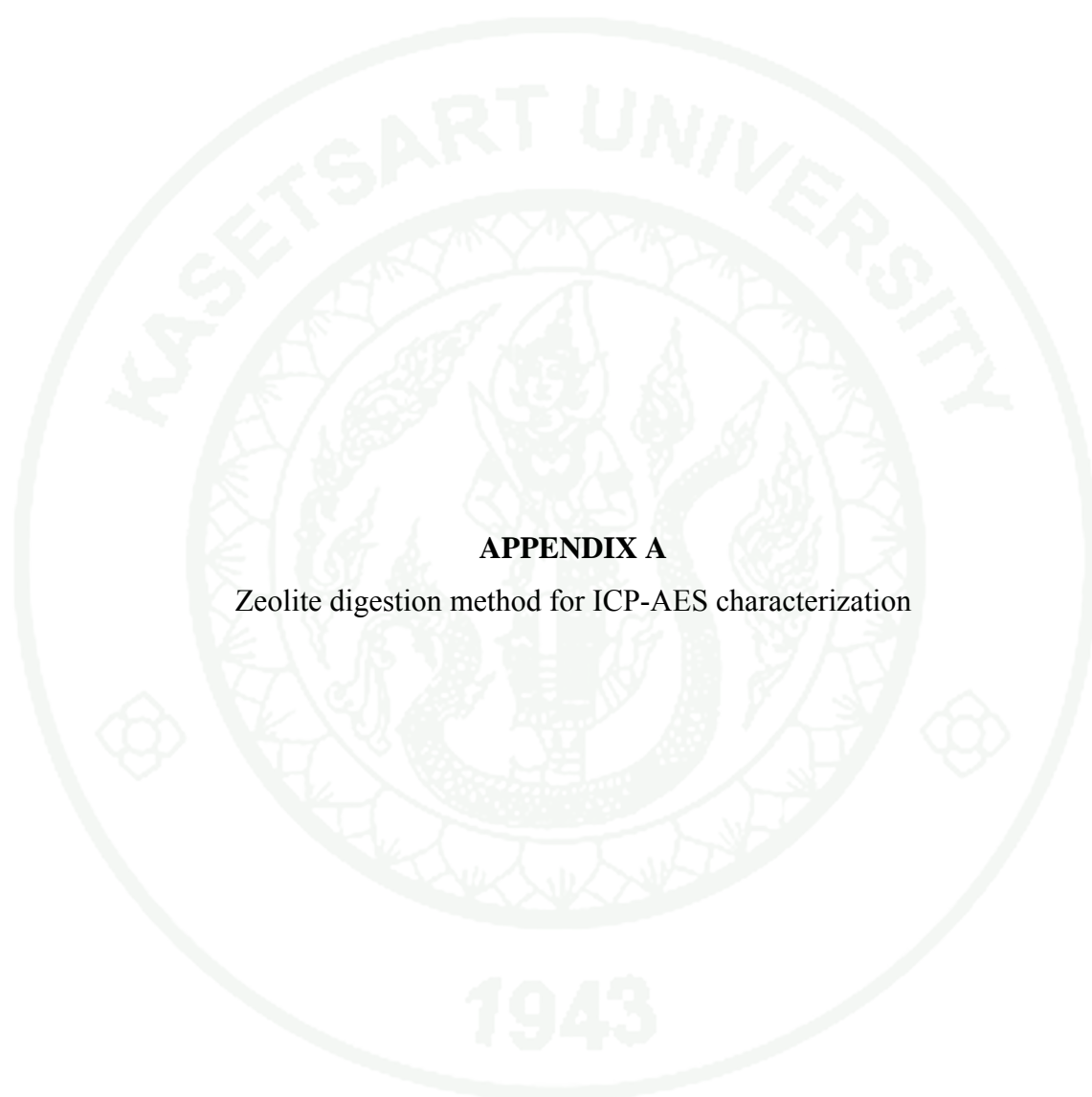
- Suits, B.H., J. Sepa, R.J. Gorte, and D. White. 2000. Molecular motion of hydrogen-bonded CH₃CN in H-MFI: A ¹H, ²H, and ¹³C multinuclear nuclear magnetic resonance study. **J. Phys. Chem. B** 104:5124-5131.
- Sun, K., H. Xia, Z. Feng, E. Hensen, R. van Santen, and C. Li 2006. Chemistry of N₂O decomposition on active sites with different nature: Effect of high-temperature treatment of Fe/ZSM-5. **J. Catal.** 238: 186-195.
- _____, _____, Z. Feng, R. van Santen, E. Hensen and C. Li 2008. Active sites in Fe/ZSM-5 for nitrous oxide decomposition and benzene hydroxylation with nitrous oxide. **J. Catal.** 254: 383-396.
- Tatlier, M. and L. Kiwi-Minsker. 2005. Catalytic activity of FeZSM-5 zeolites in benzene hydroxylation by N₂O: The role of geometry characterized by fractal dimensions. **Catal. Communications** 6: 731–736.
- Thibault-Starzyk, F., B. Gil, S. Aiello, T. Chevreau, and J.-P. Gilson. 2004. In situ thermogravimetry in an infrared spectrometer: an answer to quantitative spectroscopy of adsorbed species on heterogeneous catalysts. **Micropor. Mesopor. Mater.** 67:107–112.
- Van Koningsveld, H., H. van Bekkum, and J.C. Jansen. 1987. Diffuse scattering and disorder in urea inclusion compounds OC(NH₂)₂+C_nH_{2n+2}. *Acta Crystallogr. B* 43(2): 127.
- Veseshchagin, S.N., N.P.Kirik, N.N. Shishkina, S.V. Morozov, M.M. Shakirov, V.I. Mamatyuk, and A.G. Anshits. 2000. Hydrocarbon conversion on ZSM-5 in the presence of N₂O: relative reactivity and routes of products formation studied by GC-MS and ¹³C-NMR. **J. Mol.Catal. A** 158:337-380.

- Wang, X. , J. Long, G. Yan, G. Zhang, X. Fu, J. M. Basset, F. Lefebvre. 2008. Construction of highly dispersed mononuclear iron-oxo species in the supercages of Y zeolite by use of surface organometallic chemistry **Micropor. Mesopor. Mater.** 108: 258–265.
- Wang, Y., L. Lv, Z. Geng, G. Dai, D. Wang, H. Wang. 2005. Theoretical study of the reactivity of $X(^3P)$ ($X=Ge, Sn, Pb$) with N_2O ($X^1\Sigma$). **THEOCHEM.** 724: 185-193.
- Weckhuysen, B.M., D. Wang, M. P. Rosynek, and J. H. Lunsford. 1998. Conversion of methane to benzene over transition metal ion ZSM-5 zeolites: I. Catalytic Characterization. **J. Catal.** 175: 338-346.
- Wietkamp, J. 2000. Zeolites and Catalysis. **Solid State Ionics.** 131: 175-188.
- Wood, B.R., J.A. Reimer, and A.T. Bell. 2002. Studies of N_2O Adsorption and Decomposition on Fe–ZSM-5. **J. Catal.** 209: 151- 158.
- Wood, B.R., J. A.Reimer, A.T. Bell, M. T. Janicke, and K.C. Ott. 2004a. Nitrous oxide decomposition and surface oxygen formation on Fe-ZSM5. **J Catal.** 224: 148-155.
- _____, 2004b. Methanol formation on Fe/Al-MFI via the oxidation of methane by nitrous oxide. **J. Catal.** 225: 300-306.
- Yang, L., K. Trafford, O. Kresnawahjuesa, J. Sepa, and R.J. Gorte. 2001. An examination of confinement effects in high-silica zeolites. **J. Phys. Chem. B** 105: 935-1942.
- Yang, X.Y., Wang, Y.C., Geng, Z.Y., and Lui, Z.Y. 2006. Theoretical study of the reactivity of 4d transition metal ions with N_2O . **Chem. Phys. Letters** 430: 265-270.

- Yoshizawa, K. 2006. Nonradical mechanism for methane hydroxylation by iron-oxo complexes. **Acc. Chem. Res.** 39: 375-382.
- Yoshizawa, K., Y. Shihito, T. Yumura, and T. Yamabe. 2000. Direct methane-methanol and benzene-phenol conversions on Fe-ZSM-5 zeolites: Theoretical predictions on the reaction pathways and energies. **J. Phys. Chem. B** 104: 734-740.
- Yokomichi, Y., T. Yamabe, T. Kakumoto, O. Okada, H. Ishikawa, Y. Nakamura, H. Kimura, and I. Yasuda. 2001. Theoretical and experimental study on metal-loaded zeolite catalysts for direct NO_x decomposition **App. Catal. B** 28: 1-12.
- Yumura, T., T. Amenomori, Y. Kagawa, and K. Yoshizawa. 2002. Mechanism for the formaldehyde to formic acid and the formic acid to carbon dioxide conversions mediated by an iron-oxo species. **J. Phys. Chem. A** 106: 621-630.
- Zhao, Y. and D.G. Trulah. 2008. The M06 suite of density functionals for main group thermochemistry, thermochemical kinetics, noncovalent interactions, excited states, and transition elements: two new functionals and systematic testing of four M06-class functionals and 12 other functional. **Theor. Chem. Account** 120:215–241.
- Zhao, Y. and D.G. Trulah. 2009. Subroutines for evaluating the M05, M05-2X, M06-L, M06-HF, M06, M06-2X, M08-HX, M08-SO, and SOGGA Functionals. http://comp.chem.umn.edu/mfm/mfm_Manual_v1.2.2009.8.7.pdf.
- Zhidomirov, G.M. , A.L. Yakovlev, M.A. Milov, N.A., Kachurovskaya, and I.V. Yudonov. 1999. Molecular models of catalytically active sites in zeolites. Quantum chemical approach. **Catal. Today** 51: 397-410.



APPENDICES



The elemental analysis by Induce Coupling Plasma (ICP-AES) needs sample in the solution form. Zeolite is one of the most stable materials that can stand under high temperature and corrosive condition. From the trial during this study, the successive method for completely zeolite digestion is described as the following.

1. Reagents and apparatus

- 1.1 Nitric acid (HNO_3) 65% (Calo Erba Reagenti)
- 1.2 Hydrofluoric Acid (HF) 50% (Calo Erba Reagenti)
- 1.3 Dry zeolite samples
- 1.4 Plastic bottle (Nalgene, LDPE, size 125 ml)
- 1.5 Micro pipette (Biohit Proline pipette, 200-1000 μL) with a plastic tip
- 1.6 Ultrasonic bath (Ultrasins-H, model 200835)
- 1.7 Digital balance (AND, model HR-200, $d=0.1\text{mg}$)

2. Digestion Procedure

- 2.1 Weigh the plastic bottle (B_{w0}).
- 2.2 Weigh about 50 mg of a zeolite sample precisely (4 digit) (Z_w) and filled it into the the plastic bottle.
- 2.3 Filled about 1000 μL of HNO_3 into the bottle, shake it for well mixed
- 2.4 Added about 500 μL of HF into the bottle and shake it again for well mixed
- 2.5 Homogenized it in an ultrasonic bath for about 15 min.
- 2.6 Added about 25 ml of DI water into the solution and sonicated it again in the ultrasonic bath for about 15 min.
- 2.7 Added a makeup DI water for making the solution weight equal 100 g and then shaking for homogeneously.
- 2.8 Weigh the final weight (B_{wf}) of bottle and solution.
- 2.9 Weight about 50 ml of solution (S_{w50}).

3. Concentration calculations

The transition metal concentration in solution (mass/volume) is analyzed by ICP-AES (S_{TM}). The metal content in each zeolites are calculated as following method.

3.1 Determined the density of the solution (S_D) by weight about 50 ml of solution (S_{W50}). A density of solution in (g/L) is calculated from equation A1:

$$S_D = S_{W50} / (50 \times 10^{-3}) = 20 \times S_{W50} \quad (A1)$$

3.2 Determined the solution weight (S_W) in kilogram following equation A2:

$$S_W = B_{wf} - B_{w0} \quad (A2)$$

3.3 Determined the solution volume (S_V) in litter following equation A3:

$$S_V = S_W / S_D \quad (A3)$$

3.4 The zeolite concentration in the final solution is presents in the unit of mg/L or ppm. The prepared solution from the previous method will contain the zeolite about 500 ppm. The zeolite concentration (ppm) is calculated following equation A4:

$$Z_{ppm} = Z_W / S_V \quad (A4)$$

where :

Z_{ppm}	=	Zeolites concentration in solution (mg/L or ppm)
Z_W	=	Zeolites weight in solution (mg)
S_V	=	Solution volume (L)

3.5 Determined the metal concentration in zeolite from the metal concentration in solution (mass/volume) from the ICP-AES (S_{TM}) by equation A5:

$$TM_{ppm} = S_{TM} / Z_{ppm} \quad (A5)$$

where:

TM_{ppm} = metal concentration in zeolites (ppm in mg/kg)

S_{TM} = metal concentration in solution (ppm or mg/L)

Z_{ppm} = zeolites concentration in solution (ppm mg/L)

The Al concentration in zeolites (ppm in mg/kg) is calculated from equation A6:

$$Al_{ppm} = S_{Al} / Z_{ppm} \quad (A6)$$

where:

Al_{ppm} = aluminum concentration in zeolites (ppm in mg/kg)

S_{Al} = aluminum concentration in solution (ppm or mg/L)

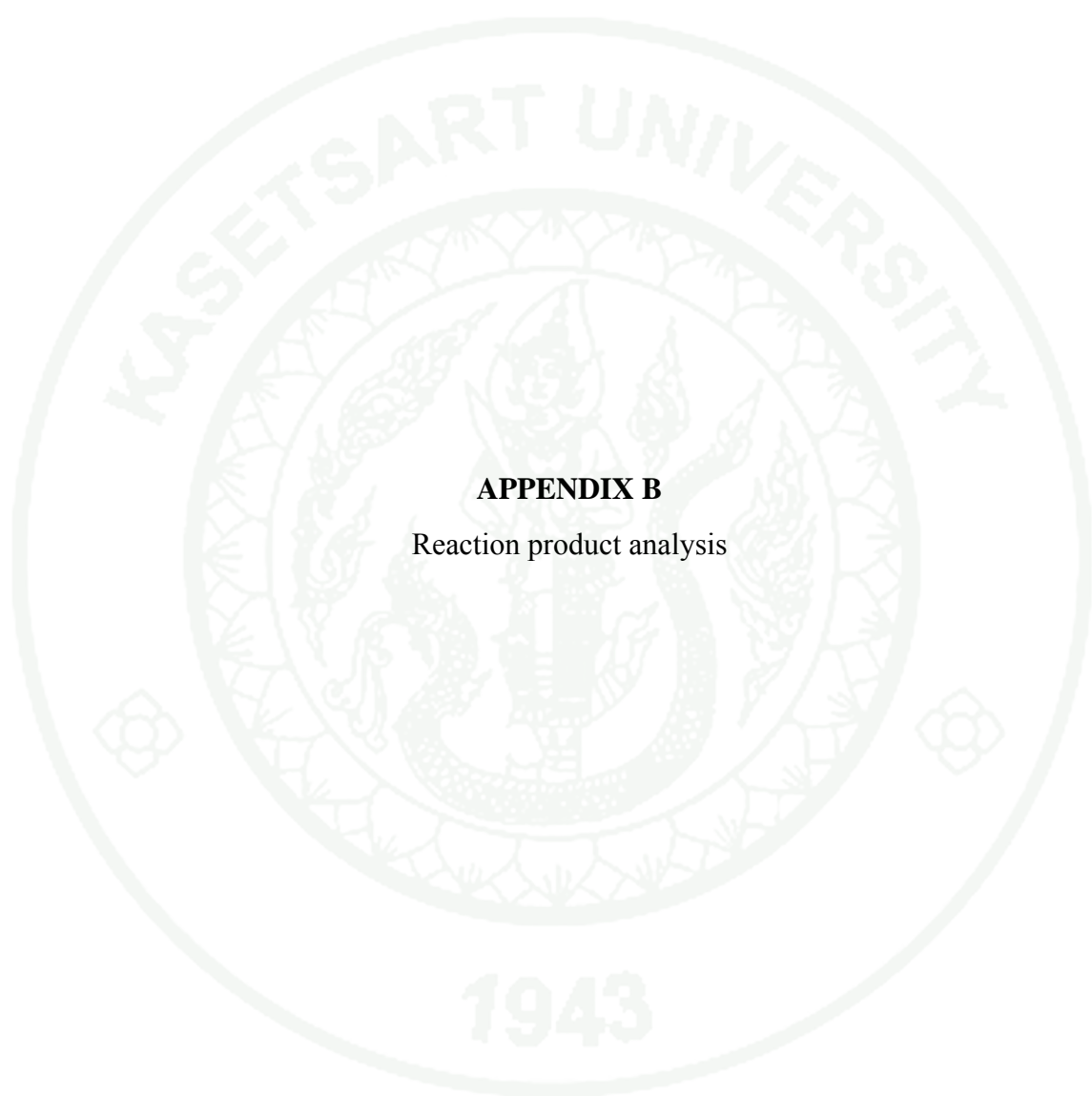
3.6 Determined the metal/aluminium atomic ratio (TM/Al) following equation A7:

$$M/Al = S_{TM} \times 26.98 / (MW_M \times Al_{ppm}) \quad (A7)$$

where:

26.98 = atomic weight of aluminum

MW_{TM} = atomic weight of transition metal ($MW_{Fe} = 55.845$, $MW_{Co} = 58.933$, and $MW_{Cu} = 63.546$ for iron, cobalt, and copper, respectively)



APPENDIX B

Reaction product analysis

In this study Mass Spectrometer (MS) and Gas Chromatography (GC) were used as the analyzers. The chemical components were quantitative characterized by the benefit of an internal standard species. The internal standard is a known quantity of a compound, different from analyte, which is added to the unknown. The internal standards addition is require for analyses in which the quantity of sample analyzed or the instrument response varies slightly from run to run for reasons that are difficult to control. In this work, the internal standard gas was added into the reactant gaseous components and simultaneously flows through the reactor with the interest species. A signal from analyte is compared with signal from the internal standard to find out how much analyte is present.

An unknown quantity can be interpreted from a response of the procedure. The response of the procedure is evaluated for known quantities of analyte (called standard) which prepared as a calibration curve. This curve is a graph showing the analytical response of analytical method (signal) as a function of the known quantity (concentration) of analyte present. Solutions containing known concentrations of analyte are called standard solutions while solutions containing all the reagents and solvents used in the analysis, but any of analyte, are called blank solutions. The response of blank is the response of the analytical procedure to impurities or interfering species in the reagents. The calibration curve is constructing as following procedure described by Harris (2003):

Step 1. Prepare known samples of analyte, covering a convenient rage of concentrations, and measure the response of the analytical procedure to the standards.

Step 2. Substract the average signal of the blank smaples from each measured signal to obtain corrected signal. The blank measures the response of the procedure when no analyte is present.

Step 3. Plot of corrected signal versus quantity of analyte, find the best straight line through the linear portion of the data.

Step 4. If analyze an unknown at the future time, run a blank at the same time. Subtract a new blank signal from the unknown signal to obtain the corrected signal.

The calibration curve is only accurate for the one set of conditions under which it was obtained. However, the relative response of the detector to analyte and standard is usually constant over a wide range of conditions. As long as the the concentration of standard is know, the correct concentration of analyte can be derived. To use an internal standard, the known mixture of standard and analyte are prepared to measure the relative response of the detector to the two species. The detector generally has different response to each component, the response of analyte to the response of internal standard is called response factor (F).

The response of X is current intensity (I_x) or peak area (A_x) of each species is depends on its concentration $[X]$ and its sensitivity. The sensitivity is the unit of signal per unit concentration or the slope of the calibration curve which plot between response of X and concentration of X. The concentration of X, can determined as equation A-8:

$$\frac{[A_x]}{[x]} = F \frac{A_s}{[S]} \quad \text{or} \quad \frac{[A_x]}{[x]} = F \frac{I_s}{[S]} \quad (\text{A-8})$$

where F is response factor

F = the response of analyte to the response of internal standard

A_x = peak area of analyte

A_s = peal area of standard

I_x = current signal of analyte

I_s = current signal of standard

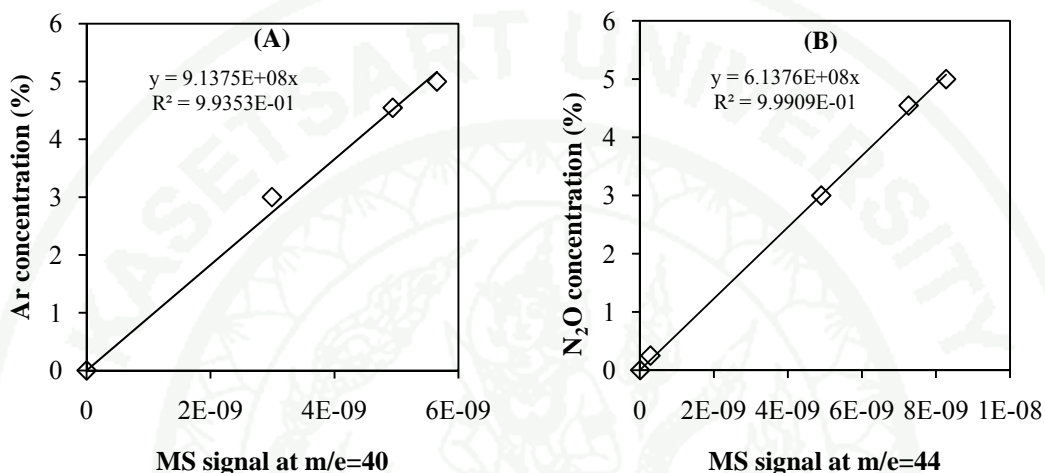
$[X]$ = concentration of analyte

$[S]$ = concentration of standard

1. Product analysis by Mass Spectrometer (MS)

In this studied MS was set to measuring with Multiple Ion Detector (MID) measurement type. In this mode one measurement on one defined mass is done per channel. The concentration of analyte was measure as mass number (m/e) and their current intensities. The MID versus time was selected to measure the data as a function of time or number of cycle.

The response factor of Ar and N₂O from MS signal is finding through the slope of appendix figure B1 (a) and (b). This slope will be defined as the sensitivity. From the plot, the slope of appendix figure B1(a) is 9.1375×10^8 for internal standard Ar and the slope of appendix figure B1(b) is 6.1376×10^8 for N₂O. The response factor (F) for N₂O is 1.488.



Appendix Figure B1. Example plot for evaluate the response factor of Ar(A) and N₂O(B) at m/e =40 and m/e=44, respectively

Then the concentration of the interest species was calculated by this equation A-9:

$$[X] = (I_x / I_s) ([S]/F) \quad (A-9)$$

The internal standard for MS detector was Ar which measure the response at m/e = 40. The signal at m/e =44 and m/e = 30 are response for N₂O species. The proportional of the response factor (1/F) for N₂O from equation A-9 when Ar was used as internal standard is 0.67. Appendix Table B1 shows the example of a one set of the MS response in this study. The calibration information contained the slope of a calibration curve, the proportional of response factor respect to the response of Ar and the equation for predicting the signal response for each analyte species. In the reaction of CH₄ and N₂O, the response at m/e=44 can be response of N₂O and CO₂ product. In this case, the N₂O concentration was determine by the response at m/e=30. The concentration of species X can calculate by equation A-10:

$$[X] = (I_x)(\text{sensitivity of } x) \quad (\text{A-10})$$

Appendix Table B1. Example of sensitivity and response factor for calculation the gas concentration from MS signal

gas	m/e	sensitivity	Proportional of response factor	
			(1/F)	Signal response
Ar	40	2.7144E+08	1.0000	y = 3.8494E-09x + base line
CH ₄	15	4.9751E+08	0.5456	
N ₂	28	2.5783E+08	1.0528	y = 3.8494E-09x + base line
N ₂ O	44	3.0104E+08	0.9017	y = 3.3199E-09x + base-line
	30	1.6389E+09	0.1656	
	28	2.9933E+09	0.0907	y = 2.1408E-10x + base-line
CO ₂	44	2.5530E+08	1.0632	y = 3.8925E-09x + base line
	28	3.7089E+09	0.0732	y = 2.6315E-10x + base-line
CO	28	2.5080E+08	1.0823	
N ₂	28	7.8842E+08	0.3443	y = 1.2659E-09x + base-line

The concentration of internal standard Ar is

$$[Ar] = I_{Ar} \times \text{sensitivity of Ar at } m/e=40$$

then

$$\frac{[x]}{[Ar]} = \frac{I_x \times \text{sensitivity of } x}{I_{Ar} \times \text{sensitivity of Ar}}$$

response factor of x = sensitivity of x/ sensitivity of Ar

$$[x] = \frac{I_x [Ar]}{I_{Ar}} \times \text{response factor of } x$$

Then the concentration of interest species are:

$$[N_2O] = \frac{I_{N_2O \text{ at } \frac{m}{e}=44} \times [Ar] \times \text{response factor of } N_2O \text{ at } \frac{m}{e}=44}{I_{Ar \text{ at } \frac{m}{e}=40}}$$

$$= \frac{I_{N_2O \text{ at } \frac{m}{e}=30} \times [Ar] \times \text{response factor of } N_2O \text{ at } \frac{m}{e}=30}{I_{Ar \text{ at } \frac{m}{e}=40}}$$

$$[CH_4] = \frac{I_{CH_4 \text{ at } \frac{m}{e}=15} \times [Ar] \times \text{response factor of } CH_4 \text{ at } \frac{m}{e}=15}{I_{Ar \text{ at } \frac{m}{e}=40}}$$

The inlet gas concentrations were calculation from the concentration of Ar. For example, the reactant gas were 5% vol Ar, 5% vol N₂O, 5% vol CH₄ and He balance then;

$$[Ar]_{in} = [CH_4]_{in} = [N_2O]_{in} = [Ar]_{out} \quad (A-11)$$

The conversions (χ) were calculated following A-12 equation:

$$\text{conversion } (\chi) = \frac{[(\text{concentration inlet}) - (\text{concentration outlet})]}{(\text{concentration inlet})} \quad (A-12)$$

$$\chi_{N_2O} = \frac{[N_2O]_{in} - [N_2O]_{out}}{[N_2O]_{in}} = \frac{[Ar] - [N_2O]}{[Ar]}$$

$$\chi_{CH_4} = \frac{[CH_4]_{in} - [CH_4]_{out}}{[CH_4]_{in}} = \frac{[Ar] - [CH_4]}{[Ar]}$$

2. Product analysis by Gas Chromatograph

A peak position is identify by compare it relation times with that of an authentic sample of the suspected compound in GC. Quantitative analysis is based on the area of a chromatographic peak. In the linear response concentration range, the area of a peak is proportional to the quantity of that component. Quantitative analysis

is performed by adding a known quantity of internal standard to the unknown. After measuring the response factor with standard mixtures as equation A-8 is used to measure the quantity of unknown.

Products compositions from the reaction of N_2O and CH_4 over zeolites catalysts were characterized by gas chromatography (GC). The product composition were separated through HayeSep®D (100/120, 10ft \times 1/8" OD, SS) pack column. Hydrocarbon products species such as small paraffin, unsaturated hydrocarbon, and some aromatic species which interested in this studied can separated by this column. In this studied oven was programmed to start at 80 °C. In the first step, oven was kept 80 °C for 1.5 min and then heating 20 °C /min to 260. Finally, oven was holding at 260 °C for 18.5 min before going to post treatment process. Flame Ionized Detector (FID) was attached to analyzed the quantities of hydrocarbon from the column outlet.

The standard liquid molecules; benzene (C_6H_6 99.8%, $F_w=78.115$, $B_p=80.1^\circ\text{C}$), toluene ($\text{C}_6\text{H}_5\text{CH}_3$, 99.8% $F_w=92.14$, $B_p=110.6^\circ\text{C}$), xylene (C_8H_{10}), methanol (CH_3OH , 99.9%, $F_w=32$, $B_p=66^\circ\text{C}$), and ethanol ($\text{C}_2\text{H}_5\text{OH}$, $F_w=52$, $B_p=78.4^\circ\text{C}$) were injected by syringe in to the GC inlet.

2.1 Calibration

2.1.1 Gas species

A molar volume of an ideal gas at STP is 22.4 L or 22400 cm^3 . At sampling detector condition at 1 atm 100°C; 1 cm^3 contain $n = PV/RT$ mole where $R = 82.0575 \text{ atm cm}^3/(\text{mol K})$ and $T = 373 \text{ K}$

$$\therefore n = (1 \times 1)/(82.0575 \times 373) = 32.671787 \text{ } \mu\text{mole}$$

In sample gas 1 cm^3 contain 32.671787 μmole .

$$\therefore \mu\text{mole of gas} = (\% \text{ gas in the total flow}/100) \times 32.671787 \quad (\text{A-13})$$

Example A pulses of C_2H_6 1 cm^3 produced peak at retention time = 4.733 min. A peak area is 16984410 a.u. is the response of 3 %vol. C_2H_6 component in the total gas flow rate and calculated to be in 0.98 μmole of C_2H_6 in 1 cm^3 .

2.1.2 Liquid species

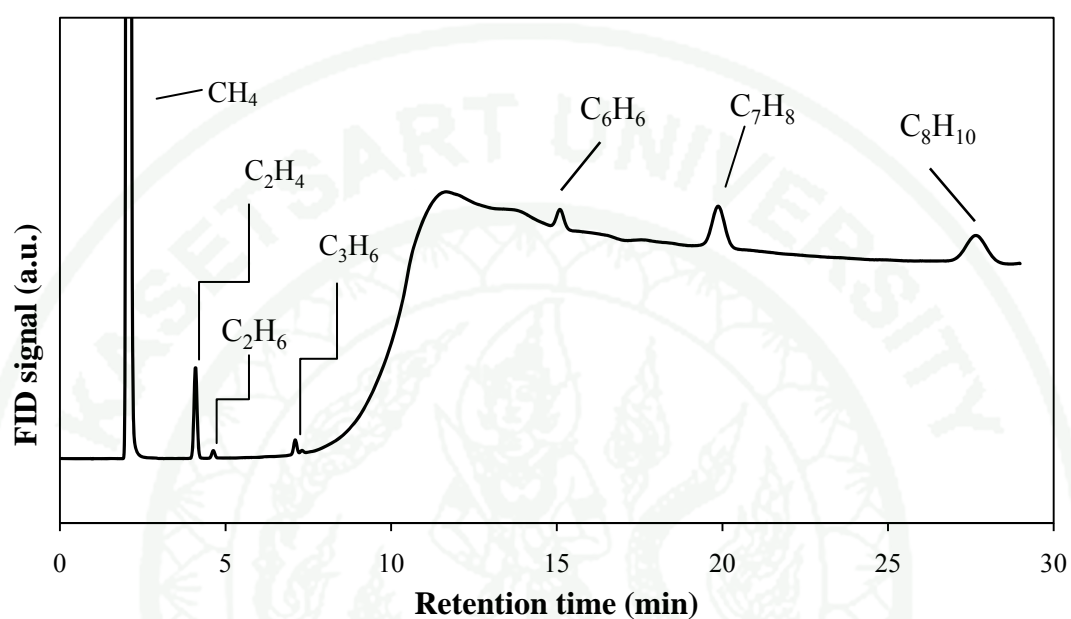
Toluene density is 0.865 g/mL at 25 °C and molecular weight is 92.14 g/mol

$$\begin{aligned}
 \therefore \text{ Toluene } 0.010\text{ }\mu\text{L} &= 0.010/1000\text{ mL} = 1 \times 10^{-5}\text{ mL} \\
 &= (1 \times 10^{-5}\text{ mL}) \times 0.865\text{ g/mL} = 8.65 \times 10^{-6}\text{ g} \\
 &= (8.65 \times 10^{-6})/92.14\text{ mol} \\
 &= 9.38789 \times 10^{-8}\text{ mol} \\
 &= 93.8789\text{ n mole}
 \end{aligned}$$

Example Toluene 93.8789 n mole produce peak at retention time 17.358 min and have a peak area equal 234000 a.u.

The relation of peak area and concentration of each standard species were plotted and collected the response factor. From GC, the peak area at specific retention times was collected to determining the products concentration of each component. The molar concentration calculated through the response factors of each species. The internal standard for this reaction is CH_4 which calculated the correct concentration from Ar in MS. The example of chromatogram from GC is showing in Appendix Figure B2. The first peak at retention time about 1.9 min is the signal from methane (CH_4). The signal at retention time 4.0, 4.3 and 7.0 min are the signal of ethane (C_2H_4), ethane (C_2H_6), and propene (C_3H_6), respectively were considered as C_2 - C_3 products. The signal at 15.0, 19.8, and 27.5 min are the signal of benzene (C_6H_6), toluene (C_7H_8) and xylene (C_8H_{10}), which considered as the aromatic products.

The production gases from the ethane dehydrogenation reaction were analyzed by TCD detector. Each component concentration was calculated by the similar method.



Appendix Figure B2 Example chromatogram from GC (from the reaction of 5%CH₄ and 2.5% N₂O in total flow 50 cm³/min over 100 mg ZSM-5(25) at 500 °C)

CURRICULUM VITAE

NAME : Miss Boonruen Sunpetch

BIRTH DATE : September 26, 1974

BIRTH PLACE : Trang, THAILAND

NATIONALITY : Thai

EDUCATION	: YEAR	INSTITUTION	DEGREE/DIPLOMA
	: 1998	Khon Kaen Univ.	B.Eng. (Chem. Eng)
	: 2002	Khon Kaen Univ.	M.Eng. (Chem. Eng.)
	: 2009	Kasetsart Univ.	Ph.D. (Chemistry)

SCHOLARSHIPS : Kasetsart University (2003-2006)
 : Postgraduate Education and Research Program in Petroleum and Petrochemical Technology (MUA-ADB) (2003-2006)

PUBLICATIONS :

1. Puntu, P., B. Boekfa, B. Sunpetch, and J. Limtrakul. Nanocavity effects on N₂O decomposition on different types of Fe-zeolites (Fe-FER, Fe-BEA, Fe-ZSM-5 and Fe-FAU): A Combined Theoretical and Experimental Study. *Chem. Eng. Comm.*195, 1477-1485, 2008.
2. Sunpetch, B. and J. Limtrakul. Interaction of CH₃CN with H-FAU, MFI zeolites: a combined QM/MM/study. Poster presentation in 227th ACS meeting (division of inorganic chemistry)